Mesoscopic Computational Haemodynamics

ACADEMISCH PROEFSCHRIFT

ter verkrijging van de graad van doctor
aan de Universiteit van Amsterdam
op gezag van de Rector Magnificus
prof. mr. P. F. van der Heijden
ten overstaan van een door het college voor promoties ingestelde
commissie, in het openbaar te verdedigen in de Aula der Universiteit
op dinsdag 14 oktober 2003, te 12:00 uur

door

Abdel Monim Mohamed Ali Mohamed Hassan Artoli

geboren te Almatamma, Soedan

Promotiecommissie:

Promotor:	prof. dr. P. M. A. Sloot
Co-promotor:	dr. ir. A. G. Hoekstra
Overige leden:	prof. dr. ir. J. S. D. Spaan prof. dr. P. de Chatel prof. dr. P. W. Hemker prof. dr. B. Chopard prof. dr. J. H. C. Reiber prof. dr. P. Hilbers dr. C. A. Taylor
Faculteit:	Faculteit der Natuurwetenschappen, Wiskunde en Informatica

The Work described in this thesis has been carried out at the Section Computational Science of the University van Amsterdam and was financially supported by the Steunfonds Soedanese Studenten, Leiden and Al Neelain University, Khartoum, Sudan.

ISBN 90 5776 112 2

Typeset with LaTeX 2ε
Printed by Ponsen & Looijen, Wageningen.
Author contact: artoli@hotmail.com

Cover figures: Velocity variation in time accross a model of the carotid artery (Front) and corresponding shear stress (Back).

To Nada, Nahla and to Naglaa

Contents

List of Figures

Chapter 1

Introduction

Physiology has widely been practised throughout time: along China's Yellow River long before the Chinese Civilisation, by the Indians along the Guanges River and by Egyptians and Nubians along the River Nile. It flourished during the time of Hippocrates (460–370 B.C.), the father of Western medicine and through the period of Aristotle (384–322 B.C.) who tutored Alexander the Great. Galen (130–200 A. D.) developed the first theories of anatomy and physiology and Ibn Sina (980–1037) made further contributions with his *Al-Qanoun*. Ibn Ul -Nafis (1210–1288) became the founder of coronary arteries circulations as we know it today and in his description of pulmonary circulation. He was the main forerunner of Servetus, Vesalius, Colombo and Harvey who in many ways proved the existence of the circulation[1] (Harvey, 1628). From this, a lot is known about how blood flows. The available literature is far too extensive to be cited in a short introduction. The book of Hippocrates on *aphorisms*, that of Aristotle *on the Parts of Animals* (384–322 BC), the Chinese book *Nei Jing* (the Internal Classic) during 472–221 BC, Ibn Ul-Nafis commentaries on medicine, and Harvey's book *On the Circulation of the Blood* (1628) are a few treasures to mention. However, all these attempts described the circulation in a qualitative way. The rules of mechanics were not yet formalised.

The seventeenth and the eighteenth centuries witnessed considerable development in mathematics, physics and related sciences. The concepts of calculus, instantaneous velocity and acceleration were introduced. Works on number theory and calculus by Fermat (1601–1665) were published for the first time as was the following three axioms of Newton (1642–1727) who also recorded the concept of viscosity (Newton, 1687). Euler (1769) formulated the use of differential equations to describe fluid flow. Cauchy (1823) introduced the concept of stress which continues to be at the basis of today's mechanics. Investigations of circulatory function in a Newtonian

[1] Ibn Ul-Nafis' book on *Sharh Tafseer al Qanoun* was translated by Andrea Alpago in 1547. In this book he stated that "The heart has only two ventricles ... and between these two there is absolutely no opening. Also dissection gives this lie to what they said, as the septum between these two cavities is much thicker than elsewhere. The benefit of this blood (that is in the right cavity) is to go up to the lungs, mix with what is in the lungs of air, then pass through the arteria venosa to the left cavity of the two cavities of the heart ..."

sense by Hales[1] established new quantitative and experimental concepts in the field of haemodynamics, the science dealing with blood flow. During the time of the French Revolution, Navier (1822) and Stokes (1845) derived the still accepted Navier-Stokes (NS) partial differential equations that fully describe incompressible viscous fluids. Following this, Poisson developed a theory that also holds for compressible fluids. Meanwhile, the nature of elasticity attracted Thomas Young who studied the relation between the velocity of propagation of the arterial pulse and the elastic properties of arteries.[2]

It did not take long for the Navier-Stokes equations to be accepted as the equations governing fluid flows. Nevertheless, these equations were, and still are very difficult to solve, except for a few idealised cases. Therefore, the approach was still highly theoretical. Moreover, with the NS solution the fluid dynamic limit (at vanishingly small mean free path) is singular at the shock regions. Thereafter, with the development of research in partial differential equations and numerical analysis, it was possible to extract useful information by finding numerical solutions to the NS equations.

During this period, relaxation methods and finite-element-like solutions were reported (Schellbach, 1851). Bessel functions were fully developed by Bessel in 1824. Hagen (1797–1884) and Poiseulle (1797–1869) established the experimental relation between flow rate and pressure gradient for steady viscous flows, which has since been worked out by Hagenbach in 1860 (see e.g. McDonald, 1974) who solved the Navier-Stokes equations for a tube flow. The Webers'[3] works on the influence of vessel elasticity and the dynamics of wave motion on blood flow, together with Moens, Korteweg and Résal has been a great contribution to understanding wave propagation in the circulation (McDonald, 1974). Formation of differential equations for problems of biological interest and attempts to solve them analytically or numerically appeared by the end of the nineteenth century. As the computational need increased, Charles Babbage (1792-1871) proposed the idea of an analytical engine as a computing machine. These are just a few of the great names associated with the historical development of haemodynamics before the start of the twentieth century.

Theories on atomic constituents of matter and sooner, laws of statistical mechanics and thermodynamics were under control since the beginning of last century. Clausius, Maxwell and Boltzmann (1844-1906) are to be regarded as the founders. Statistical mechanics explains how the properties of atoms such as mass, charge, and structure determine the visible properties of matter such as viscosity, thermal conductivity,

[1] Hales, among other achievements, measured the arterial blood pressure (in the horse) for the first time. He also introduced the concept of peripheral resistance. For his many achievements, he deserves the title 'father of haemodynamics', as suggested by McDonald, a pioneer in haemodynamics of the last century.

[2] It is worth noting that Young, who was a practising physician as well as a physicist, gave an interesting lecture to the Royal Society on the function of the heart and arteries (Young, 1809) in which he said " The mechanical motions, which take place in animal body, are regulated by the same general laws as the motions of inanimate bodies... the circulation of the blood depends on the muscular and elastic powers of the heart and of the arteries, supposing the nature of those powers to be known, must become simply a question belonging to the most refined departments of the theory of hydraulics."

[3] Weber brothers also pioneered in electrophysiology.

pressure, and diffusion. Instrumentation enhanced as a consequence of war demand. In the mean time, a new era of haemodynamics has flourished.

The early twentieth century started with a clear theoretical and experimental idea about the mechanics of the circulation. Manometers capable of measuring pulsatile flow were invented by Otto Frank (1903), leading to a huge accumulation of measured data on pressure pulse. Before and during World War I, sophisticated calculations, with the aid of a Pascal calculator, and reasonably precise measurements of the macroscopic world have been made. The discovery of the string galvanometer and its use in electrocardiography (*het tele-cardiogram*) by Willem Einthoven in 1906[1] opened a new chapter in the study of haemodynamics. Just before World War I, vascular anastomosis and transplantation to treat stenosis and thrombosis were remarkably successful (Carrel[2], 1912). Thereafter, Frank (1927), Womersley (1955a, 1955b; 1955c) and McDonald (1955; 1960) introduced Fourier harmonics and came up with the Womersley solution for pulsatile flow. From there on, theoretical development about pulsatile flow has been completed; the Womersley solution well describes the macroscopic nature of pulsatile flow in arteries. Interests were then shifted towards closer investigation of blood rheology, and fluid-structure interaction. Theories on non-Newtonian fluids and effects were developed and questions on high and low-shear-limits were raised.

Since the middle of the twentieth century, the arterial system has been treated as being in a steady-state oscillation produced by repeated heart beats and the cardiac pulse was represented by its Fourier harmonics.

Computers of the first generation were hardly used by physiologists since they were not widespread. Physiologists, like other researchers in fluid mechanics started to think of modelling flow in more complex geometries. A need for computer simulations was then realised. However, the history of computing during the 1950's and the 1960's is of less importance to the development of haemodynamics, although it is not the case for fluid mechanics. For instance, one of Mark I's applications was to solve ordinary differential equations by the Runge-Kutta method. Iterative solutions of multidimensional partial differential equations were reported (e.g. Stone, 1968).

Numerical fluid dynamics, later called computational fluid dynamics (CFD) was identified (see Garrett Birkhoff in Nash (Ed.), (1990) for extended survey), but mostly engaged in developing and understanding the fluid mechanics of war machines and in space dynamics. However, shortly after the availability of computing facilities, mathematical models and simulations of a biological nature began to develop (e.g. Turing, 1952; Lindermayer, 1968). With the development in computer power, finite difference method and the finite volume method were then ready to solve flow in complex geometries. Primitive versions of the finite-element method were introduced during the 1950's (e.g. Argyris, 1952; Turner *et al.*, 1956; Clough, 1960) and landmarks in its development were established during the 1960's (Przemieniecki *et al.*,

[1]The first cardiogram can be seen at http://www.einthoven.nl/images/fotos/eh002.jpg

[2]Carrel is also known with his "Man the Unknown" book (1935) in which he said "We must arise and move on. We must liberate ourselves from blind technology and grasp the complexity and the wealth of our own nature."

1965). Although the finite difference (e.g. Roache, 1972) and finite volume methods (e.g. Spalding, 1981) were the ones most commonly used, significant difficulties in modelling complex geometries and applying local grid refinement techniques to resolve flow in regions of large velocity gradients were faced until the finite element method was matured in the late 1970's (e.g. Girault and Raviart, 1979). However, it was believed that the finite element method could not be applied to un-symmetric operators, and therefore, use of the methods for solving fluid flow problems was not realised until the first works on solutions of NS equations with the finite element methods appeared (e.g. Oden, 1970; Oden and Somogyi, 1968, Aziz, 1972). Thereafter, the mathematical theory, including priori error estimates was fully developed and from that time the finite element method has become popular in solving many engineering problems.

Until the middle of 1980's, finite elements methods were not fully formulated to deal with unsteady flow simulations in realistic geometries (van de Vosse, 1987). It is worth noting that till that time, it was not possible to measure time-dependent flow *in vivo* with the available techniques. This gave computational modelling a chance to grow in order to fill this gap. During this period, hypotheses on arterial wall shear stress and its relation to atherosclerosis were tested (e.g. Caro *et al.*, 1969; Zamir, 1977). It may be stated that in vitro, idealised models, and animal experiments were the main modes of cardiovascular investigations during the 1970's.

During and since the 1980's, a new era of computational haemodynamics has been initialised, associating the dramatic increase in computational power, and enhancements in imaging techniques and computational methodology. The localisation of cardiovascular diseases in certain segments of hydrodynamic complexity has been reported (e. g. DeBakey *et al.*, 1985; Thubriker and Robicsek, 1995). Since then, the finite element methods have become adequate and widespread in solving fluid flow problems. In this thesis, most of the cited literature about computational haemodynamics involve the finite element method as a flow solver.

However, the finite element method consumes both memory and computational time. This is attributed to the time consuming generation of the body fitted computational grid, and to the explicit nature of solving the Poison equation. With the development of computer power and advances in parallization methods, the computational time for finite element methods was significantly reduced. Nevertheless, a high demand on interactive simulations is raised. The finite element methods are still far from being interactive. An average simulation time for solving flow in a geometry like the abdominal aorta may take half a day on a single processor of today's technology. Since the computational grid is body fitted, parallization of finite element method is not straightforward as it is for Cartesian grids. Therefore, a tendency to prefer Cartesian grids is slowly growing. In addition, recent years have seen a growing interest in developing numerical algorithms for compressible multi fluids with the need to model multi-component flows. The difficulty in measurement of multi-component flow properties (e.g. Baker, 1991) with traditional computational fluid dynamics solvers, as they are faced with a challenge to produce physically correct solutions (e.g Igra and Takayama, 2002; Fedkiw, 2002) raised a high demand in adopting new robust

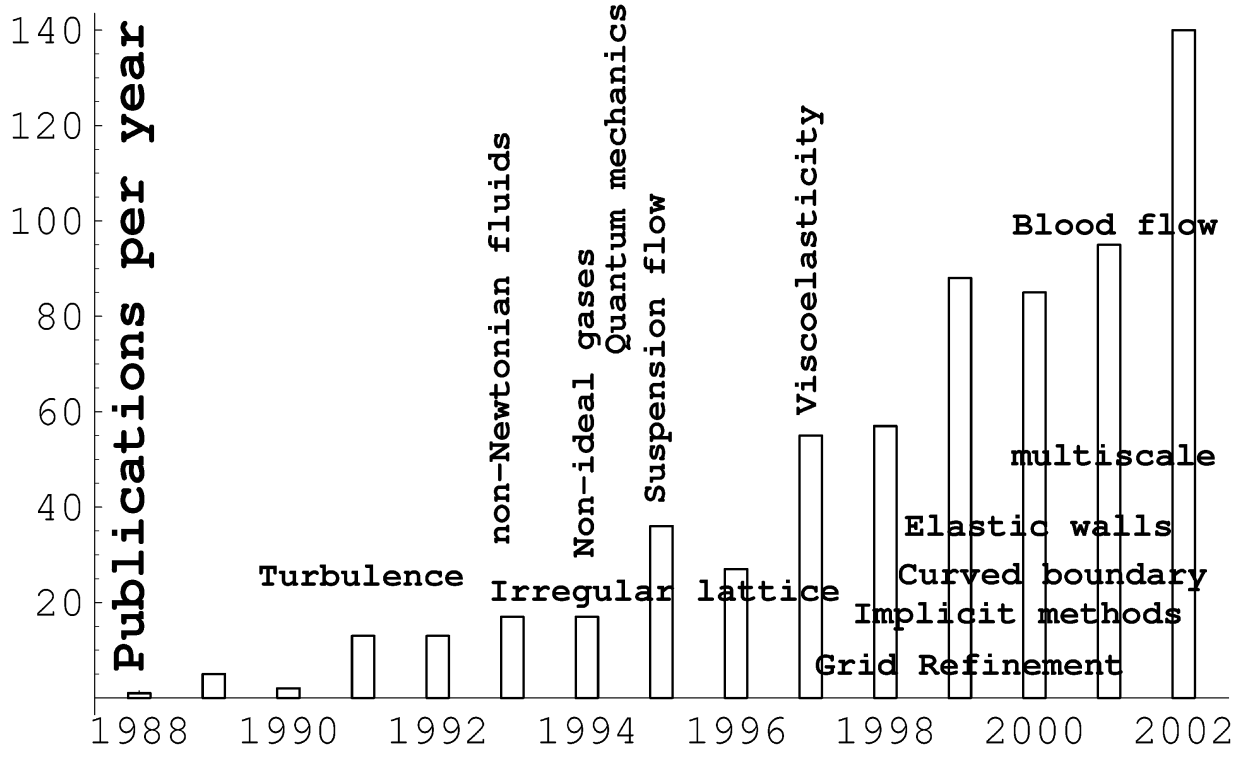

Figure 1.1: Evolution of lattice Boltzmann models in terms of applications (text) and annual number of publications (columns). The graph is generated using the ISI Web of Science and Science Direct digital databases.

techniques. Mixed finite elements techniques (Raviart, 1984) is now being used as a standard way of deriving high-order conservative approximations.

New particle based methods such as dissipative particle dynamics, lattice gases and lattice Boltzmann methods have been developed and matured (McNamara and Zanetti, 1988; Higuera and Succi, 1989; Qian *et al.*, 1992; Aharonov and Rothman, 1993; Behrend, 1995). These mesoscopic techniques have been proved successful in many applications (see Fig. 1.1) and may be quite useful for haemodynamic research, as, among other features, they are more flexible in modelling suspensions.

1.0.1 Going Mesoscopic

It is well known that accurate predictions of the behaviour of fluids is possible with the standard macroscopic representation in which the continuum hypothesis[1] and local thermodynamic equilibrium are assumed. The validity of a macroscopic approach holds only if all macroscopic length and time scales are considerably larger (a few

[1]Matter is assumed to occupy every point of the space of interest, regardless of how closely the material is investigated.

hundreds) than the largest molecular length and time scales[1] (e.g. 60 nm and 0.1 sec for nitrogen). The Navier-Stokes equations treat the fluid macroscopicly. Therefore, they are only valid when the length and time scales are such that the fluid is in local thermodynamic equilibrium. With large spatial and temporal gradients, local thermal equilibrium may not be guaranteed over the macroscopic time sclaes and the NS equations would not be an accurate mathematical model to solve. For a better understanding of macroscopic behaviour, and for more accuracy, one may investigate the microscopic world of cells and atoms. The question of whether it is time to go microscopically in haemodynamics may be argued for some time to come, but it may be realised, even now, that microscopic details about rheology of blood and the nature of cardiovascular diseases are needed, and the only way to understand that is by avoiding idealistic simplifications when investigating blood mechanisms. For instance, the non-Newtonian behaviour of blood flow, the chemical interaction with the enzymes produced in the arterial system and the drug-blood relation are all challenging us. It can be argued that this is enough to try different approaches in haemodynamics. Solving the NS equations, which are based on Newtonian mechanics of the macroscopic world, is not enough to handle this problem. Unfortunately, the computational power is far behind performing molecular dynamics simulations[2] even in a tiny arterial segment[3]. As one cannot construct a fully deterministic theory of many particles in motion, the introduction of statistical mechanics by Maxwell (1866) and Boltzmann (1872)[4] provides an alternative approach with which the high abstraction of macromechanics is limited. Statistical mechanics suggests Boltzmann transport equation as an alternative mesoscopic approach to Newton's laws of motion. This has been recognised as a real breakthrough in theoretical physics.

The Boltzmann equation is still hard to solve and only perturbative approximations are used in fluid dynamics (Caflisch, 1983). Numerical solutions of the Boltzmann equation have many applications, ranging from nuclear reactor design, through medical radiation physics, to high energy physics. Both deterministic and stochastic approaches are widespread. Deterministic solutions are fast, but are usually associated with discretization errors. Monte Carlo methods are more accurate but are quite slow. Recently, considerable efforts have been made in both directions.

[1] The length scale is usually taken as the mean free path between collisions while the time scale is represented by the time between successive collisions.

[2] In molecular dynamics, the interaction between individual molecules is computed for the whole system.

[3] For 100k atoms, it takes a week to simulate a nanosecond on an Athlon cluster of 32 processors with NAMD, a molecular dynamics code designed for high-performance simulation of large biomolecular systems. See http://www.ks.uiuc.edu/Research/namd/

[4] Boltzmann was the first to show that the entropy increases with time. His atomic hypothesis gave him a hard time that he didn't survive to see being proved one year after his death.

1.0.2 Choice of the Numerical Method

Just after World War II, the ENIAC computer was built. This changed the world of computing in many aspects. The early Monte Carlo calculations[1] and sampling techniques were made possible (e.g. Richtmyer and Metropolis, 1949) and with the introduction of the cellular automata by von Neumann in 1948 (the universal computing machine, to mimic the complexity of nature), computers have been recognised as a kind of experimental laboratory rather than just number processing devices. Since then, Lattice Gas automata (LGA), a special category of cellular automata, were developed and have been proved to model hydrodynamics in a much simpler way than the conventional computational fluid dynamics solvers. Although it may be considered as a particular class of cellular automata with some additional constraints (Rivert and Boon, 2001), lattice gases can be described, from a physical point of view, as a simple fully discrete microscopic model of a fluid in which fictitious particles reside on finite regions of a regular Bravais lattice. It is therefore a particle-in-cell method, in which the continuous physical domain is broken-up into a number of discrete states. Particles move with discrete velocities, stream to neighbouring sites where they collide under collision rules and stream again in a continuous way till a predefined equilibrium state is reached. Currently there are a considerable number of lattice gas models, being adapted to simulate specific applications. More details on lattice gas hydrodynamics were described in the recent books of Rothman and Zaleski (1997), Chopard and Droz (1998), and Rivet and Boon (2001).

Although they proved successful in returning the elegance of Physics, lattice gas models were met with two major difficulties: they are very noisy due to their Boolean nature[2], and they do not satisfy Galilean invariance[3] due to the velocity dependent density in the equations of motion.

Being established to overcome these problems, the lattice Boltzmann method (LBM) may be considered as an attractive alternative to conventional computational fluid dynamics solvers such as the finite elements and the finite difference methods. This is due to its simple implementation, straightforward parallelism, easy grid generation and its proven capability in simulations of multi-component flows and complex geometry. The lattice Boltzmann method is nowadays considered as a matured computational fluid dynamics flow solver. The method competes with traditional Navier-Stokes solvers by directly obtaining the pressure without a need to solve the Poisson equation and obtaining the stress tensor without using simulated velocity gradients. This strong argument is not yet taken seriously since the method is still developing while the conventional solvers are quite mature.

This motivated us to test the capability of the method in the field of haemodynamics, in which it is hardly used, although it has often been argued that the method has many capabilities that may attract researchers in haemodynamics. Pioneering work

[1] It is believed that Enrico Fermi (1901-1954) was the first to use what was to be called later the Monte Carlo method in studying the moderation of neutrons in 1930's in Rome (see Nash (Ed.), 1990).

[2] The lattice gas intrinsic fluctuations may be used to capture the essentials of actual fluctuations in real fluids. For more details see Rivet and Boon(2001).

[3] A frame of motion is Galilean invariant if the equations of motion do not change in all other frames.

in this direction was done by Krafczyk *et al.* (1998).

1.0.3 Objectives of This Study

As the complex nature of blood flow in the human arterial system is still gaining more attention, and since cardiovascular diseases are considered a leading cause of death in the developed world and are now becoming more prevalent in developing countries (World Health Organisation, 2002), the main objective of this thesis is to better understand the nature of blood flow in realistic geometry (namely patient specific geometry produced from medical scanners) through solving the mesocopic Boltzmann transport equation with a simple to generate grid via the lattice Boltzmann method. Other objectives include testing capabilities, robustness, accuracy and performance of the lattice Boltzmann method for unsteady flows and development of tools to enhance them towards interactive simulations. Relevant flow quantities will be validated through experimental and/or macroscopic numerical data. The outcomes of the study will be used to develop a computer-aided surgical planning environment in a Grid-supported virtual environment.

1.0.4 Thesis Overview

In Chapter 2, we briefly review the basics of haemodynamics, focusing on recent development in mathematical modelling of blood flow circulation. Then we present model considerations. This chapter is based on available literature which may be referred to for further details.
A derivation of the lattice Boltzmann method from the Boltzmann equation and the discussions on its benefits and drawbacks are dealt with in Chapter 3. Formal error analysis and its relation to hydrodynamics non-dimensional parameters for time-dependent flows is presented. The advances in the theory of lattice Boltzmann methods are highlighted with a special focus on features related to time-dependent flows.
As the grid is Cartesian, discretization errors are eliminated in a two-dimensional benchmark simulations, aiming at understanding the error behaviour of the lattice Boltzmann method in detail. This is presented in Chapter 3 which involves steady flow in simple 2D geometries. A comparison with a conventional computational fluid dynamics solver is made.
Although the lattice Boltzmann method is easy to implement, it is not yet fully developed to deal with boundaries different than fluid ones. There are a number of boundary conditions that may be used but they are highly sophisticated and may violate the conservation laws and the stability of the system. However, there are some boundary conditions that are now popular due to their robustness in dealing with complex geometries. In this study, we focus only on those boundary conditions we believe can be used without difficulty in computational haemodynamics. In Chapters 4, 5, 6 and 8 initial and boundary conditions are studied.
In Chapter 5 three-dimensional pulsatile flow benchmarks are investigated. The Womersley solution is recovered within a very high accuracy.

One objective of this thesis is to seek a possibility of using the lattice Boltzmann method as a core for an interactive simulation environment believed to be useful in so called predictive medicine. Reasonably, computational aspects of the standard lattice Boltzmann method are discussed in Chapter 6, while Chapter 7 discusses acceleration techniques for time dependent flows.
Simulation results of steady and unsteady flow in a model of the human aortic bifurcation reconstructed from Magnetic Resonance Angiography are presented in Chapter 8 as a typical haemodynamic application. Velocity profiles and shear stress are presented and visualised. Qualitative and quantitative analysis of the flow fields and the shear stress are presented.
Although some studies on flow in elastic tubes were investigated by the author and others (Hoekstra *et al.*, 2003), results on flow in elastic structures are not discussed in this thesis.
Chapter 9 concludes the thesis with a brief summary, concluding remarks and plans for future work. Acknowledgement is given at the end of the thesis.

Chapter 2

Model Considerations

"Life is short, Art is long"

Hippocrates

Haemodynamics comprises three major problems: the physics of pressure and flow in the circulation, its role in the living systems and the use of this knowledge for diagnostic and clinical activities. This chapter is concerned with the physical principles of the mechanics of the circulation in large blood vessels. The governing equations of motion are studied and major flow characteristics in simplified geometries are investigated. Most of the brief treatment in this chapter follows some of that available in literature (McDonald, 1974; Pontrelli, 1998)

2.1 Blood

Blood is a suspension of formed blood cells and some liquid particles (the chylomicrons) in an aqueous solution (the plasma). The most important mechanical property of blood that influences its motion is the apparent viscosity η, which relates the shear rate γ and the shear stress σ. If this relationship satisfies the Newton's law of viscosity

$$\sigma = -\eta\,\gamma \tag{2.1}$$

where the viscosity η is independent of the shear rate γ, the fluid is known to be Newtonian. In this sense, blood is a non-Newtonian fluid, especially when the shear rate is small, in small vessels and arterioles. Experimentally, it has been reported that when the shear rate is about $1000\ sec^{-1}$, a typical value in large vessels, the non-Newtonian behaviour becomes insignificant and the apparent viscosity asymptotes to a value in the range $3-4$ cP[1] (Caro *et al.*, 1978), while for low shear rate ($\gamma < 1\ sec^{-1}$) it rises steeply. The red cells are in part responsible for the non-Newtonian behaviour. More details can be found in literature (e.g. Caro *et al.*, 1978). The rheological properties of

[1]The poise (P) is the CGS unit of viscosity. $1P = 1\ g\ cm^{-1}sec^{-1}$. The centipoise (cP) is one hundredth of a Poise.

non-Newtonian fluids are quite different from those of the Newtonian ones. The shear rate dependent viscosity, normal stress differences, secondary flows, stress relaxation and creep are all challenging behaviours that need to be handled carefully. Numerous empirical models for the viscosity of non-Newtonian fluids have been proposed (e.g. Chrochet and Walters, 1983; Pontrelli, 1997). These can be categorised into two main groups (see e.g. Bird, Stewart and Lightfoot, 1960); two-parameter models (e.g. Bingham model and Ostwald-de Waele model, known as the power law) and three-parameter models (e.g. Ellis model and Reiner-Philippoff model). For blood, the viscosity depends mainly on the protein concentration of the plasma, the deformability of the blood cells, and the tendency of blood cells to aggregate (Fung, 1993). Consequently, the viscosity of blood varies with the shear rate of the flow. It increases with decreasing shear rate[1], increasing haematocrit, decreasing temperature, and with the tendency of cells to aggregate. Additional factors may affect the viscosity in micro-vessels.

For some unsteady flows, such as blood flow in the human circulation, the liquid generally demonstrates both a viscous and an elastic effect, both of which determine the stress-strain relationship. Such liquids are called viscoelastic. Blood plasma shows viscosity, while whole blood is both viscous and elastic. The viscosity is related to the energy dissipated during flow, while elasticity is related to the energy stored during flow due to orientation and deformation of red blood cells (Thurston, 1972; Lowe and Barbenel, 1988; Kasser *et al.*, 1989; Sharpa *et al.*, 1996). The Newtonian model can be generalised into $\sigma = \eta(A)A$ where $A = L + L^T$ with $L = \nabla\vec{v}$ and

$$\eta(A) = \eta_\infty + (\eta_o - \eta_\infty)\left[\frac{1 + log(1+\Gamma\dot{\gamma})}{1+\Gamma\,\dot{\gamma}}\right] \tag{2.2}$$

where $\dot{\gamma} = \sqrt{\frac{tr(A^2)}{2}}$, η_o and η_∞ are the asymptotic apparent viscosities as $\dot{\gamma} \to 0$ and ∞ respectively, and Γ is a positive material constant (dimension of time) representing the degree of shear-thinning. The dot over a variable denotes the substantial derivative D/Dt given by $D/Dt = \partial/\partial t + \vec{v}\cdot\nabla$.

Another model for viscosity is the Oldroyed-B model (Oldroyd, 1950 and 1958) three-parameter shear-thinning model, given by

$$\sigma + \lambda_1\,(\dot{\sigma} - L\sigma - \sigma L^T) = \eta(A + \lambda_2(\dot{A} - LA - AL^T)) \tag{2.3}$$

in which η is a constant, λ_1 and λ_2 are two constants usually known as the relaxation and retardation constants, respectively.

A recently accepted model for blood viscosity is that proposed by Pontrelli (1998), which combines the generalised Newtonian model with the Oldroyd-B model which considers the creep, the normal stress and the stress relaxation effects with constant viscosity. This yields

$$\sigma + \lambda_1\,(\dot{\sigma} - L\sigma - \sigma L^T) = \eta(A)\,A + \eta_0\lambda_2(\dot{A} - L\,A - A\,L^T) \tag{2.4}$$

[1]In some fluids, known as shear-thickening fluids, viscosity increases with shear rate. In others, known as shear-thinning fluids, viscosity decreases with increasing shear rate. In blood, both thickening and thinning behaviour is observable.

where σ is the extra stress[1], $L = \nabla \vec{v}$,$A = L + L^T$ and the viscosity $\eta(A)$ is computed from the Generalised Newtonian model, as given by Eq.(2.2). This generalised Oldroyd-B model (GOB) captures most of the important characteristics of blood. For details on evaluations of these models, we refer to the Ph. D. thesis of Yeleswarapu (Yeleswarapu, 1996).

2.1.1 Simplifications

Experimentally, three main regions that categorise the relationship between shear rate and blood viscoelasticity have been observed:

- at low shear rate ($\gamma < 10\ sec^{-1}$) the cells are clustered in large aggregates with diminishing nature as the shear rate is increased. The viscosity and the elasticity are of O(10^{-1}) Poise. In this region, blood is absolutely non-Newtonian.
- at medium shear rate ($10 < \gamma < 100\ sec^{-1}$), the clusters are disintegrated and forced to be oriented. The viscosity is of O(10^{-3}–10^{-2}) Poise, decreasing with increasing shear rate. The elasticity is of O(10^{-1}) Poise but slightly less than at low shear rate.
- with increasing shear rate ($\gamma > 100\ sec^{-1}$), the cells are deformed and they tend to form layers that slide on plasma. To a fair approximation, blood can be treated as Newtonian in this region.

In this study our focus is on large blood vessels, such as the abdominal aorta in which the shear rate exceeds $100\ sec^{-1}$ and therefore, to the first approximation, we consider blood to be Newtonian. Available numerical studies on non-Newtonian behaviour have shown minor influences on the flow in large vessels (e.g. Gijsen *et al.*, 1999; Cole *et al.*, 2002). We also assume that blood is an isotropic, homogeneous and incompressible fluid.

2.2 Fluid-Structure Interaction

The walls of an artery are distensible tubes of complex elastic behaviour. The diameter of the vessel varies with the pulsating pressure. Being elastic, it also propagates pressure and flow waves generated by the heart at a velocity of magnitude mainly determined by the elastic parameters of the wall and the pressure gradient. It is to be noted that, the distensibility of wall vessels is essential for the wave to propagate, as for a fluid like blood flowing in a rigid tube, the wave would unrealistically propagate with the speed of sound in blood (about 1500 m/sec) (McDonald, 1974).
However, fluid-structure interaction is rather a challenge in haemodynamics. This is due to the complex structure of the arterial wall (fibrous elastin and collagen supported in a fluid) and its *elastomer* behaviour[2]. With the advances in Computa-

[1]The Caushy stress tensor is $T = -pI + \sigma$ with p the pressure.
[2]Elastomers are easily extensible

tional Fluid Dynamics (CFD) and development of computing power, studies on fluid-structure interactions have been reported. In lattice BGK models, this field is under development (Chopard and Marconi, 2002) and only a few applications are present in the literature (e.g. Fang *et al.*, 2002; Hoekstra *et al.*, 2003). The promising future of new imaging techniques such as magnetic resonance elastography (Weaver, 2001) may allow accurate estimation of elastic properties of the vessels and motivate the need for more complex simulation models. However, the Poisson ratio[1] for arterial walls is approximately 0.5, making the deformation nearly isovolumetric.
In large vessels, such as the aorta and the carotid, a maximum change of 10% in the vessel diameter is expected. This results in the same change in the Womersley parameter ($\alpha = R\sqrt{\frac{\omega}{\nu}}$, with ω the angular frequency and ν the kinematic viscosity) and the Reynolds number ($R_e = UD/\nu$ with U the velocity and D the diameter). For the aorta under resting conditions, the Womersley parameter is 16 if the wall is rigid and is in the range $14.5 - 17.6$ under elastic assumption, while the Reynolds number is 1150 for rigid wall approximation and is in the range 1035–1265. The effect is therefore quite minor for large arteries. Therefore, to first approximation, rigid wall assumption is reasonably valid in large arteries.

2.3 Equations of Motion

Even with the above simplifications, it is still difficult to mathematically describe the mechanics of the circulation for the whole body. One way to study this complex system is to consider flow in an isolated single segment. The whole system may be studied using electric network similarity (see e.g. Berger, 1993).
For an isothermal fluid, the equations of conservation of mass and momentum fully describe the macroscopic behaviour of the viscous flow. The rate of mass accumulation is always equal to the difference between the rate of incoming and outgoing masses. This leads to the well known equation of continuity

$$\frac{D\rho}{Dt} + \rho(\nabla \cdot \vec{v}) = 0 \tag{2.5}$$

which simplifies to

$$\nabla \cdot \vec{v} = 0 \tag{2.6}$$

for incompressible fluids. The conservation of momentum follows from Newton's second principle: Mass per unit volume times acceleration is equal to the sum of three forces; the pressure force, the viscous force and, if exists, the external force, all per unit volume

$$\rho\frac{D\vec{v}}{Dt} = -\vec{\nabla}p - \vec{\nabla}\cdot\sigma + \rho\vec{G} \tag{2.7}$$

In these equations, ρ is the density ($\rho = 1.05 gm/cm^3$ for blood), D/Dt is the substantial derivative, p is the pressure, σ is the stress tensor (symmetric and second order) and

[1] It is the ratio of transverse to longitudinal strain

$\vec{G}$ is the external force. There are five unknowns (velocity components, pressure and density) in four equations. It follows that one more equation is needed to uniquely determine the solution of the system. This equation is provided by applying a boundary condition. Boundary conditions are equations in the unknowns, holding only in three dimensions (any three of x,y,z,t in Cartesian coordinate system). The general specifying equation for the boundary conditions may be written in the form

$$F(p,\rho,\vec{v},x,y,z,t) = 0\ . \tag{2.8}$$

Assigning a boundary condition to the equations of motion results in a simplified set of equations suitable for a specific type of flow problems. For example, assuming constant density and viscosity results in the celebrated Navier-Stokes equations for incompressible Newtonian fluids

$$\rho\frac{D\,\vec{v}}{D\,t} = -\vec{\nabla}p + \mu\vec{\nabla}^2\vec{v} + \rho\vec{G}, \tag{2.9}$$

and for negligible viscous effects, $\vec{\nabla}\cdot\sigma = 0$, this reduces to the Euler equation

$$\rho\frac{D\vec{v}}{Dt} = -\vec{\nabla}p + \rho\vec{G}. \tag{2.10}$$

The energy equation will not be used in this study and therefore, is not presented here. We assume that the system is isothermal. In this study, analytic solutions for the used benchmarks will be presented whenever needed. It is understood that the equations presented here are the fundamental equations used to derive these solutions and therefore, it will not be necessary to derive the analytical solutions for these benchmarks.

2.3.1 The Boltzmann Equation

From a CFD point of view, the Navier-Stokes equations are adequate enough to describe macroscopic fluid flow phenomena through simple structures. As mentioned in the introduction, there is always a need to go more complex in order to understand the complexity of nature. Going complex may involve a choice of going microscopic up to the molecular dynamics, or even more.
In kinetic theory, an alternative description for monatomic gas dynamics is given through the Boltzmann equation (Boltzmann, 1872)

$$\frac{\partial f}{\partial t} + \vec{\xi}\cdot\frac{\partial f}{\partial \vec{x}} + \vec{G}\cdot\frac{\partial f}{\partial \vec{\xi}} = Q(f,\ f) \tag{2.11}$$

where $f = f(\vec{x},\ \vec{\xi},t)$ is the distribution function, $\vec{x}$ and $\vec{\xi}$ are the position and velocity vectors of a molecule, $\vec{G}$ is the force per unit mass acting on the molecule, $Q(f,\ f)$ is the quadratic collision operator and t the time. This equation can be used to describe

fluids in the limit of small mean free path between molecular collisions, which enters the equation as a collision rate. This implies that f should not be far from the Maxwellian[1]

$$g = \rho(2\pi RT)^{-D/2}\, exp[-\ (\vec{u} - \vec{\xi})^2/2RT] \tag{2.12}$$

where R is the ideal gas constant, T the absolute temperature of the fluid, D the spatial dimension and $\vec{u} - \vec{\xi}$ is the peculiar speed. The speed of sound in kinetic theory is defined as (Chapman and Cowling, 1970)

$$c_s = \sqrt{\gamma R\, T} \tag{2.13}$$

with $\gamma = 1 + 2/D$ the ratio of specific heats. By applying conservation laws to the Boltzmann equation, and assuming that f is Maxwellian, one can derive the compressible Euler equation for the hydrodynamic variables.

2.3.2 Solution of the Boltzmann Equation

As it is difficult to solve the Boltzmann equation, numerical perturbation approaches have been introduced. There are a few different ways to find asymptotic solutions for the Boltzmann equation and bridge the link between the mesoscopic Boltzmann equation and the macroscopic hydrodynamic. Examples are:

- **Hilbert expansion**: The Boltzmann equation is solved by expanding *both* the velocity distribution function and the macroscopic variables in a power-series of the Knudsen number (Cercignani, 1971; Sone *et al.*, 2000). The leading terms of the resulting equations involve the Euler equations but *not* the Navier-Stokes equations.

- **Chapmann-Enskog expansion**: Here the velocity distribution function is expanded while the macroscopic variables are not. The leading terms of the resulting equation include, in addition to the Euler equation, compressible Navier-Stokes equations, which approximate to incompressible Navier-Stokes equations in the limit of low Knudsen numbers. Higher order defects are reported (Sone *et al.*, 2000). This technique is still the most popular in the lattice Boltzmann community and will be adopted in this study, although it is more complex than the other approaches.

- **Diffusive scaling**: By considering the finite discrete velocity model of the Boltzmann equation and scaling of $\vec{x} \to \vec{x}/\varepsilon$ and $t \to t/\varepsilon^2$, the generalised lattice Boltzmann equation is obtained. Adopting the diffusive scaling and equivalent moment techniques lead directly to the incompressible Navier-Stokes equations (Inamuro *et al.*, 1997; Junk *et al.*, 2002). This way, the accuracy of the lattice Boltzmann equation can be realised as second order in space and first order in time.

[1]The Maxwellian distribution function describes equilibrium states as characterised by no heat flux or stresses other than the isotropic pressure. The Maxwellian is not an exact solution of the Boltzmann equation.

In addition to variational methods (Cercignani, 1983). More details on the solution of the Boltzmann method by means of the Chapmann-Enskog expansion are discussed in the next chapter.

2.3.3 The Hydrodynamic Stress Tensor

For its importance in haemodynamics, it is worth adding a short note about the hydrodynamic stress tensor. If a fluid is viscous, energy is dissipated during its motion due to thermodynamic irreversibility of internal friction and thermal conduction. This will affect the fluid motion. Dissipation of energy is always associated with momentum flux whose density can be described by the symmetric tensor Π_{ik} which gives the ith component of the amount of momentum flowing in unit time through unit area perpendicular to the x_k-axis. The momentum flux density tensor in a viscous fluid of mass density ρ and viscosity η moving with velocity $\vec{v}_i$ takes the form (Landau and Lifshitz, 1975)

$$\Pi_{ik} = \rho v_i v_k - \sigma_{ik} \ , \tag{2.14}$$

where

$$\sigma_{ik} = -p\delta_{ik} + \eta(\frac{\partial v_i}{\partial x_k} + \frac{\partial v_k}{\partial x_i}) = -p\delta_{ik} + 2\eta S_{ik}, \tag{2.15}$$

is the stress tensor for an incompressible fluid, p is the scalar pressure, δ_{ik} denotes the unit tensor, and

$$S_{ik} = \frac{1}{2}(\frac{\partial v_i}{\partial x_k} + \frac{\partial v_k}{\partial x_i}) \tag{2.16}$$

is the strain rate tensor. In order to estimate the stress tensor components of an incompressible fluid, derivatives of the corresponding velocity profiles are conventionally computed from the measured or simulated velocity profiles. However, the lattice Boltzmann methods obtains it directly, as will be seen in the next chapter.

2.4 Specifying Simulation Parameters

In order to simulate flow in a model representing a segment of the cardiovascular system, different input parameters must carefully be selected. Some of them are addressed here.

2.4.1 Flow Rate

As it is patient specific, choosing a flow rate for a study is not an easy task. However, for a new computational method like the lattice Boltzmann model, validation with existing studies is needed. Therefore, we have selected two existing flow rates, recently studied by Moore *et al.* (1994a) and Taylor *et al.* (1998). The two flow rates are similar in shape and their average does not differ. The shape of the flow rate will be shown together with simulation results produced by it.

It is more important to remark that the flow is derived mainly by the pressure gradient and not the pressure itself. It is to be noted also that the Poiseulle formula, which relates the pressure gradient and the flow rate for steady flows, is not valid here (see McDonald, 1974 for valid relationships). In our simulations of realistic geometry, the flow rate waveform is Fourier transformed up-to the 8th harmonics (a constant + 8 sines + 8 cosines). Frequently, we also use the oscillatory components of a pressure gradient derived from a measured aortic pulse to reproduce oscillatory Womersley solution.

2.4.2 Viscosity

In a Newtonian sense, viscosity may be defined as the force required to move a unit area through a fluid to create a unit velocity gradient. Viscosity is also patient dependent and is quite sensitive to many parameters, especially the haematocrit and temperature. The value taken for blood, with a haematocrit of 45%, is acceptably taken as 4.0 cP at 37^o.

2.4.3 Dimensionless Numbers

In fluid flows, each of the pressure, viscous and transient forces dominates under certain conditions. In order to investigate the importance of each of these forces, the equations of motion are written in a dimensionless form, through defining dimensionless parameters. The major dimensionless numbers used in this study are

- **The Reynolds number** which indicates the relative significance of the viscous effect compared to the inertia effect. It is defined as

$$R_e = \frac{UD}{\nu} \tag{2.17}$$

  where D is a characteristic length (such as the tube diameter), $\nu = \frac{\mu}{\rho}$ is the kinematic viscosity and U is the maximum velocity[1]. A large Reynolds number indicates that the convective inertia forces are dominant, while at low Reynolds numbers the shear forces influence the flow. The Reynolds number gives an idea about how far from turbulence we are. Experimentally, three regions can be recognised: laminar flow at low Reynolds numbers ($0 < R_e < 2300$), transient flow ($2300 < R_e < 4000$) and turbulent flow ($R_e > 4000$). For the flow in the circulation, since the geometry is not regular, the characteristic length is defined as $D = 4m = \frac{4A}{C}$ where m is the mean hydraulic depth, A is the cross section of the vessel (the vascular bed) and C is its circumference. Typical Reynolds numbers in the circulation are $R_e = 6000$ in the ascending aorta, $R_e = 1150$ in the abdominal aorta, $R_e = 500$ in the carotid artery, and can be as small as one in the arterioles. It is to be noted that, in the circulation, the Reynolds number should not be used as the only measure of the stability of the flow, as early turbulence,

[1]The Reynolds number may be also defined in terms of the average velocity.

flow mixing, vortex formation and back-flow may occur due to the complex geometry of the arterial system. The best way to describe qualitatively flow in the circulation is to call it "disturbed flow".

- **The Womersley Number** which is the ratio of the transient inertia force to the shear force
$$\alpha = \frac{D}{2}\sqrt{\frac{\omega}{\nu}} \tag{2.18}$$
where $\omega = 2\pi f = \frac{2\pi}{T}$ is the angular frequency, with f the frequency and T the period of oscillation. If α is large, the transient inertia force dominates, while the viscous force dominates at low Womersley numbers. Typical values for the Womersley number in the circulation are $\alpha = 16$ in the abdominal aorta and $\alpha = 9$ in the carotid artery under resting conditions. Under exercise conditions, the Womersley parameter increases as a consequence of the increase in the heart rate.

- **The Strouhal Number** which determines the time available for vortex formation to occur. It is defined as
$$St = \frac{Df}{U} \tag{2.19}$$
which can be rewritten as $St = 2\frac{\alpha^2}{\pi R_e}$. It therefore combines the influence of Reynolds and Womersley numbers. Typical values in the circulations are $St = 0.14$ in the abdominal aorta and $St = 0.10$ in the carotid artery.

- **The Mach Number** which measures the velocity of a fluid relative to the speed of sound in the fluid. It is only important when dealing with compressible fluids. Although it is accepted that blood is an incompressible fluid, the Mach number plays an important role in this study due to the compressible nature of the used lattice Boltzmann solver (see Chapter 7).

There are many other non-dimensional parameters that are useful in fluid mechanics, but in this study we will deal only with the above mentioned.
In the next chapter, we review the numerical method involved and discuss the influence of these parameters on the error behaviour of the method.

Chapter 3

Numerical Method

"It is the People's method."

Li-Shi Luo, Shanghai, Discrete Fluids Conference, 2002.

"Reaching full maturity is just a matter of time and labour, no conceptual hurdles in sight."

Sauro Succi, 2001.

In this chapter, the theory of lattice Boltzmann methods is reviewed. The advantages and drawbacks in comparison with the classical computational fluid dynamics (CFD) techniques are highlighted. The accuracy and performance of the method are briefly discussed.

3.1 Introduction

For many years to come, a necessity for efficient and robust numerical CFD solvers will be demanded by computational scientists who work at the edge of available computer power. It has been realised by many authors that transport phenomena can be studied from a kinetic theory point of view (e.g. Caflisch, 1983; Ramaswamy, 2001), where an alternative description is given through the Boltzmann equation for the density function $f(t, \vec{x}, \vec{\xi})$ for particles of velocity $\vec{\xi}$ at point $\vec{x}$ and time t. The Boltzmann equation is derived from Newton's laws of motion in the limit of a large number of particles. Although the Boltzmann equation was mainly developed for ideal gases, nevertheless, in the limit of small mean free path between molecular collisions, a gas may be considered as a continuum fluid[1]. The main advantage over solving the Boltzmann equation instead of the Navier-Stokes equations is that Navier-Stokes equations are not adequate to model flows in which the local Knudsen number lies in the continuum regime, since they are based on small deviation from local thermodynamic equilibrium, while the capability of the Boltzmann solution to

[1]The number of gas molecules in a cubic centimetre is given by Loschmidt number $N = p/kT$.

capture complex fluid behaviour even near shocks is a fact (see Cerignani (1975) for details and Pareschi and Russo (2001) for recent developments). After the link between the Boltzmann equation and hydrodynamics was well established (Cercignani 1971; Caflisch, 1983), a need for efficient solvers was raised, since the Boltzmann equation is hard to solve. Perturbation techniques such as the Chapmann-Enskog and Hilbert techniques were the common numerical solvers (Cercignani, 1971), with the solutions obtained as asymptotes to the Boltzmann equation, after simplifying the collision operator.

Soon after Frisch, Hasslacher and Pomeau (1986) introduced the lattice gas cellular automata (LGCA), an automata that is capable of capturing complex fluid nature by just obeying conservation laws, a few shortcomings of LGCA were recognised and intensively investigated. Those are, among others, the lack of Galilean invariance, statistical noise[1], low Reynolds number (high viscosity) and exponential complexity of the collision operator (Succi, 2001; Rothman and Zaleski, 1997; Chopard and Droz, 1998). The earliest lattice Boltzmann method was introduced by McNamara and Zanetti (1988) and Higuera and Jimenez (1989) to circumvent these shortcomings. Although the idea was simply to replace the Boolean LGCA occupation numbers n_i with ensemble-averaged populations $f_i =< n_i >$, the system became capable to capture many features in the evolving nature, but complex enough, due to the complexity of non-equilibrium statistical mechanics, needed to understand it. In the next section a brief review on the hydrodynamics of the lattice Boltzmann method will be presented for completeness. More details on the theory behind the lattice Boltzmann method and the developments in that direction are available in literature (e.g. Qian *et al.*, 1992; Succi *et al.*, 1993; Qian, 1993; Flekkϕy and Herrmann, 1993; Chopard and Droz, 2001; Succi, 2001) and interested readers may consult the last two books or the proceedings of the 9th (2000), the 10th (2001) International Conferences on Discrete Simulation of Fluid Dynamics, the DFG and Konwihr Workshop on Lattice Boltzmann methods (LSTM Erlangen, 2001) and the 11th International Conference on Discrete Simulation of Fluid Dynamics and Condensed Matter Physics (Fudan University, 2002). There exist a number of lattice Boltzmann models, based on more complex collision operators (known as Generalised LBE models) than the BGK approximation. As a first step, however, we believe that the lattice Boltzmann BGK (simply the lattice BGK) model is quite adequate for the recent study that deals with Newtonian fluids under laminar regimes. Use of Generalised models is recommended in future work.

[1] An insight can be gained from these 'physically sound' fluctuations. For details see Rivet and Boon (2001).

3.2 The Lattice Boltzmann Model

Although the lattice Boltzmann model historically evolved from the lattice gas automata, it was soon realised as a special discretisation of the Boltzmann equation

$$\frac{\partial f}{\partial t} + \vec{\xi} \cdot \vec{\nabla} f = -J_i(f_i) \tag{3.1}$$

with the collision term $-J_i(f_i)$ later simplified by Bhatnagar Groos and Krook (BGK) in 1954
to describes the evolution of the single particle distribution function $f \equiv f(x, \vec{\xi}, t)$ for particles that move with a microscopic velocity $\vec{\xi}$, collide with collision relaxation time λ till they relax to the Maxwell-Boltzmann equilibrium distribution function g. Equation 3.1 then becomes

$$\frac{\partial f}{\partial t} + \vec{\xi} \cdot \vec{\nabla} f = -\frac{1}{\lambda}(f - g), \tag{3.2}$$

A numeric solution for f is obtained by discretising Eq. (3.2) in the velocity space $\vec{\xi}$ using a finite set of velocities $\vec{e}_i$, $i = 0, 1, ..., N$, without violating the conservation laws of the hydrodynamic moments. This gives

$$\frac{\partial f_i}{\partial t} + \vec{e}_i \cdot \vec{\nabla} f_i = -\frac{1}{\lambda}\left(f_i - f_i^{(eq)}\right). \tag{3.3}$$

where $f_i(\vec{x},\ t) \equiv f_i(\vec{x},\ \vec{e}_i,\ t)$ and $f_i^{(eq)} = f_i^{(0)}(\vec{x},\ \vec{e}_i,\ t)$ are the distribution function and the equilibrium distribution function of $\vec{e}_i$, respectively. The equilibrium distribution function, obtained by Taylor expansion of the Maxwellian distribution, usually takes the following form in the limit of low Mach number

$$f_i^{(eq)} = \rho w_i \left(1 + \frac{3}{v^2}\vec{e}_i \cdot \vec{u} + \frac{9}{2v^4}(\vec{e}_i \cdot \vec{u})^2 - \frac{3}{2v^2}\vec{u} \cdot \vec{u}\right), \tag{3.4}$$

where w_i is a weighting factor, $v = \delta_x/\delta_t$ is the lattice speed, and δ_x and δ_t are the lattice spacing and the time step, respectively. The values of the weighting factor and the discrete velocities depend on the used lattice Boltzmann model (LBM) and can be found in the literature (see e.g. Mei *et al.*, 2000). In this chapter, without loss of generalisation, we use the D2Q9 model (Chen and Doolen, 1998) and and its incompressible candidate D2Q9i, which has three types of particles on each node; a rest particle, four particles moving along x and y principal directions with speeds $|\vec{e}_i| = 1$, and four particles moving along diagonal directions with speeds $|\vec{e}_i| = \sqrt{2}$. The hydrodynamic density, ρ, and the macroscopic velocity, $\vec{u}$, are determined in terms of the particle distribution functions from

$$\rho = \sum_i f_i = \sum_i f_i^{(eq)} \tag{3.5}$$

and

$$\rho\ \vec{u} = \sum_i \vec{e}_i\ f_i\ =\ \sum_i \vec{e}_i\ f_i^{(eq)}\ . \tag{3.6}$$

Equation (3.2) is then discretised in space and time into the well-known lattice BGK equation

$$f_i(\vec{x}+\vec{e}_i\ \delta_t,\ t+\delta_t)\ -\ f_i(\vec{x},\ t) = -\frac{1}{\tau}[f_i(\vec{x},\ t)\ -\ f_i^{(0)}(\vec{x},\ t)] \tag{3.7}$$

where $\tau = \frac{\lambda}{\delta_t}$ is the dimensionless relaxation time. Taylor expansion of Eq. (3.7) up to $O(\delta_t^2)$ and application of the multi-scale Chapmann-Enskog technique (e.g. Chopard and Droz, 1998) by expanding f_i about $f_i^{(0)}$ and introducing two time scales[1] $t_0 = t$ and $t_1 = t\delta_t$ (assuming that $\lambda \sim \delta_t$), we can write the evolution equation as

$$(\partial t_0\ +\ \vec{e}_i \cdot \vec{\nabla}) f_i^{(0)}\ =\ -\frac{1}{\tau} f_i^{(1)} \tag{3.8}$$

to the first order, and

$$\partial t_1 f_i^{(0)} + (\partial t_0 + \vec{e}_i \cdot \vec{\nabla})(1 - \frac{1}{2\tau}) f_i^{(1)} = -\frac{1}{\tau} f_i^{(2)} \tag{3.9}$$

to the second order. From the last two equations, the macroscopic density, ρ, and velocity, $\vec{u}$, can be obtained to the first and the second order in δ_t by taking the sum of Eq.(3.8) over all directions and velocities to yield the continuity equation

$$\partial t_0 \rho + \vec{\nabla} \cdot (\rho \vec{u}) = 0 \tag{3.10}$$

to the first order. Also, by multiplying Eq.(3.10) by $\vec{e}_i$ and taking the summation over all directions and velocities, we reach

$$\partial t_0 (\rho \vec{u}) + \vec{\nabla} \cdot \Pi^{(0)} = 0 \tag{3.11}$$

where

$$\Pi_{\alpha\beta}^{(0)}\ =\ \rho\ c_s^2 \delta_{\alpha\beta} + \rho u_\alpha u_\beta \tag{3.12}$$

is the momentum flux tensor, to the first approximation. Here, c_s is the speed of sound which is given by

$$c_s = \sqrt{C}\ v \tag{3.13}$$

where C is a geometric parameter which depends on the used lattice Boltzmann model. For the D2Q9 and D3Q19 models, $C = 1/3$. Similarly, from Eq.(3.9) we get

$$\partial t_1 \rho = 0, \tag{3.14}$$

and

$$\partial t_1\ (\rho\ \vec{u}) + \vec{\nabla} \cdot \left(1 - \frac{1}{2\tau}\right) \Pi^{(1)} = 0, \tag{3.15}$$

[1]Using the full Taylor expansion of the Boltzmann equation does not need two time scales. A single time scale approach is adopted by Holdych *et al.* (2002).

where

$$\Pi^{(1)}_{\alpha\beta} = \sum_i f_i^{(1)} \vec{e}_{i\alpha} \vec{e}_{i\beta}$$
$$= \delta_t v^2 \tau \left[(\frac{c_s^2}{v^2} - C)\delta_{\alpha\beta} \vec{\nabla} \cdot (\rho \vec{u}) - C(\partial_\beta \rho u_\alpha + \partial_\alpha \rho u_\beta) \right] \tag{3.16}$$

is the momentum flux tensor, to the second order approximation (e.g. Chopard and Droz, 1998). For incompressible fluids, $\vec{\nabla} \cdot (\rho \vec{u}) = 0$, and therefore Eq. (3.16) becomes

$$\Pi^{(1)}_{\alpha\beta} \; = \; \rho \delta_t v^2 \tau \left[- \, C \, (\partial_\beta \, u_\alpha + \partial_\alpha \, u_\beta) \right] \tag{3.17}$$

or, equivalently,

$$\Pi^{(1)}_{\alpha\beta} = - \; 2\rho \; \delta_t \; v^2 \; \tau \, C \, S_{\alpha\beta}. \tag{3.18}$$

The strain rate tensor is therefore

$$S_{\alpha\beta} \; = \; - \frac{1}{2 \, C \, \delta_t \, v^2 \, \tau \, \rho} \, \Pi^{(1)}_{\alpha\beta}. \tag{3.19}$$

The Navier-Stokes equation can be derived from Eq. (3.7):

$$\partial_t \, \vec{u} \; + \; (\vec{u} \; \cdot \; \vec{\nabla}) \vec{u} = - \frac{1}{\rho} \vec{\nabla} \; p + \nu \; \vec{\nabla}^2 \; \vec{u} \tag{3.20}$$

where $p = \rho c_s^2$ is the scalar pressure and ν is the kinematic viscosity of the lattice Boltzmann model, given by

$$\nu = C \, v^2 \; \delta_t \; (\tau - \frac{1}{2}) \tag{3.21}$$

Substituting these formulas for the pressure and viscosity into Eq. (2.15) yields

$$\sigma_{\alpha\beta} \; = \; - \rho c_s^2 \; \delta_{\alpha\beta} \; - \; \left(1 - \frac{1}{2\tau} \right) \sum_{i=0} f_i^{(1)} e_{i\alpha} \; e_{i\beta}. \tag{3.22}$$

This equation gives the stress tensor components in lattice units and is valid for all of the known lattice BGK models. We emphasise that the quantity $f_i^{(1)} e_{i\alpha} \; e_{i\beta}$ is usually computed during the collision process. Therefore, the stress tensor components can be obtained without almost any additional computational cost. This significantly enhances the lattice Boltzmann BGK method, as other CFD methods are more elaborate and estimate the stress tensor components from the simulated velocity field. As this approximation is of second order in the Knudsen number, the stress tensor components are also accurate up to the second order in the Knudsen number.

3.3 A Priori Error Analysis

There have been many theoretical investigations on the analysis of the lattice Boltzmann method under study. Realisation of the error behaviour depends on the way it is analysed. However, the method is in general of second order in space and first order in time. The following paragraphs briefly attempt to analyse the lattice Boltzmann equation.

3.3.1 Analytical Solutions

Analytical solutions for the lattice Boltzmann equation have been obtained for some flows in the context of simple and exact boundary conditions. Luo *et al.* (1991) solved the generalised hydrodynamics of two-dimensional lattice-gas automata in the linearised Boltzmann approximation and derived the dependence of the transport coefficients upon wave number. Cornubert *et al.* (1991) analytically solved the Kramers problem[1] and classified the boundary conditions into two categories, producing isotropic and anisotropic Knudsen layers. Ginzbourg and Adler (1995) computed first and second order deviations of f_i from their equilibrium. Machine accuracy was obtained by Noble *et al.*(1995) for the plain Poiseuille flow with lattice BGK. This was later analysed by Zou *et al.* (1995), He *et al.* (1997) and Luo (1997) who analytically solved the lattice BGK for the Poiseulle and the Couette flow (see next chapter). Recently, kinetic theory approach to the lattice Boltzmann methods has flourished (He and Luo, 1997b and 1997c; Abe, 1997; Shan and He, 1998). These studies have remarked that the lattice Boltzmann schemes are directly connected to the mescoscopic Boltzmann equation. A need to link lattice Boltzmann models to LGA is no more needed, except for historical reasons. Although studies on formal error analysis of the lattice Boltzmann methods for unsteady flows are quite rate (He and Luo, 1997a; Artoli *et al.*, 2001; Holdych *et al.*, 2002), additional conclusions may be drawn from studies on steady flows, especially those by Holdych *et al.*, (2002). In the last-named reference it was shown that the error varies with the product of Δx^2 and polynomials in the relaxation time τ that multiply high order derivatives and suggested the roots of these polynomials as optimum values for τ. The analysis is performed by inserting a Taylor series expansion of the equilibrium distribution f_i^{eq} into the lattice Boltzmann equation. The compressibility error C.E. and the momentum error M.E. were then computed for 2D models. Although a lot has been done in order to understand the error behaviour in three dimensions, the most popular way is via performing benchmark simulations, as it is very difficult to isolate compressibility errors, momentum errors and discretisation errors in three dimensional Cartesian grids. We will study both approaches (see Chapter 4 and Chapter 5).

[1] A standard problem in kinetic theory caused by the modification of the bulk equilibrium by an obstacle.

3.4 Accuracy of the Lattice Boltzmann Equation

In numerical solvers, differential operators are usually replaced with corresponding finite difference discretisations. The accuracy of a numerical method is said to be of degree n (or n^{th} order accurate), where n is the degree of the polynomial after which the error vanishes (Succi, 2001).
It can be shown that the lattice Boltzmann equation is equivalent to a second order discretisation of the Navier-Stokes equation if the viscosity is defined by Eq. 3.21 and the pressure is defined as $p = \rho c_s^2$. Therefore, the hydrodynamic quantities can be computed with the lattice Boltzmann equation up to second order accuracy in both space and time[1] (Succi, 2001). This accuracy may be enhanced by considering influence of more neighbours through adding further discrete speeds (Succi, 2001). On the other hand, the accuracy of LBE is commonly degraded by four major sources. These are the boundary conditions, the compressibility error, the discretisation error and the momentum error. These errors will not be discussed here in details unless necessary, depending on each benchmark case. Nevertheless, a short briefing would complete the idea of the behaviour of this numerical scheme.

3.4.1 Discretisation Errors

Although Cartesian grids are quite comfortable to work with in parallel computing, they produce large errors when representing fluid boundaries of non-uniform geometry such as vessel structures. Three ways to deal with discretisation errors are to consider realistic models by the aid of scanning techniques (such as magnetic resonance and Computed Tomography), to use curved boundary conditions or finite volume-like LBMs, and to use fine grids at regions of interest. The first treatment is limited by scanner resolution and the other two techniques exploit computational power. Nevertheless, even with a very coarse grid, the lattice Boltzmann solvers return acceptable accuracy, far better than the required engineering accuracy, as will be seen in the next few chapters.

3.4.2 Boundary Conditions

As mentioned above, Kramer's problem arises when the fluid meets an obstacle. Therefore, accurate boundary conditions are needed. The role of a boundary condition in lattice Boltzmann schemes is to give the evolving fluid information from the obstacle which is normally of different physical characteristics (solid, another fluid, gas, etc.). This information is transported by particle distributions streaming from the obstacle into the fluid bulk. As they are unknown (due to the fact that the number of specifying equations is less than the number of the unknowns), heuristic assumptions

[1]First order accuracy in time may be theoretically argued. The lattice Boltzmann equation is a first order in time discretisation of the original Boltzmann equation. I am grateful to Li-Shi Luo who explained to me the potential for confusion in a short remark "It depends on the way you look at it."

are needed to close the system at the boundary. These heuristics depend on the nature of the boundary, whether it is an inlet, outlet or a containing surface. Since this issue is sophisticated, and since the boundary conditions are numerous, only the used boundary conditions will be discussed in association with the models implementing them. For an introduction on Boundary conditions the reader is referred to a chapter written by Succi (2001) and to cited literature in this study.

3.4.3 Compressibility Errors

The lattice Boltzmann method is a compressible discretisation of the Boltzmann equation. Under the fluid dynamic limit, the incompressible NS equations can be derived. This makes the compressibility effect an undesired error source when dealing with incompressible fluids. To correct this, a few incompressible models have been proposed (Zou *et al.*, 1995; He and Luo, 1997; Guo *et al.*, 2000; Guo and Zhao, 2002), most of them are for steady flows. Although some can be used for unsteady flow, they may either complicate the model or hardly enhance the overall error unless more restrictions are fed into the system. Moreover, three dimensional incompressible lattice BGK models are not well tested in the literature. In this study, the standard lattice BGK is used for the sake of simplicity. The compressibility effects are reduced by inventing a new technique based on reducing the Mach number on the fly (see Chapter 7).

3.4.4 Momentum Error

This is the error that appears in the momentum equation and is usually a function of the dimensionless hydrodynamic numbers. It was shown by Holdych *et al.*(2002) that if the viscosity is considered as the independent parameter, this error is a multiple function of Δx^2 and polynomials in the relaxation parameter τ, which include the Reynolds number and the viscosity. The major terms suggest that the error increases linear with the Reynolds number. The τ- dependent polynomials suggests some values for τ at which the error is minimum (solutions for the polynomials). It was shown in the same study that the momentum error is inversely proportional to the Reynolds number if Δt is seen as the independent variable in the error analysis[1].

3.5 Summary

Many solution methods have been developed to solve various flow problems on High Performance Computers, and several new techniques were used to enhance their performance. It may be very difficult to compare between these methods in accuracy and performance, and we can hardly draw constructive conclusions from such comparisons. However, it would be possible to justify why some numerical solvers such as the lattice Boltzmann schemes are superior to other ones in certain cases.

[1] We need to remember that $\Delta x = c\Delta t$.

An elegant flow solver, nevertheless, is required to satisfy many desired features, the most important of which are accuracy and performance. In terms of accuracy, lattice Boltzmann is known to be of second order in space and time. The stress tensor is obtained from the non-equilibrium parts of the distribution functions without any need to approximate the shear-rate. This last featureis of help to researchers in haemodynamics since the shear stress is believed to play a major role in the development of arterial diseases.
For its orthogonal (Cartesian) grid, grid generation in lattice Boltzmann methods is negligible when compared to that in body fitted grid methods. Although Cartesian grid generation is coarse, many near-obstacle features are captured with comparable accuracy to body fitted grids.
The Cartesian grid is an advantage when solving large scale applications in parallel computing environment, as, for instance, load balancing can be satisfactorily achieved. The lattice Boltzmann is also an adaptive method (see next chapter). The explicit nature of time discretisation is another feature that is useful for simulating time-dependent flows.
On the other hand, the lattice BGK is quasi-compressible, thermodynamically inconsistent, very difficult to stabilise at high Reynolds numbers and may harldly involve fluid-structure interaction. So far, many achievements have been made to enhance the method. Many of these drawbacks can be eliminated with the use of the generalised lattice Boltzmann equation (GLBE) (d'Humieres *et al.*, 1992; D'Humeres *et al.*, 2002), but at a cost of 15% in performance (D'Humeres *et al.*, 2002). The method has also been developed to model fluid turbulence (see e. g. Chen et al., 2003 for higlights of benefits over the NS solvers).
Although only recently developed, this study proves that the method is useful in computational haemodynamics. Bearing in mind the hydrodynamic constraints in this study, the lattice-BGK is adequate enough in dealing with simplified blood flow models such as Newtonian flow in the aorta.
In the next chapter, simple 2D steady flow benchmarks are used to test the accuracy of the method while Chapter 5 deals with pulsatile flows. Computational issues are discussed afterwards.

Chapter 4

Error Analysis for Steady Flow Simulations

In this chapter we perform three initial tests for the lattice Boltzmann method with BGK approximation. In all cases, steady flow simulations are investigated. The first two categories present and discuss results obtained from 2D simulations of the channel flow and the Couette flow benchmarks and study the error behaviour in velocity and shear stress. We study different boundary conditions and compare them for the two benchmarks. Machine accuracy is reproduced for the channel flow under certain conditions. The third category discusses simulation results performed on a symmetric bifurcation in a range of Reynolds numbers. The obtained simulation results are compared to a finite volume simulation for the same geometry under the same conditions, all showing excellent agreement.

4.1 Channel Flow

As a simple benchmark, channel flow between two fixed parallel plates separated by a distance h is investigated. If the flow is in the positive x-direction, the analytical solution for the channel flow is

$$u_x = \frac{4U_c}{h^2} y(h-y) \tag{4.1}$$

where y is the distance from the lower wall, $U_c = -\frac{1}{2\eta}\frac{dp}{dx} \equiv \frac{h^2 G}{8\rho\nu}$ is the centreline velocity derived by a pressure drop per unit length, dp/dx, or a body force G, and $\eta = \rho\nu$ is the fluid viscosity. The stress tensor components obtained by using Eq. (3.22) are to be compared with those defined by Eq.(2.15). The stress tensor components defined by Eq.(2.15) yield

$$\sigma_{xy} = \eta\frac{\partial u_x}{\partial y} = \frac{4\eta U_c}{h^2}(h-2y), \tag{4.2}$$

$$\sigma_{xx} = -p(x) \tag{4.3}$$

which is linear along the channel, and

$$\sigma_{yy} = -p(y) \tag{4.4}$$

which is constant across the channel. To verify our numerical model, we have carried out a number of simulations for the channel flow at $R_e = 10$ and $R_e = 90$. The system size $N_x \times N_y$ ranges from 20×10 lattice points for the coarsest grid to 100×50 for the finest grid. The system is initialised with zero velocity. The algorithm uses double precision to obtain the velocity profiles, the pressure and the stress tensor components, all being computed over the whole grid after the transients have died out. We have implemented two types of boundary conditions: the bounce-back rule for the walls and periodic boundary conditions in the horizontal direction, and the velocity boundary conditions (VBC) proposed by Zou and He (1997). For Poiseuille flow, since the centreline velocity is given by $U = \frac{h^2 G}{8\rho\nu} = \frac{R_e \nu}{h}$ (He et al., 1997), a uniform body force $G = 8\rho R_e \nu^2 / h^3$ along the x-direction is applied. The amplitude of this body force is changed with the grid resolution while keeping fixed both the Reynolds and the Mach numbers. He *et al.* (1997) analytically proved that the LBM has a solution for the velocity u_x for the channel flow, given by

$$u_x = \frac{4U_c}{n^2} y(n-y) + U_s, \tag{4.5}$$

where U_s is the slip velocity at the boundary. In the case of the bounce-back on the links, they claimed that the slip velocity is given by

$$U_s = \frac{2U_c}{3n^2}[(2\tau - 1)(4\tau - 3) - 3n] \tag{4.6}$$

where U_c is the centreline velocity without slips at the boundaries, $h = n\delta_x$ the width of the channel and n the number of nodes representing the width of the channel. The analytical solution for the shear stress in this case therefore becomes

$$\sigma_{xy} = \eta \frac{4U_c}{n^2}(n - 2y). \tag{4.7}$$

This equation is equal to the analytical solution of the shear stress for the channel flow (see Eq. (4.2)). This shows that with the bounce-back rule, the shear stress is not affected by the slip velocity, and therefore, it can be computed up to machine accuracy. For the shear stress, we have observed errors of the order of 10^{-15}, which is of the order of the roundoff error.

On the other hand, we have used the VBC proposed by Zou and He (1997) to implement a parabolic velocity profile at the inlet, a constant density at the outlet, and no slip conditions at the upper and the lower boundaries. On the boundaries, values for the distribution functions are computed at each time step from the imposed velocity or density and the known distribution functions streaming from the fluid to the boundary. The bounce-back scheme is assumed to be valid for the non-equilibrium

part of the particle distributions normal to the boundary. The densities at the corner points are assigned values from their nearest neighbouring fluid nodes. With VBC, the system is initialised with zero velocity components.

As mentioned before, the Kramer problem degrades the analytical solution near the boundary and the accuracy depends on the used boundary condition assigned at the obstacle. The simulation results are in good agreement with the expected theory when VBC is used, but obtaining machine accuracy has not been possible with the standard lattice BGK model. This is due to the influence of compressibility errors. We will present the error analysis for the shear stress in the channel flow together with the error analysis for the shear stress in the Couette flow problem in section 4.3.

4.2 Plane Couette Flow

We have selected this benchmark as a simple example of a two-component flow which has an exact analytical solution but is not an exact solution of the lattice BGK equations (He *et al.*, 1997). For the Couette flow with vertical injection at the upper and the lower boundaries, we consider the lower wall to be fixed while the upper wall moves along the horizontal direction with velocity u_n. The vertical injection speed is assumed to be $u_y = constant$. The two plates are separated a distance h. Since the lower wall is fixed, the analytical solution for the horizontal fluid velocity is (He *et al.*, 1997)

$$u_x = \frac{exp\left(\frac{R_e}{h}y\right) - 1}{exp(R_e) - 1} u_n \tag{4.8}$$

where the Reynolds number is defined as $R_e = u_y h/\nu$. Consequently, the analytical solution for the shear stress component is

$$\sigma_{xy} = A\ exp\left(\frac{R_e}{h}y\right), \tag{4.9}$$

where $A = \frac{\eta u_n R_e}{h(exp(R_e)-1)}$ is the value of the shear stress at the lower boundary. The other two components of the stress tensor are

$$\sigma_{xx} = -p(x) \tag{4.10}$$

which is constant along the channel when using periodic boundary conditions, and

$$\sigma_{yy} = -p(y) \tag{4.11}$$

which is also constant across the channel.

The analytical lattice BGK solution for the Couette flow with injection is (He *et al.*, 1997)

$$u_x = \frac{\lambda^j - 1}{\lambda^n - 1}(u_n + U_s^n) + \frac{\lambda^n - \lambda^j}{\lambda^n - 1}(u_0 + U_s^0) \tag{4.12}$$

where $\lambda = (2+R)/(2-R)$ with $R = u_y\delta_x/\nu$, u_0 is the velocity of the bottom wall ($u_0 = 0$ in our case), U_s^n and U_s^0 are the slip velocities at the top and the bottom walls, respectively. This solution is a second order approximation for the Navier-Stokes analytical solution given by Eq. (4.8). If the shear stress is computed from the derivative of this velocity, it yields

$$\sigma_{xy} = B\lambda^j \tag{4.13}$$

where

$$B = \frac{\eta ln(\lambda)}{\lambda^n - 1}\left[(u_n + u_0) - (U_s^0 + U_s^n)\right] \tag{4.14}$$

In our case, as the bottom wall is fixed, while using the no-slip VBC are used, B will have the simple form

$$B = \frac{\eta ln(\lambda)}{\lambda^n - 1}u_n \tag{4.15}$$

which is equal to A in Eq. (4.9) when we replace the Reynolds number R_e with $R_e^* = n\ ln(\lambda)$. The difference between the two Reynolds numbers reflects the finite difference errors.

The first order behaviour has also been studied in the case of the Couette flow problem, by assigning the equilibrium distributions to the distribution functions at the walls and periodic boundaries in the x-direction. With the equilibrium distribution boundary conditions, the slip velocities have the analytical lattice BGK forms (He *et al.*, 1997)

$$U_s^0 = -\frac{(\tau-1)(\lambda-1)(\tau\lambda-\tau-\lambda)}{\lambda^n(\tau\lambda-\tau+1)+\lambda(\tau\lambda-\tau-\lambda)}(u_n-u_0), \tag{4.16}$$

and

$$U_s^n = \frac{(\tau-1)(\lambda-1)\lambda^n(\tau\lambda-\tau+1)}{\lambda^n(\tau\lambda-\tau+1)+\lambda(\tau\lambda-\tau-\lambda)}(u_n-u_0), \tag{4.17}$$

which are of first order in space. The initial value of the shear stress in this case can be obtained by substituting Eqs. (4.16) and (4.17) into Eq. (4.15). It can be proved that as $\delta_x \to 0$, the slip values of the shear stress at both walls are proportional to $1/n$.

Hence, we have three formulae for computing the shear stress:

- from the analytical Navier-Stokes solution, as given by Eq. (4.9),
- from the analytical lattice BGK solution, as given by Eq. (4.13), and
- directly from the non-equilibrium parts of the distribution functions, as given by Eq. (3.22).

To compare these methods, we have carried out numerical simulations for this Couette flow problem at $R_e = 10$. The size and the initial state of the system are the same as those described previously for the channel flow problem. For the boundaries, we have first implemented the VBC for the upper and the lower boundaries and periodic

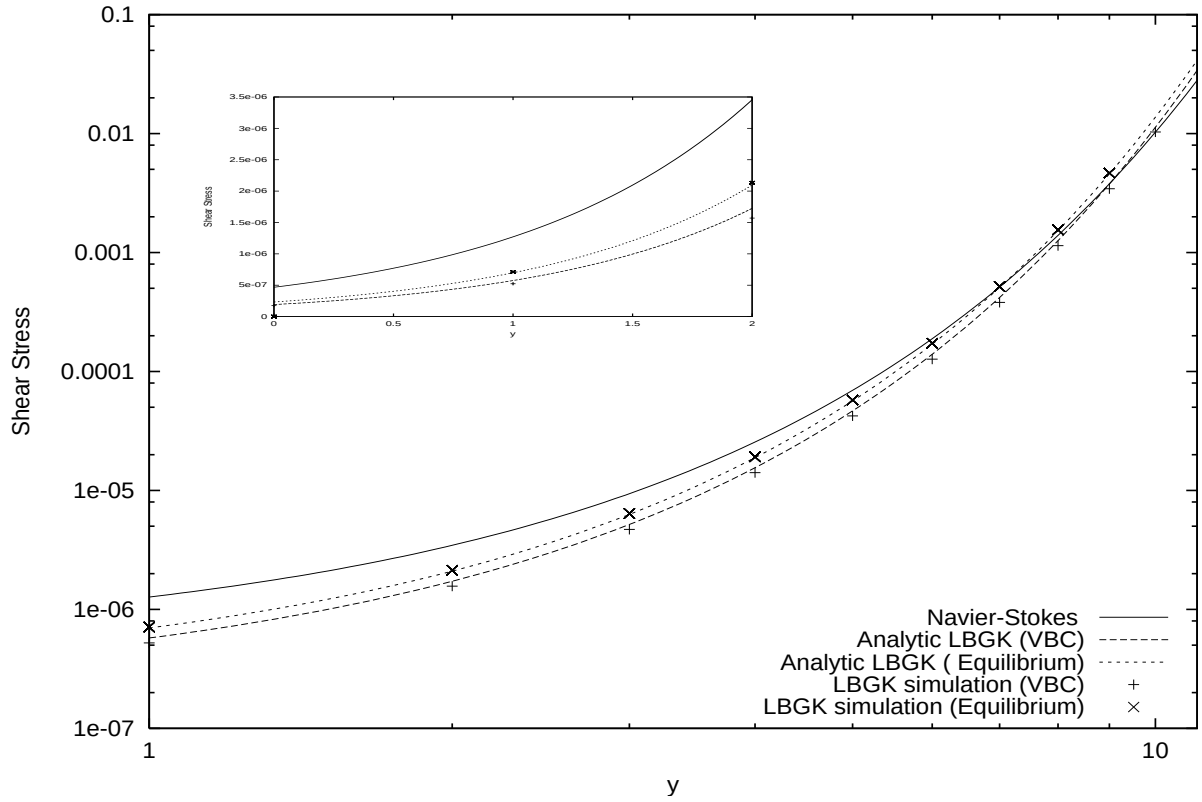

Figure 4.1: Shear stress computed from the distribution functions (Eq. (3.22)) compared to that computed from the Navier-Stokes solution (Eq. 4.9) and the derived lattice BGK analytical solutions (Eq. 4.13), using VBC and equilibrium distributions, for $R_e = 10$, in the Couette flow benchmark. Values at $y = 0$ are zoomed inside the figure.

boundaries in the horizontal directions. We have also performed a similar simulation for the Couette flow problem using the equilibrium distributions at the boundaries and periodic boundaries in the x-direction. In each case, good agreements with analytical solutions have been obtained, as can be seen from Fig. 4.1, from which we also notice that the equilibrium distributions yield zero values for the shear stress at the boundaries. This is attributed to the fact that $f_i^{(1)} = 0$, and may be maintained by using Eq. (4.13) or extrapolating from the nearest points. We are interested in the equilibrium distributions because they are easy to use for non-uniform inlet and outlet boundaries (see Chapter 8).

4.3 Error Analysis

Although these two benchmarks have been classically investigated by many authors, here we find it necessary to test the accuracy of the used algorithmand investigate

the accuracy of the stress tensor for these simple benchmarks.
We have carried out a number of simulations with different grid sizes at constant values of the relaxation parameter τ at various Reynolds numbers in the range 1–100 for both the channel flow and the Couette flow with injection. The measured error Ev in the velocity is calculated using the formula

$$Ev = \frac{\sum_{x,y} |u_x - u_x^*|}{\sum_{x,y} |u_x^*|} \tag{4.18}$$

where u_x^* is the analytical solution for the velocity at the given grid location and the summations are taken over the whole grid. Similarly, the error Es in the shear stress component is computed from

$$Es = \frac{\sum_{x,y} |\sigma_{xy} - \sigma_{xy}^*|}{\sum_{x,y} |\sigma_{xy}^*|} \tag{4.19}$$

where σ_{xy}^* is the analytical solution for the shear stress component at the given grid location. While using the VBC, the error behaviour for the channel flow and the Couette flow with injection at the boundaries is shown in Fig. 4.2 for $R_e = 10$. For $R_e = 10$, the slopes of the lines are -2.0 for the channel flow and -1.8 for the Couette flow with injection. Similar results have been obtained for $R_e = 90$, where the slopes are -2.0 for the channel flow and -1.7 for the Couette flow with injection. From this figure, we observe that the error in the shear stress behaves the same as the error in the velocity fields, which is a second order error for the VBC. Moreover, the error in the shear stress is approximately of the same magnitude as that of the velocity, as predicted from theory. However, we have obtained machine accuracy with the incompressible D2Q9i model proposed by Zou *et al.*(1995).

Since the Reynolds number is a critical parameter in the case of the Couette flow with injection, we have carried out a number of simulations with $R_e = 6$, $R_e = 30$ and $R_e = 60$ at $\tau = 1$ for this benchmark. The results are shown in Fig. 4.3. For the shear stress, the slopes are approximately -1.9 for the three Reynolds numbers. However, the order of the error increases with the Reynolds number and more grid refinement is needed to recover the same accuracy. For $R_e = 30$ and $R_e = 60$, the grid is respectively 25 and 100 times larger than the case for $R_e = 6$.

Using the bounce-back rule for the channel flow, we have observed errors of the order of 10^{-15} for the stress tensor while a first order error has been obtained in the velocity. The error in the velocity in this case is attributed to the slip velocity which can be subtracted to yield the same order as the shear stress. This shows that, with the simple bounce-back rule, the shear stress yields perfect agreement with the analytical solutions. This result has a direct impact on haemodynamics, as will be realised later.

For the Couette flow benchmark, while assigning the distribution functions their corresponding equilibrium distributions at the walls and periodic boundaries in the x-direction, the error in the shear stress is of first order. However, as shown in Fig. 4.1,

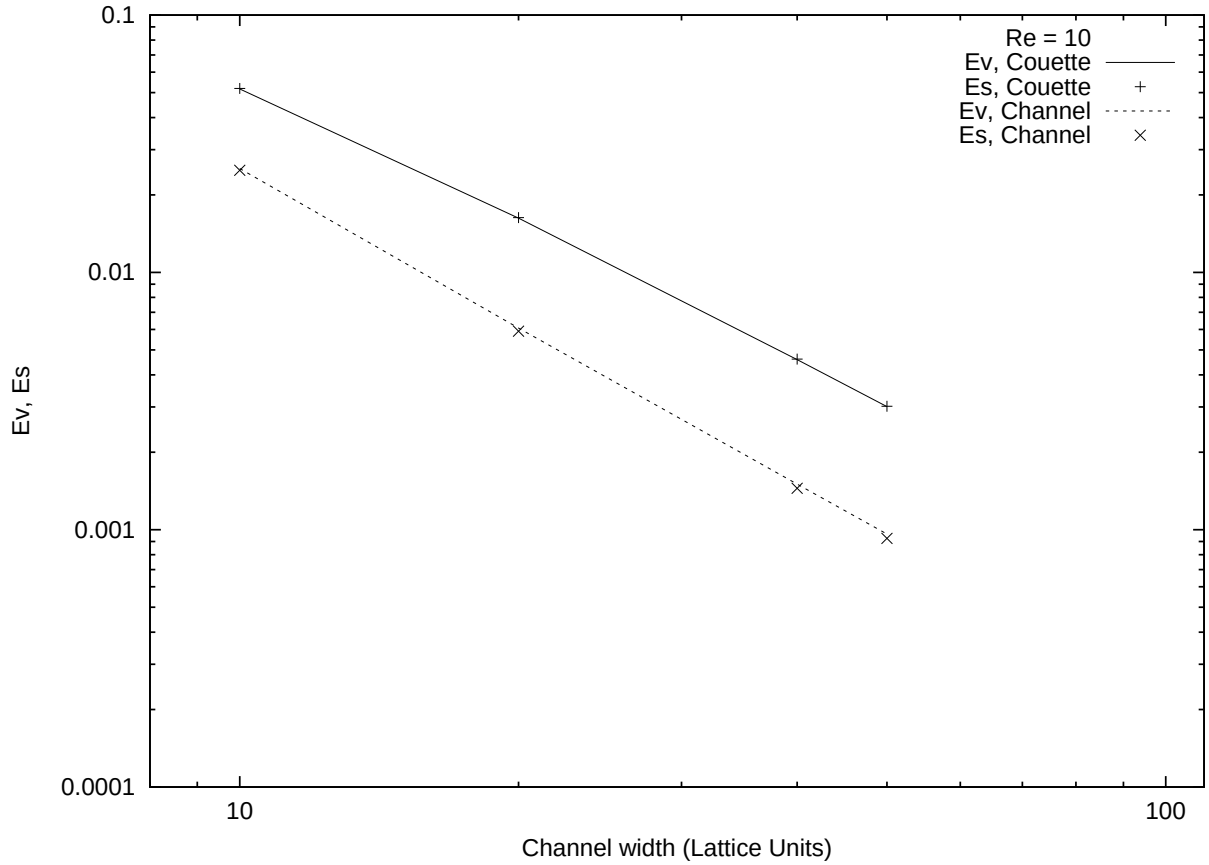

Figure 4.2: Relative errors in v_x and σ_{xy}, using the LBM with the velocity boundary conditions for $R_e = 10$, in the channel and the Couette flows.

the shear stress obtained by using equilibrium distributions is not different from the shear stress computed from the derivative of the analytical lattice BGK solution for the velocity, except at the boundary nodes where the theory fails. It is also clear from the figure that with the equilibrium distributions, the shear stress inside the flow domain has values closer to the shear stress derived from the analytical Navier-Stokes solution for the velocity than values obtained by the second order VBC. This may be attributed to the fact that VBC are derived by assuming that the bounce-back is valid for the non-equilibrium parts of the distribution function, from which the shear stress is computed.

4.4 Convergence Behaviour

As assumed by the Boltzmann equation, approach towards equilibrium shall be guaranteed when the Boltzmann equation is correctly solved by any means. Figure 4.4 shows the error magnitude as the simulation creeps towards its Maxwellian equilibrium with different lattice sizes. It is to be noticed that, at the beginning, coarse grids may be more accurate than finer ones. The reason for this is that the number

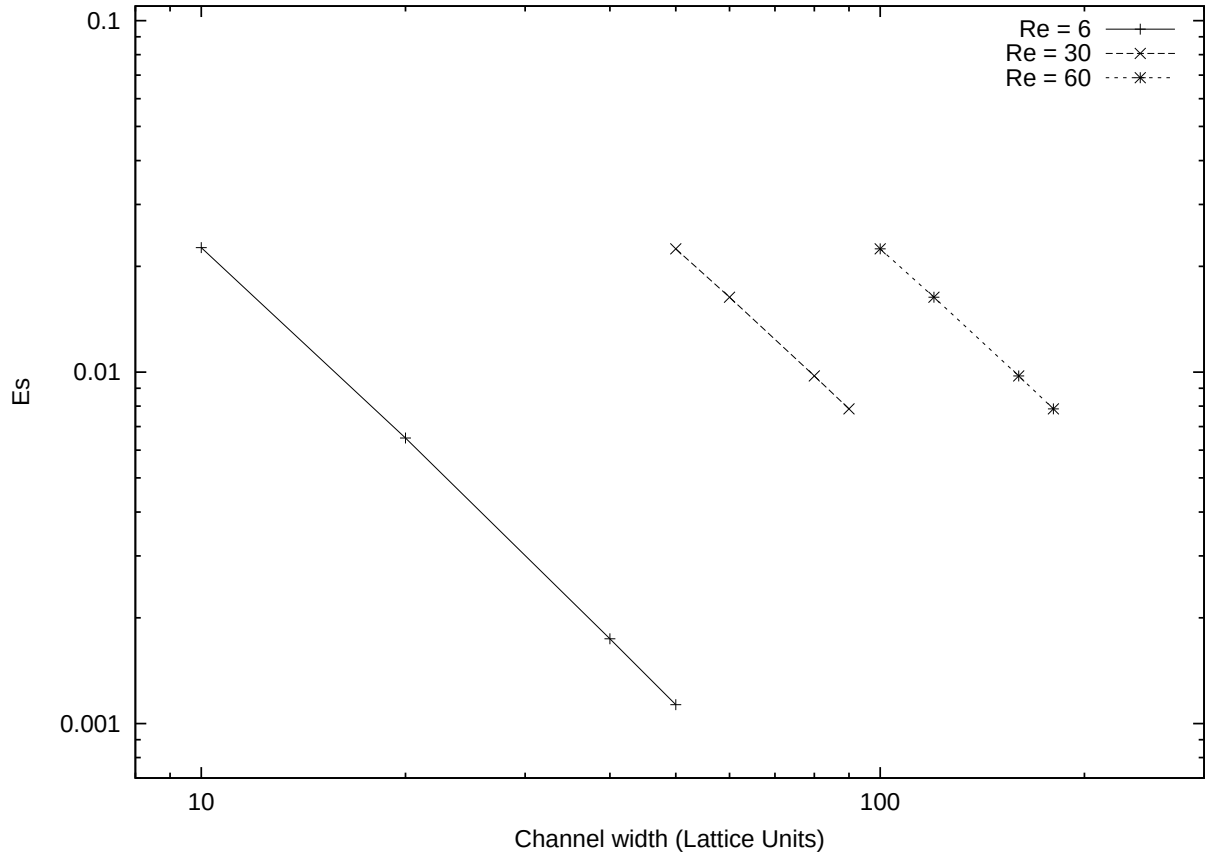

Figure 4.3: Relative errors in σ_{xy}, using the LBM with the velocity boundary conditions, for $R_e = 6, 30$ and 60 , in the Couette flow benchmark.

of unknowns increases with the number of nodes[1], and therefore the system needs more simulation time before it updates all the nodes of the fine grids, at the right edge of the figure. For interactive or real-time simulations, coarse grids may therefore be preferable than fine ones, unless certain small-scale flow characteristics are of interest. However, there is a minimum number of grid points that allows a stable solution. This depends strongly on the compressibility error which increases with δ_x and the Reynolds number.

4.5 The Symmetric Bifurcation

We are interested in the symmetric bifurcation as a more complex two-dimensional benchmark to investigate the accuracy of the shear stress in the LBM. This benchmark will be used later as an investigative benchmark for interactivity and robustness of the lattice Boltzmann method (see Chapter 7).
As we mentioned before, there is a direct relation between the shear stress and

[1]This is similar to real fluid streaming behaviour.

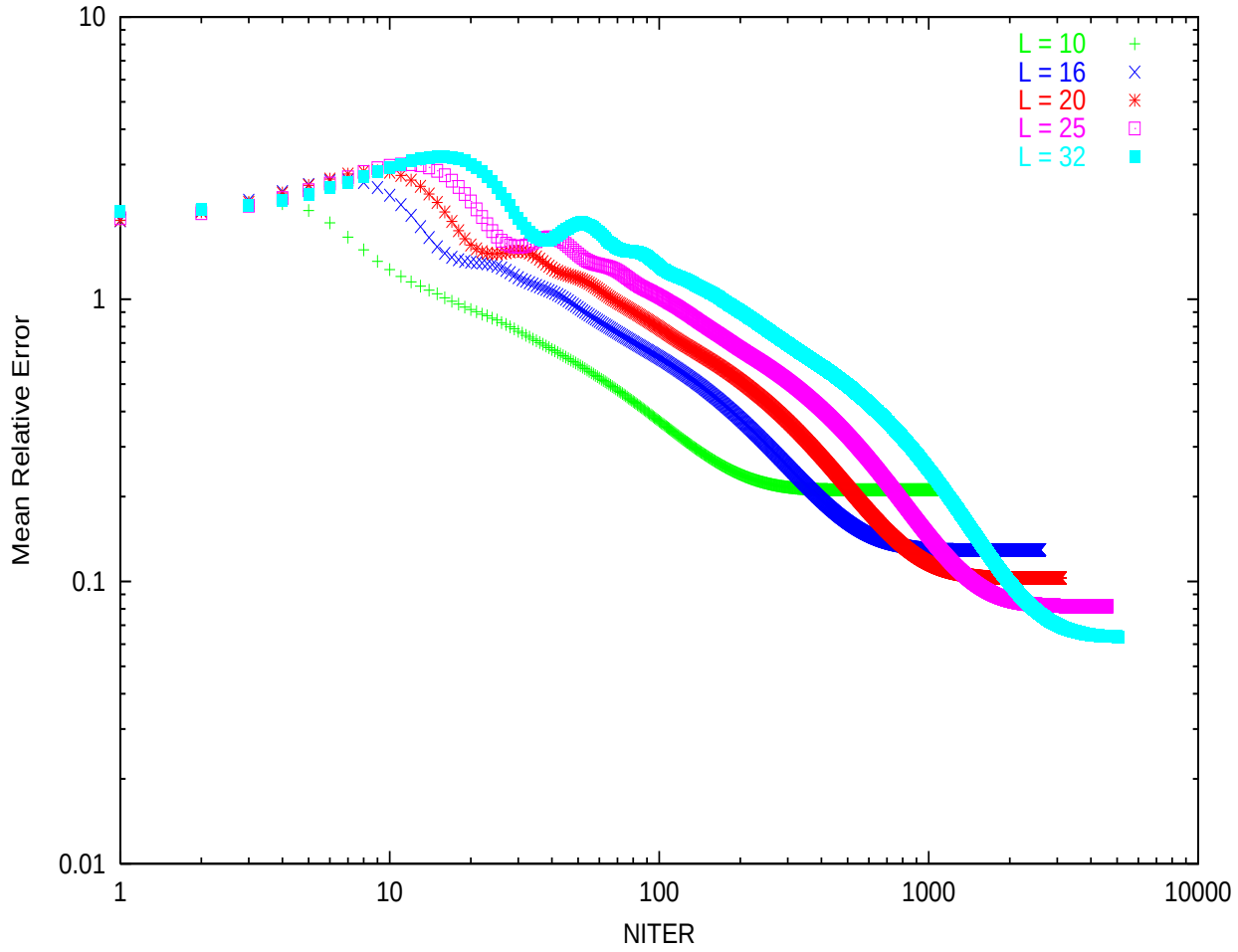

Figure 4.4: Temporal error behaviour in the Couette flow problem.

Atherosclerosis, which is a highly localised disease in areas of the carotid, coronary and femoral arteries and abdominal aorta. All these locations have complex geometry, such as branching and bifurcation, complex flow patterns, secondary flow and complex shear stress.

Several numerical and experimental models of fluid flow in large arteries and bifurcating tubes have been extensively studied (e.g. Friedmann *et al.*, 1974, Ojha, 1994;Qiu and Tarbell, 2000). However, in these attempts, the use of the derivatives of the velocity fields to get the shear stress was quite common. Within the LBM community, this benchmark did not receive much attention. This may be attributed to three reasons. Firstly, the analytical solution for the symmetric bifurcation is not known. Secondly, it is not easy to implement accurate and flexible boundary conditions at the outlets. Finally, this application is a good benchmark in biomechanics and the lattice Boltzmann method is just recently being used in this field. However, studying the

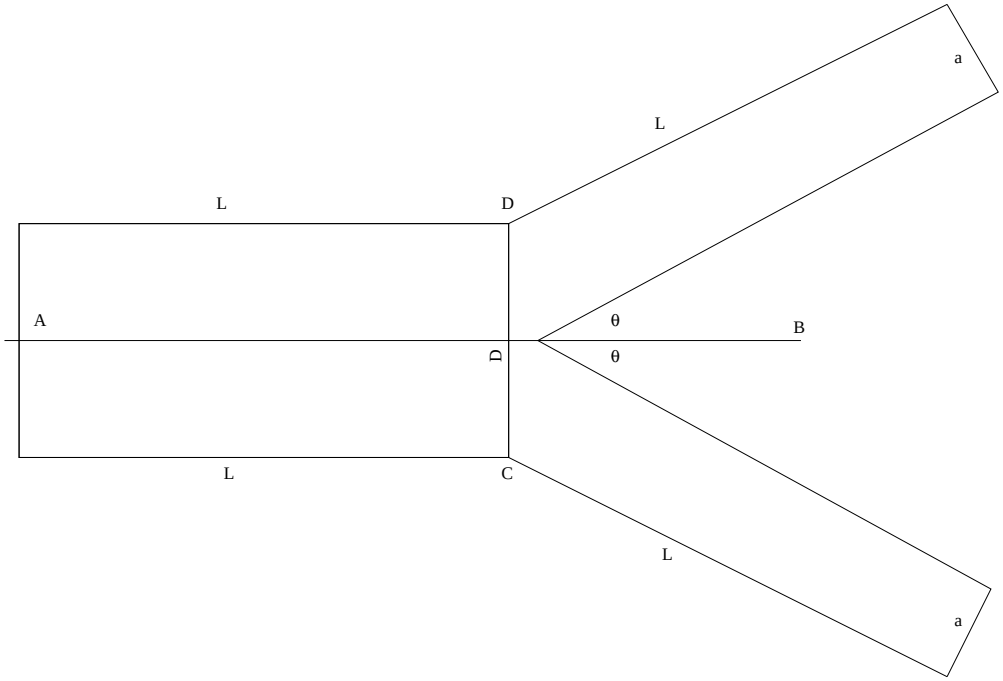

Figure 4.5: Geometry of the simulated symmetric bifurcation

symmetric bifurcation as a benchmark for blood flow problems gives us a clearer idea about the complexity of the flow field and the shear stresses at locations of interest. Additionally, it allows us to investigate implementation of several boundary conditions before using them for more complex geometry.

In this study, we consider a simplified model of a two-dimensional symmetric bifurcation that consists of one main tube of diameter D and length L and two branches at the end of the main tube, each of which has an outer length L and diameter $a = D/2$. The angle θ between each branch and the centerline AB that passes horizontally across the divider is set to be equal to 30^o. The geometry of the symmetric bifurcation is illustrated in Fig. 4.5 in which the centerline AB and the cross line CD will be reference axes for measurements and comparisons of the flow fields and the components of the stress tensor.

It can be shown that the cross sectional area of this two-dimensional bifurcation model does not change, as long as $a = D/2$. Using this result and applying the continuity equation to the model, we can prove that the average velocity in the main branch is equivalent to the average velocity in the daughter branches. This allows us to impose consistent velocity values at the inlet and outlet boundaries. On the other hand, the pressure gradient in the branches can be compared to that in the main branch by assuming that the Poiseuille formula still holds in regions far from the divider region and applying the continuity equation to end up with the conclusion that the pressure gradient in the branches is four times larger than the pressure

drop in the main branch. Assuming that the Poiseuille formula is still valid for locations of fully developed flow in the bifurcation, the shear stress in these areas will not differ significantly from values obtained from a similar channel flow. Therefore, the only region which needs further investigation is the region close to the divider. The geometry of the symmetric bifurcation whose vascular area does not change, makes the region just before the divider an expanding region. This additional area has to be filled by the fluid. As a result, both the pressure and the velocity will drop near to the divider before they enter the branches, where the velocity accelerates towards the fully developed flow and the pressure drops faster than the pressure in the main branch.

In order to obtain a more quantitative picture of the flow, we have carried out a number of LBM numerical simulations for the symmetric bifurcation at $R_e = 1$, $R_e = 200$ and $R_e = 1250$, where $R_e = DU_0/\nu$ is the Reynolds number. The diameter of the main branch is represented by 40 lattice points on the coarsest grid and 320 lattice points on the finest grid. At the inlet, we have set a flat velocity U_0 of magnitude corresponding to the required Reynolds number. The distribution functions and the density at the inlet are computed using the VBC, as described before. For the outlets, we have assumed that the flow is fully developed at a distance far from the divider by setting parabolic profiles at each outlet and forcing the distribution functions to their equilibrium values. Finally, for the other walls, we have implemented the simple bounce-back scheme.

For validation purposes, we have used the FLUENT program (Fluent, 1998) which uses a finite volume method (FVM) solver, to carry out a number of simulations for the same bifurcation at the three Reynolds numbers[1]. The comparison is made along the centerline *AB* and the cross line *CD*.

The velocity profiles and the shear stress as obtained by LBM are shown in Figs. 4.6 (a–f) for the three Reynolds numbers. As shown from these figures, the flow field fully develops just after the inlet region for $R_e = 1$. However, for the larger Reynolds numbers, the flow field is not yet fully developed when entering the divider region. At the outlets, the flow is fully developed (as we assumed) for $R_e = 1$ and $R_e = 200$. For $R_e = 1250$, it appears that the flow is not fully developed at the outlets, but this doesn't have significant effects on the flow closer to the divider (experiments of varying lengths of the branches didn't show significant difference (data not shown)) . It can also be observed that the flow near the divider becomes complex. As the region before the divider is an expansion region, the velocity flow pattern drops before entering the branches. We also observe that the velocity skews towards the inner walls inside the daughter branches and each of the two streams are bent because of the influence of the secondary motion, with the highest velocities near the outer walls of the bend. All these features are in agreement with the literature (Caro *et al.*, 1978;

[1]The finite volume simulations were carried out in collaboration with Huub Hoefsloot. See Artoli *et al.*, 2003d

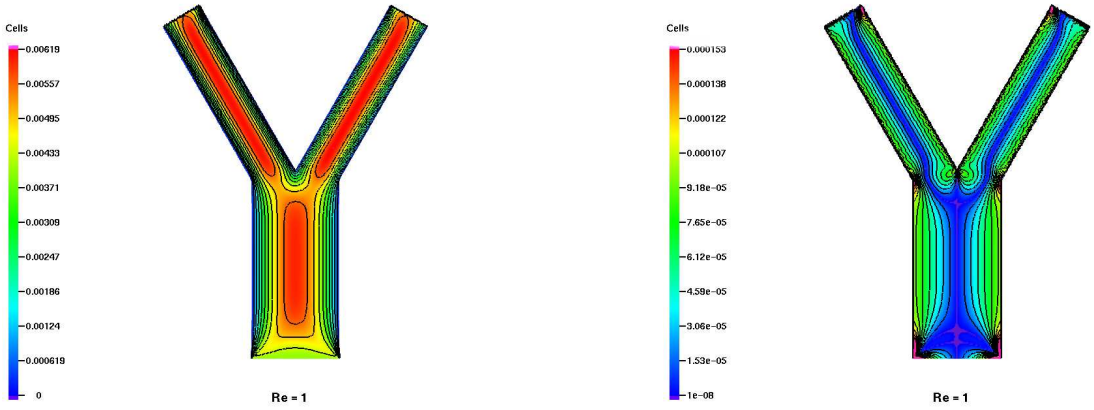

(a) (b)

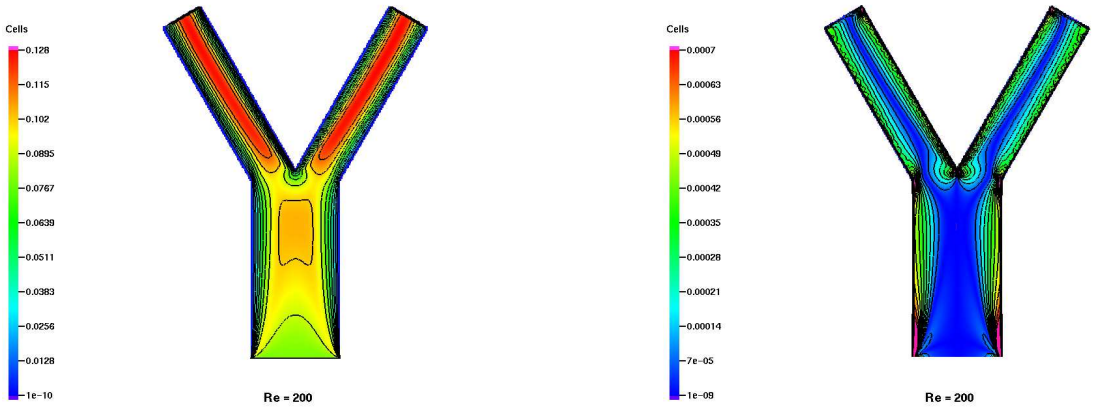

(c) (d)

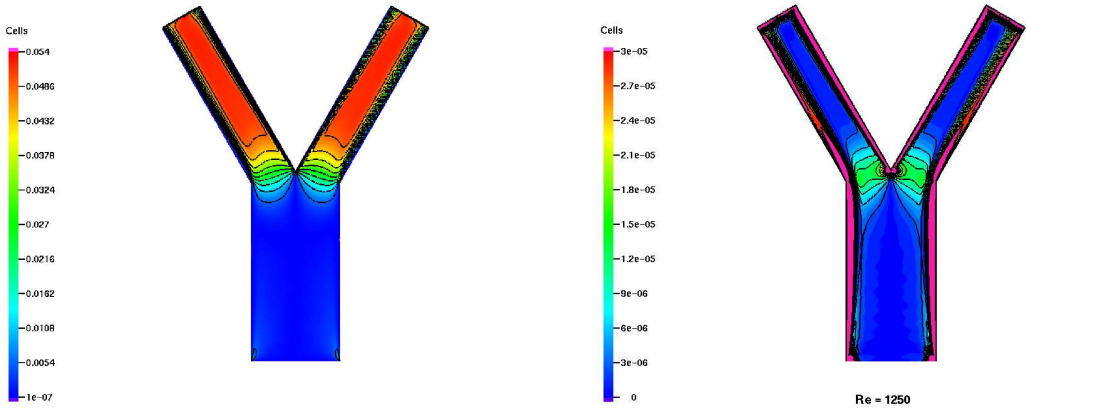

(e) (f)

Figure 4.6: Contours of velocity magnitudes and shear stress in Lattice Units for $R_e = 1(dx/dt = 0.0091$ m/sec), $R_e = 200(dx/dt = 0.0912m/sec)$ and $R_e = 1250(dx/dt = 0.5706m/sec)$.

Berger and Jou, 2000) and with the solutions of the FVM results.

The σ_{xy} components at the inlet are very close to zero, because of the imposed flat velocity profile. The corner points C and D and the divider region show higher stress values. The stress in the inner walls of the daughter branches is larger than that at the outer walls. As the Reynolds number increases, the shear stress behaves more complex, especially around the divider.

Next, results obtained from the LBM are compared to those obtained by the FVM, by taking measurements along the cross line CD. Acceptable agreement between the results obtained from the LBM and the results obtained from the FVM has been achieved when comparing the two components of the velocity (Figs. 4.7 (a–c) for v_x and (d) for v_y). The two methods show that the maxima of v_x are shifted towards the outer walls before entering the expansion region and these maxima approach the wall as the Reynolds number increases (since the velocity component increases). As it is shown in Fig. 4.7 (a) for $R_e = 1$, the maximum difference in the x-component of the velocity occurs at the centre point which faces the divider for $R_e = 1$. This is because of the flexibility of the finite volume method in performing local grid refinements at complex regions. For $R_e = 200$ and $R_e = 1250$, the differences are less than one percent. We also observe that the LBM solution approaches the FVM solution as the grid refines (see e.g. Fig. 4.7 (a)).

The stress tensor component, σ_{xy}, shows good agreement for both methods, as is shown in Figs. 4.7 (e–g) for the three Reynolds numbers. We can observe that σ_{xy} becomes quite complex in the case of $R_e = 1250$, where the shear stress changes sign more frequently. It is worth noting that the bounce back rule yields good results for the shear stress close to the wall, since it is not affected by the slip velocity. On the other hand, assigning the equilibrium distributions at the outlets yields completely wrong values of the stress tensor near to the wall. This is clearly seen from the contour lines of the shear stress at the outlets, specially for $R_e = 1$.

While looking at the results along the centerline AB, we have observed good agreement between the two numerical methods for v_x (data not shown). However, discrepancy in the pressure drops has been observed for small Reynolds numbers. The maximum difference between the two solutions is about 20% , which occurs at low Reynolds number, near to the divider. This may be attributed to the minor artifacts in the lattice BGK approximation and can be eliminated by considering generalised models.
For the stress tensor components along the centerline, the off-diagonal components, σ_{xy} has zero values far from the divider in both the LBM and the FVM. Since $\frac{\partial v_y}{\partial y} = 0$ on the line AB, it turns out that $\sigma_{yy} = -p$ (see Eqs. 4 and 5). This presents a good consistency check for LBM. In Fig. 4.7(h) we compare σ_{yy}, calculated by Eq. (3.22), with $-p = -\rho c_s^2$, for the three Reynolds numbers. In all cases, good agreement is observed.

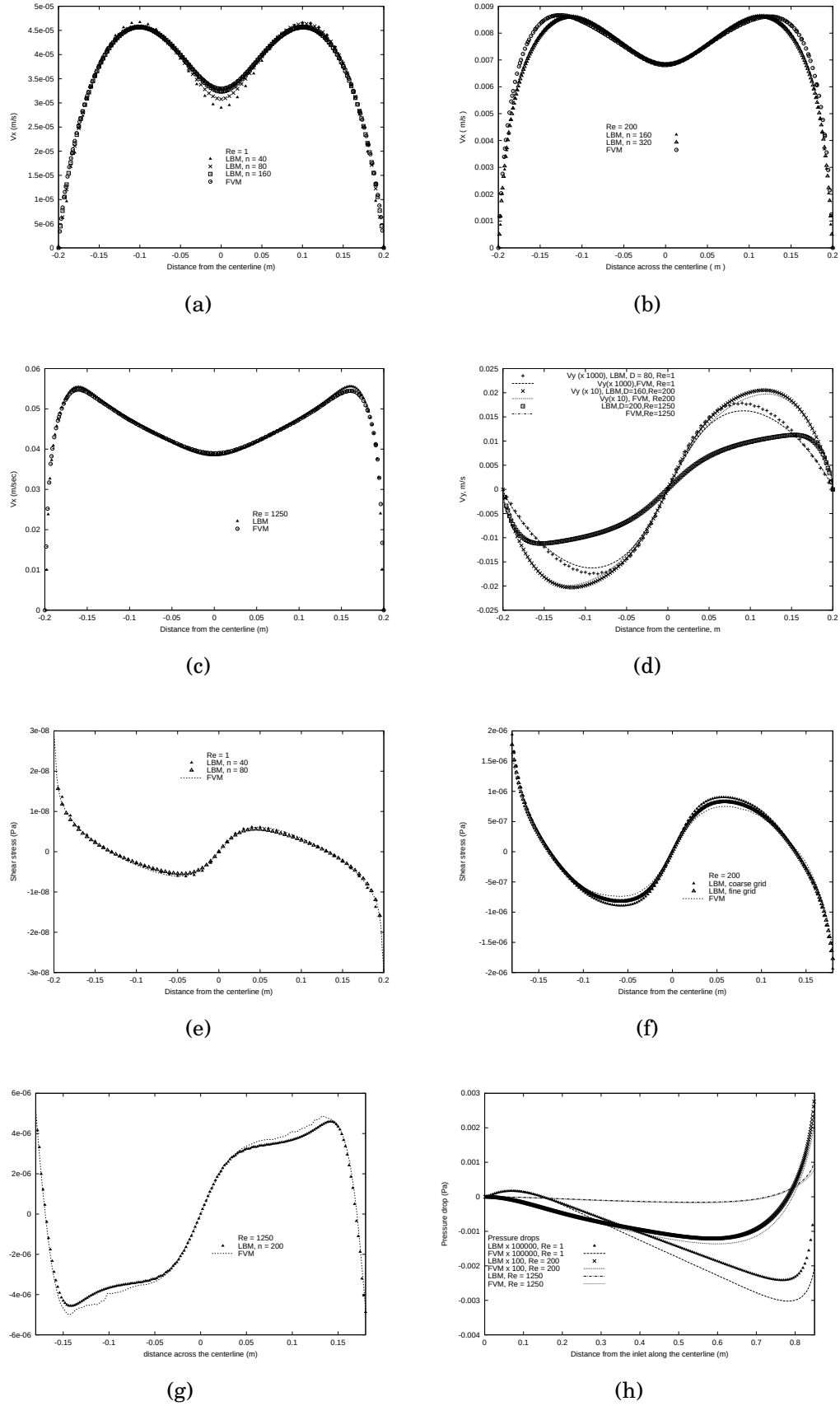

Figure 4.7: Comparison of LBM velocity profiles (upper four graphs) and shear stresses (lower left) with the FVM solution along the line CD of the symmetric bifurcation for $R_e = 1,\ 200$ and 1250 with different grid resolutions. The lower right graph shows the pressure drop along the centerline AB.

From this experiment we conclude that although the flow near the divider of a symmetric bifurcation is complex, we can obtain results of comparable accuracy to the finite volume method, by computing the stress tensor components from the non-equilibrium parts of the distribution functions, commonly computed during the collision process of the lattice BGK simulations.

4.6 Summary

Three independent 2D numerical simulations have been used to validate the lattice BGK for simple steady flows: the channel flow, the Couette flow with injection at the boundaries and the symmetric bifurcation. We have implemented a number of boundary conditions known to the LBM community. We have also shown that the accuracy of obtaining the stress tensor from the LBM follows the accuracy of the implemented boundary condition, except for the bounce-back rule, where the error is of the order of the machine accuracy in the case of channel flow. We have also compared the obtained results with the analytical solutions derived from the analytical lattice BGK solution for the velocity field which has been obtained by He *et al.* (1997) and the Navier-Stokes solution for the shear stress in the Couette flow with injection. In the case of the symmetric bifurcation, the results are comparable to the FVM results. It has been shown that, close to the walls, the wall shear stress can be computed with high accuracy using the lattice BGK. The method proved to be successful in computing the stress tensor in complex geometry, in the limit of low Mach number. As there is an increasing interest in applying the LBM in haemodynamics, we argue that similar formula for the stress tensor for non-Newtonian fluids may be worked out. Further experimental and simulation studies on 3D flows are necessary for validation and more enhanced boundary conditions for the outlets may be required. These issues will be discussed in the next chapter.

Chapter 5

Pulsatile Flow Benchmarks

In the last chapter, we have shown that the lattice BGK works well for steady flow benchmarks. The advantages and drawbacks of the method were discussed in Chapter 2. In this chapter, detailed analysis of the accuracy of the lattice BGK method in simulating pulsatile flow in a 2D channel and a 3D tube is presented. The influence of different boundary conditions on the accuracy is discussed.

5.1 Introduction

Recently, it has been demonstrated that the lattice BGK method is useful to simulate time-dependent fluid flows (Krafczyk *et al.*, 1998). As demonstrated in Chapter 2, for steady flow, the lattice BGK is second order accurate in the velocity fields and the stress tensor, when second order boundary conditions are applied. Although the accuracy has been studied extensively for steady flows, studies on the accuracy of lattice BGK for time dependent flows are quite rare (He and Luo, 1997; Artoli *et al.*, 2002c).

Pulsatile flow characteristics are quite important in haemodynamics. It is believed that the shear stress and other haemodynamic factors play a dominant role in diagnosis and treatment of cardiovascular diseases (e.g. Wooton and Ku, 1999). These factors are either studied by building experimental or simulation models for locations of interest. Depending on the geometry of these locations, appropriate approximations such as rigidity of the wall, circular cross section and assuming blood to behave as a Newtonian fluid commonly take place. The role of Computational Haemodynamics is well recognised in this field and proved to be of great help in understanding the nature of blood flow in diseased locations (Vorp *et al.*, 2001).

As mentioned before, with lattice BGK, it is possible to compute the local components of the stress tensor without a need to estimate the velocity gradients from the velocity profiles. In addition, the equation of state defines the pressure as a linear function of the density, which makes it easy to obtain the pressure from the density gradient. All these advantages make the lattice BGK a suitable candidate for simulating time-dependent blood flow in arteries.

In this chapter, we investigate the accuracy of the lattice BGK model in recovering analytical solutions for oscillatory two dimensional (2D) channel flow and three dimensional (3D) tube flow. The 2D simulations are performed to test and validate the model, while the 3D simulations are performed to model a straight rigid segment of a large artery. Typical values from haemodynamics are used to cover a range of Womersley and Reynolds numbers.
The standard lattice BGK model works well as long as the Mach number M is low ($M^2 << 1$) and the density fluctuations are small. However, modelling unsteady flows involves higher density fluctuations, since the only way to model time-dependent pressure in lattice BGK is by incorporating time-dependent density. Also, compressibility errors at high Mach numbers are expected. It has been reported that, with compressible lattice BGK models, when the pressure gradient is time-dependent, compressibility effects may arise and using an incompressible model is necessary (He and Luo, 1997). Realizing this defect, other incompressible lattice BGK models have been developed (Zou *et al.*, 1995; He and Luo, 1997; Guo *et al.*, 2000) here referred to as D2Q9i, D2Q9ii and D2Q9iii, respectively. The difference between the D2Q9 and the D2Q9i is that the density in the equilibrium distribution is inside the brace of Eq. (3.4) for the D2Q9i. The D2Q9ii assumes the pressure to be the independent dynamic variable instead of the density, and is equivalent to D2Q9i when the density is equal to unity. The D2Q9iii introduced a different equilibrium distribution function with which it is possible to exactly derive the incompressible Navier-Stokes equations in the limit of a low Mach number. As the incompressible D2Q9i model has already been tested for steady flows, for which it was proposed, we test it here for unsteady flows after noting that the D2Q9i is a special case of the D2Q9ii.

5.2 Boundary Conditions

As stated before, with the lattice Boltzmann methods, the no-slip boundary condition is not automatically recovered at the boundaries. Therefore, the walls require special treatment. A number of boundary conditions have been proposed which are either of first or second order accuracy in space and may or may not have slip velocities at the walls. In this study, we distinguish four types of wall boundary conditions:

1. The bounce-back on the links, referred to later as BBL, in which particles coming to the walls simply return back to the fluid in the direction where they came from. Collision is not performed at the boundary nodes while using this boundary condition. It is simple, computationally efficient, and can be used for a complex geometry, but is of first order and is known to yield a slip velocity which in turn can be minimised by increasing the grid size and tuning the viscosity.

2. The bounce-back on the nodes, referred to as the BBN, in which collision is allowed at the boundary nodes. The bounce-back on the nodes is known to be of second order accuracy, but still has a slip velocity, except when $\tau = 1$.

3. Recently, Bouzidi *et al.* (2001) introduced another version of the bounce-back on the links which allows using the bounce back for the curved geometry, and we will refer to it as the bounce back on a curved boundary (BBC). The idea of this boundary condition is to add a linear or a quadratic interpolation term to the streaming step by considering the first or both the first and the second fluid points together with the bounce back rule. The bounce-back on the links is a special case of this boundary condition.

4. The non-slip velocity and pressure boundary conditions presented by Zou and He (1997) have been used to set a specific velocity or pressure at the boundary by assuming that the bounce-back is valid for the non-equilibrium parts of the distribution functions and explicitly computing the unknown distributions.

5.3 Simulations in 2D

We have conducted a number of 2D simulations for time dependent flow in a channel. Various boundary conditions have been tested. For the walls, we have used the bounce-back on the nodes and non-slip boundary conditions; for the inlet and outlet, we have used periodic boundaries in combination with body forcing or velocity and pressure boundaries. For all simulations described below, unless otherwise specified, the flow is assumed to be laminar ($R_e < 2000$) and the Mach number is assumed to be low ($M < 0.1$).

5.3.1 Oscillatory Channel Flow

We have studied the flow in an infinite 2D channel due to an oscillatory pressure gradient $\frac{\partial P}{\partial x} = Asin(\omega t)$, where A is a constant. The pressure gradient is implemented by applying an equivalent body force G or by appropriate oscillating pressure difference between the inlet and outlet. The analytical solution for the velocity in this case is given by the Real part of (Pozrikidis, 1997)

$$v(y,t) = -\frac{A}{\rho\omega} e^{-i\omega t} \left(1 - \frac{cosh\left[\sqrt{b}(y - L/2)\right]}{cosh\left[\sqrt{b}L/2\right]} \right) \tag{5.1}$$

where ρ is the fluid density, L is the width of the channel, and $b = -i\omega/\nu$.
To check the accuracy of the lattice BGK model, we have performed a number of simulations. The Reynolds number is defined as $R_e = \frac{UL}{\nu}$, the Womersley number is defined as before; $\alpha = R\sqrt{\frac{\omega}{\nu}}$, and the Strouhal number is defined as $St = \frac{R}{UT}$, where $R = L/2$, ν is the kinematic viscosity, $\omega = \frac{2\pi}{T}$ is the angular frequency and T is the sampling period. The velocity U is given by $U = -\frac{-1}{2\nu\rho}\frac{dp}{dx} \equiv \frac{L^2 G}{8\nu\rho}$, the average density of the system is $\rho = 1.0$ and the pressure gradient is sinusoidal with amplitude A.

At first, we have used the bounce-back on the nodes (BBN) which is quite simple and is known to be of second order accuracy. Periodic boundary conditions are used for the inlet and the outlet boundaries. Both the Reynolds and the Womersley numbers were kept fixed by fixing the distance L between the two plates and varying the relaxation parameter τ, the period T and the body force G. The error in velocity at each time step is defined by

$$Ev = \frac{\sum_{i=1}^{n} |\vec{v}_{th}(\vec{x}_i) - \vec{v}_{lb}(\vec{x}_i)|}{\sum_{i=1}^{n} |\vec{v}_{th}(\vec{x}_i)|} \tag{5.2}$$

where $\vec{v}_{th}(\vec{x}_i)$ is the analytical solution for the horizontal velocity, $\vec{v}_{lb}(\vec{x}_i)$ is the velocity obtained from the lattice BGK simulations and n is the number of lattice nodes representing the width of the channel. The overall average error, $< Ev >$, is averaged over the period T. The relaxation time ranges from $\tau = 0.6$ to $\tau = 3.0$, the body force ranges from $G = 25 \times 10^{-5}$ to $G = 0.04$ and the sampling period lies in the range $500 - 20$, giving corresponding values of $0.2 - 5.0$ for δ_t, with $\delta_t = 1$ corresponding to the case where $\tau = 1$. The system was initialised by setting the velocity to zero everywhere in the system. The convergence criterion is attained by comparing simulation results from two successive periods and the stop criterion is when this difference is less than 10^{-7}. The agreement between the simulation and the analytical solutions is quite good, as is shown in Fig. 5.1 in which the obtained velocity profiles (point) for $\alpha = 4.34$ at $t = 0.75T$ are compared to the theory (dashed line). However, there seems to be a small shift in time between the simulation and the theory. This shift is a function of time and τ. We have found that if we assume that the theory lags the simulation with a half time step, i.e $t_{lb}\delta_t = t_{th} + 0.5\delta_t$, the error reduces at least one order of magnitude for all τ values. Figure 5.1 shows a typical simulation result compared to the analytical solution with (solid line) and without (dashed line) shifting the time coordinate. We have used this observation to compare the simulation results with the shifted analytical solution which leads to excellent agreement for all values of time, as shown in Fig. 5.2 The error as a function of time is shown in Fig. 5.3 from which it can be seen that the error is minimum at $\tau = 1$, since there is no slip velocity at this specific case (He *et al.*, 1996). An error of the order of the round-off error could be reached for the special case when $\tau = 1$, when the bounce-back on the nodes is used, and assuming the 0.5 time shift (the asterisks, *, in Fig. 5.3). From Fig. 5.3 we also observe that the error is maximum at a quarter period in time. This may be attributed to the large pressure gradients at this time.

This shift in time has been observed before by Matthaeus (2001). It may be attributed to the way the driving force is imposed in the simulation and details of the specific lattice BGK model (force evaluation). We also believe that the way in which time coordinates are discretised may have some effects on this shift. For the other cases, when $\tau \neq 1$, the effect of the slip velocity dominates. Up to now, the slip velocity has analytical expression for the steady channel flow, but not yet for the unsteady flow. In the next sections we will investigate the influence of boundary conditions and flow parameters such as the Reynolds number on this shift.

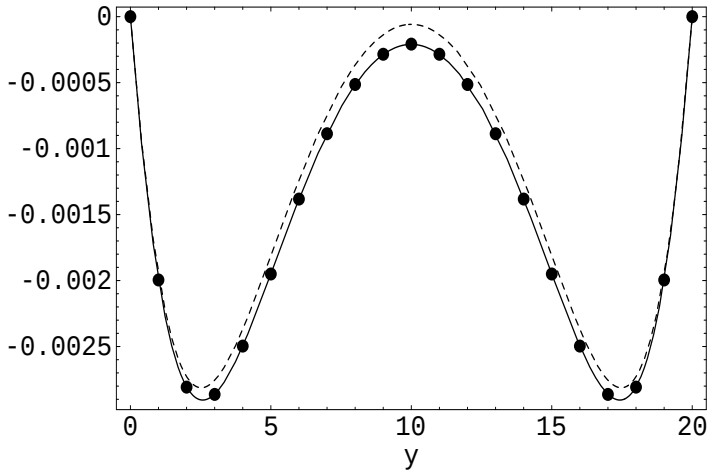

Figure 5.1: Velocity profile (in Lattice Units) at $t = 0.75T$ with $\tau = 1$, $\alpha = 4.34$, $R_e = 10$ and $St = 0.6$ in a 2D oscillatory channel flow using the BBN. The dots are the lattice BGK results. The dashed line is the analytical solution and the solid line is the analytical solution with a shift of 0.5 time step.

5.3.2 Non-Slip Boundary Conditions

In order to remove errors arising from the slip velocity, we have conducted similar simulations with the no-slip velocity boundary conditions explained in section 5.2(4) at the walls and periodic boundary conditions at the inflow and the outflow boundaries. The body force that corresponds to a desired Reynolds number drives the flow. The Strouhal number is kept constant by fixing both the Reynolds and the Womersley numbers and looking at the accuracy in time. This is done by fixing the width L and assigning the corresponding values for the sampling period T, the body force G, and the relaxation parameter τ. In this way, δ_t will change. The results are shown in Fig. 5.4 which shows the average error $< Ev >$ as a function of δ_t. From this figure, we clearly see that the lattice BGK is of first order accuracy in time (slope = 0.9). The error is again decreased when the half-time step correction is used, specially at $\tau = 1$, as shown in the same graph. From this experiment, we conclude that the shift in time does not depend on the used boundary condition.

5.3.3 Influence of the Reynolds Number

We have conducted another set of simulations to see the influence of the Reynolds number on the error in the flow fields. Here, the relaxation parameter is kept fixed at the value $\tau = 1$, the width of the channel is varied to achieve higher Reynolds numbers and the period is changed accordingly to keep the Womersley parameter constant. The length of the channel is $5L$. In summary, we change the Reynolds

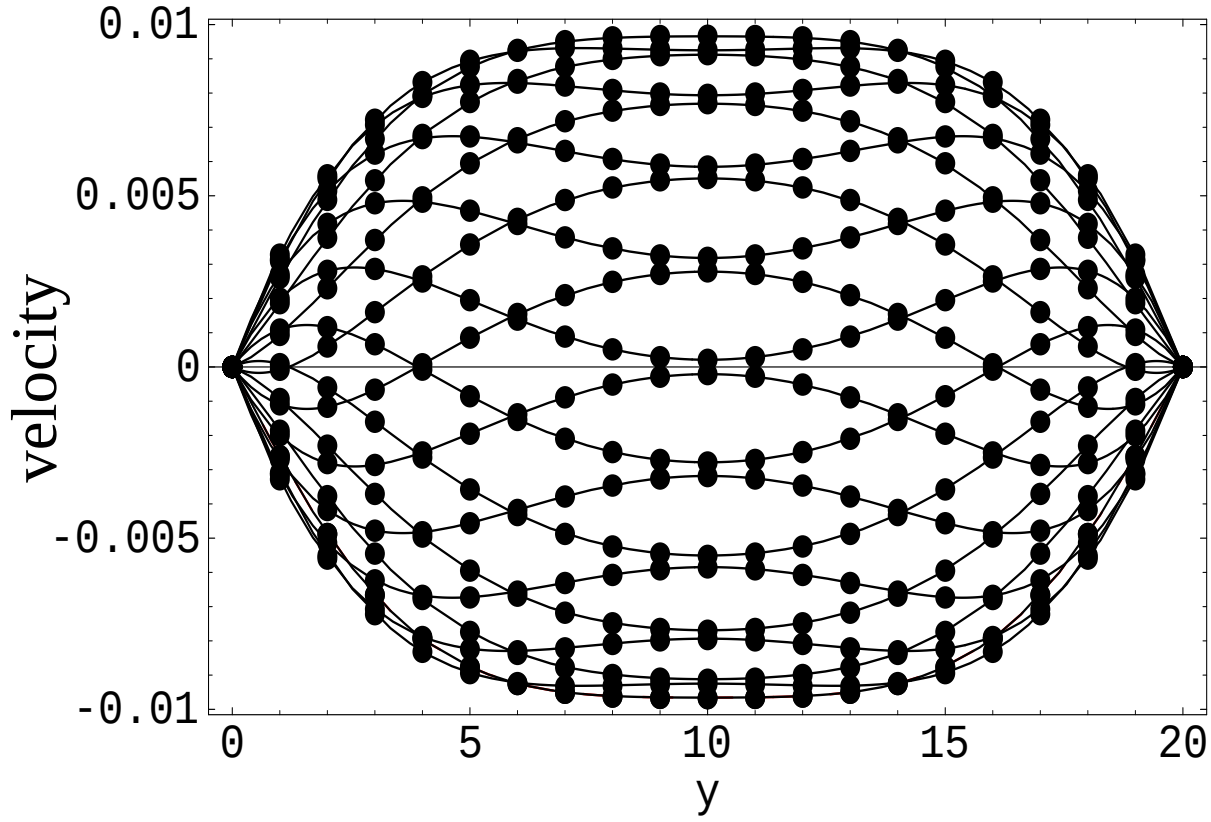

Figure 5.2: Obtained velocity profiles (in Lattice Units) over a complete period (dots) compared to the shifted theory (lines) with $\tau = 1$, $\alpha = 4.34$, $R_e = 10$ and $St = 0.6$. The measurements are taken at the middle of the channel, at each $t = 0.05nT$ where $n = 0, 1, ..., 20$.

number R_e, the body force G, the width L and the period T. Simulations for Reynolds numbers in the range $1 \rightarrow 200$ at $\alpha = 15.533$ were performed. Figure 5.5 shows comparisons of numerical and analytical solutions of the velocity profile for $R_e = 200$ at $t = 0.2T$. Similar agreements between theory and simulations have been observed for the whole period at different Reynolds numbers (data not shown). When compared to the analytical solutions, with and without shift in time, the error decreases from $< Ev >= 0.0085$ to $< Ev >= 0.00024$ for $R_e = 200$.
We observe that the difference between the two analytical solutions (the original and the shifted) becomes less as the Reynolds number increases. This suggests that the shift is inversely proportional to the applied body force which may have direct influence on it. It is therefore necessary to conduct another set of simulations in which the body force has no influence (i.e. is absent).

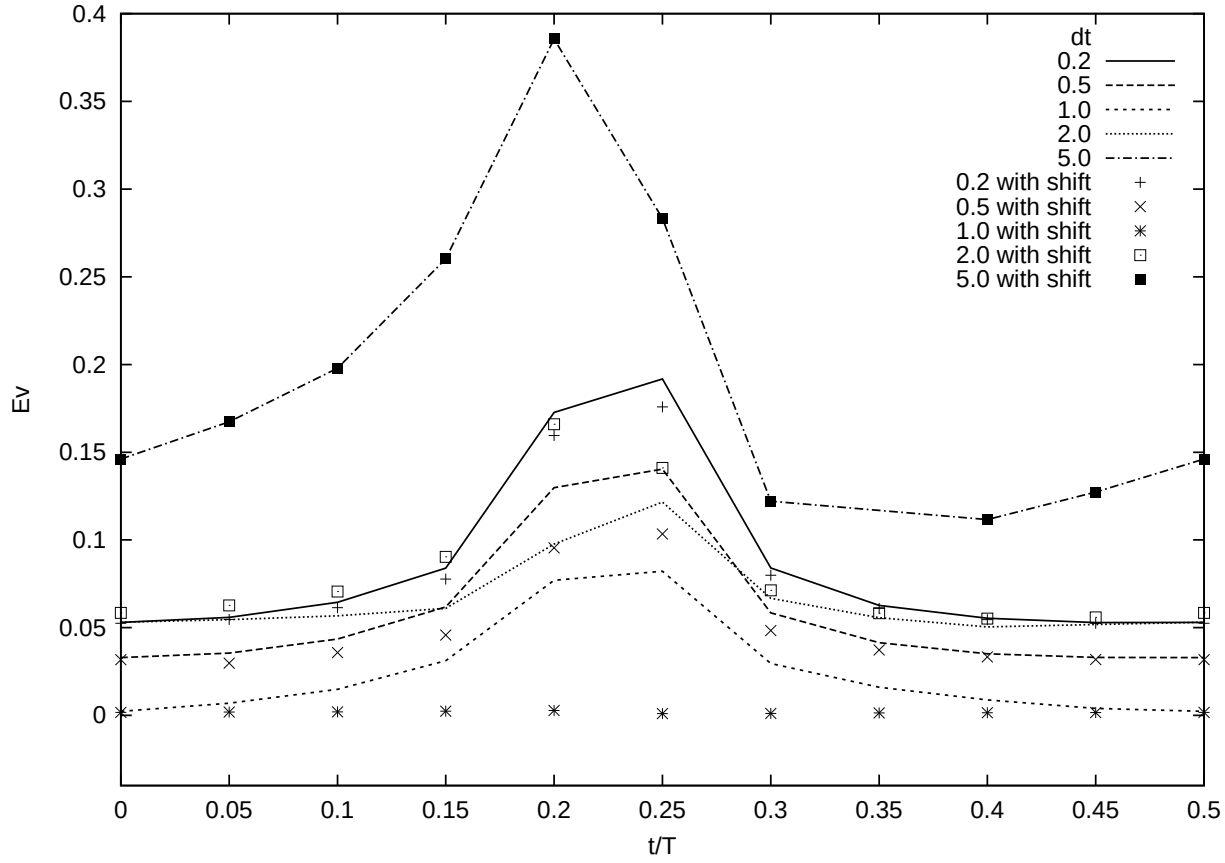

Figure 5.3: Error behaviour over a half cycle for different values of δ_t as a function of the fractional time t/T without (lines) and with (points) time-shift correction for $\alpha = 4.34$, $R_e = 10$ and $St = 0.6$ in a 2D oscillatory tube flow using the BBN boundary condition.

5.3.4 Inlet and Outlet Pressure Boundary Conditions

In order to remove the influence of the body force, we have conducted another set of simulations in which the flow in a 2D channel is driven with a sinusoidal pressure gradient of magnitude $A = 0.001/L_x$ where L_x is the length of the channel. The length of the channel is 10 times the width and the period of the driving pressure is $T = 1000$. The density at the inlet is $1 + Asin(\omega t)$ and is set to be 1.0 at the outlet. The convergence criterion is attained by comparing simulation results from two successive periods with a stop criterion less than 10^{-7}. All the flow fields were initialised from zero. We have again observed good agreement with the theory, as is shown in Fig. 5.6 The shift in time has diminished in magnitude, but it is still there ($< Ev >= 0.019$ without shift and reduces to $< Ev >= 0.017$ with shift).

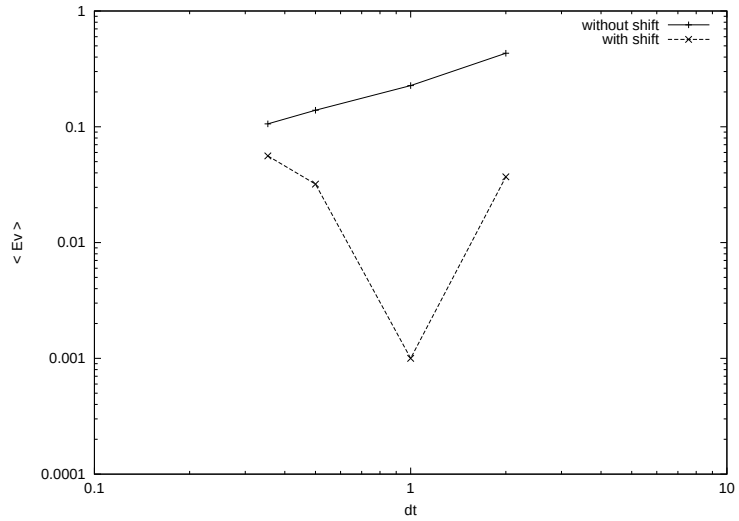

Figure 5.4: Relative Error in velocity, averaged over the whole period, versus the time step for $\alpha = 15.53$, $R_e = 10$ and $St = 7.68$ in a 2D oscillatory channel flow. The slope of the straight line is 0.90. The dashed line is the error with reference to the shifted in time analytical solution. A second order BBN boundary condition is used here.

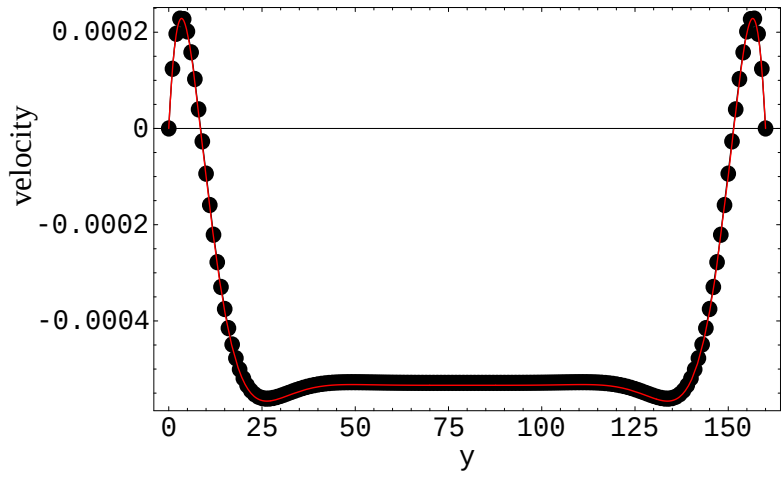

Figure 5.5: Velocity profiles (in Lattice Units) obtained from lattice BGK simulations (dots) for $\alpha = 15.53$, $R_e = 200$ and $St = 0.38$ in a 2D oscillatory channel flow, showing excellent agreement with the analytical solutions (lines). The effect of time shift is not observable.

5.4 Simulations in 3D

To have a complete picture about the accuracy of the lattice BGK, we have conducted a number of 3D simulations of sinusoidal flow in a tube using a parallel lattice BGK

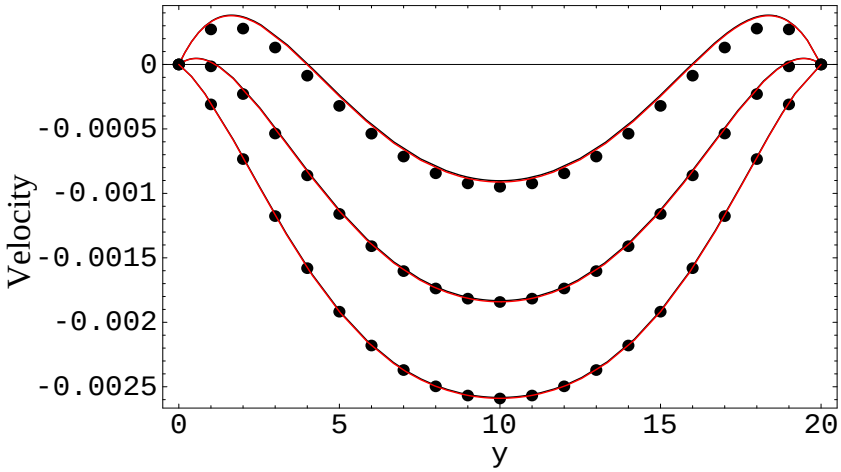

Figure 5.6: Velocity profiles obtained from lattice BGK simulations (dots) for $\alpha = 4.00017$, $R_e = 10$ and $St = 0.51$ in a 2D oscillatory channel flow when inflow and outflow boundary conditions are used. Selected simulation times are shown. The shift in time has little effect but is still there.

solver developed in our group (Kandhai *et al.*, 1998) with added functionalities for dedicated in- and outlets, solid boundary and shear stress calculations (Artoli *et al.*, 2002). The diameter of the tube is represented by 39 lattice nodes and the minimum tube length is $L = 50$ lattice nodes. First, we have used the BBL together with periodic boundaries to simulate oscillatory flow in the tube. The simulation period is set to be $T = 800$, the relaxation parameter is $\tau = 0.625$ and the amplitude of the body force G is chosen to be 4.687×10^{-6} in order to have a Womersley number $\alpha = 8.4661$. Initialisation of the system and the stop criterion is the same as that for the 2D case. The simulations were performed on 4 nodes of a Beowulf cluster using slice decomposition. The time per iteration is about 0.2 seconds.
The obtained velocity profiles for a half cycle are shown in Fig. 5.7, compared to the analytical solution

$$u(y,t) = Re\left[-\frac{A}{\rho\omega}e^{-i\omega t}\left(1 - \frac{J_0\left[\sqrt{b}y\right]}{J_0\left[\sqrt{b}R\right]}\right)\right], \tag{5.3}$$

where J_0 is the zeroth order Bessel function of the first type and again $b = -i\omega/\nu = -i(\alpha/R)^2$. Similar velocity profiles have been obtained for the complete period and for a range of Womersley parameters and relaxation times. The overall average error is about 15 % and is maximum at the centres and near to the walls where the flow reverses. This large error may be attributed to, among others, the stairing geometry of the boundary, the way of implementation of the body force, the slip velocity of the bounce back rule and the compressibility effect.

There are at least two ways to reduce the error; to use an incompressible 3D model, and/or to have more advanced boundary conditions. As there exist more advanced boundary conditions which are well tested (see for e.g. (Zou and He, 1997; Mei *et al.*, 1999; Bouzidi *et al.*, 2001), as a first step, we have applied the curved boundary conditions recently proposed by Buzaidi *et al.* (2001) which is simple and easy to implement. It has been realised by the author that the Bouzidi boundary condition slightly violates mass conservation. This has a very little effect on the final solution. With the curved boundaries, the system size and the simulation parameters are the same as those for the bounce-back. The accuracy is significantly enhanced, as shown in Fig. 5.4 which shows both the simulation results (points) and the analytical solutions. The shift in time was not clearly observed here. This may be attributed to the different nature of the quasi compressible D3Q19 Model in which we have combined errors from stairing and compressibility effects.
The error behaviour is studied by keeping fixed both the Reynolds and the Womersley numbers via fixing the diameter R and varying the relaxation time τ, the body force G and the period T. Defined as above, the error behaviour as a function of the sampling period is shown in Fig. 5.9, from which we observe that the error enhances as the number of sampling points representing the period increases. This is expected as the time step decreases with increasing T. The error behaves as first order in time (slope of the fitted line is about 1.0). Furthermore, as a typical Reynolds number in the Abdominal aorta is 1250 we have performed another set of simulations at this Reynolds number with $\alpha = 7.7284$ by setting $T = 1200$ and $\tau = 0.6$. Figure 5.10 shows the simulation results compared to analytical solutions. The average error per time step is about 0.07 which is in the worse case still two times more accurate than when the BBL is used, even if they are both of first order accuracy. As we are interested in blood flow simulations, periodic boundary conditions are not suitable, since there are different flow conditions at the outlets of the arteries. Therefore, we have tried an inlet-outlet boundary condition in which we have assumed stagnant flow at the inlet and no flux at the outlet. This is done by copying the densities from inside the flows to the inlet and the outlet, computing the velocity near the outlet and assigning equilibrium distributions to the outlet distribution functions, and applying a body force or a pressure gradient to drive the flow. We have obtained comparable results for periodic boundary conditions (the difference in error is about 0.004).

5.5 Shear Stress

As mentioned previously, the shear stress is an important factor in haemodynamics and is known to play a dominant role in the localisation of cardiovascular diseases such as atherosclerosis. We have shown in a previous article (Artoli *et al.*, 2001) that the components of the stress tensor in the lattice Boltzmann BGK method can be computed from Eq. (3.22)

$$\sigma_{\alpha\beta} = -\rho c_s^2 \delta_{\alpha\beta} - \left(1 - \frac{1}{2\tau}\right) \sum_{i=0} f_i^{(1)} e_{i\alpha} e_{i\beta}. \tag{5.4}$$

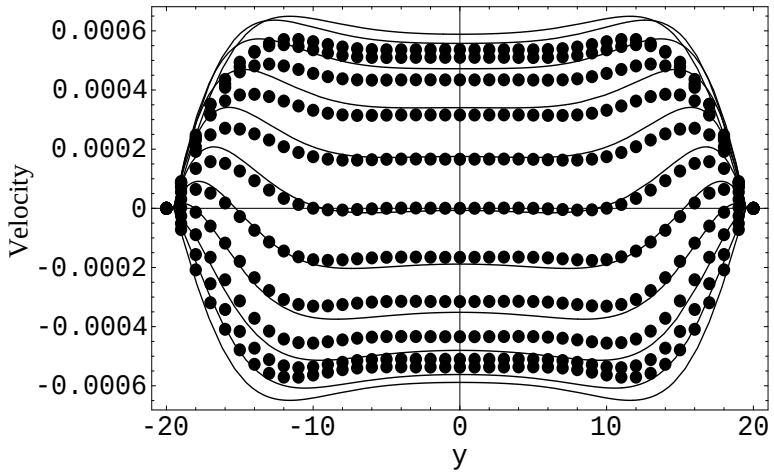

Figure 5.7: Obtained velocity profiles (dots) compared to the analytical Womersley solutions (lines), for $\alpha = 8.4661$ and $R_e = 10$ in a 3D oscillatory tube flow using the bounce-back on the links. The overall average error is about 15%.

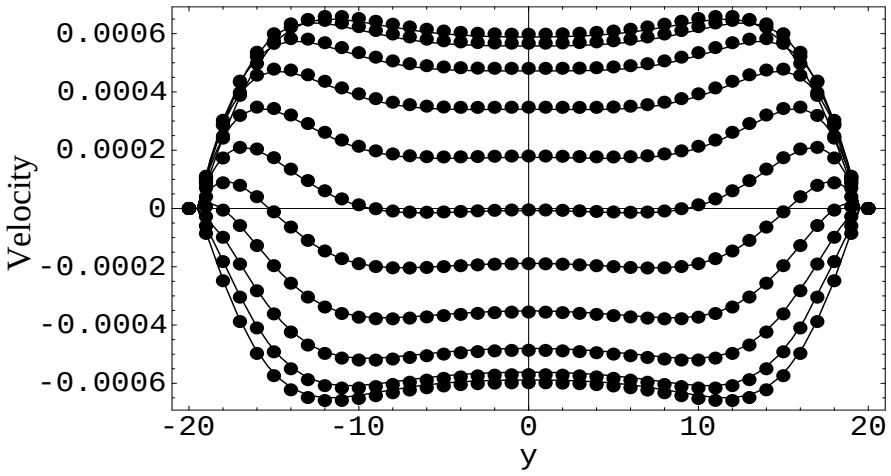

Figure 5.8: Obtained velocity profiles (dots) compared to the analytical Womersley solutions (lines), for $\alpha = 8.4661$, $R_e = 10$ and $St = 2.2815$ in a 3D oscillatory tube flow using the BBC. The overall average error is about 7 %.

in lattice units, where the quantity $f_i^{(1)} e_{i\alpha} e_{i\beta}$ is usually computed during the collision process. Therefore, the stress tensor components can be obtained without almost any additional computational cost. This extensively enhances the lattice Boltzmann BGK method, as other CFD methods are more elaborate and estimate the stress tensor components from the simulated velocity field. We have used this formula to compute the shear stress for pulsatile flow and compare the simulation results with the ana-

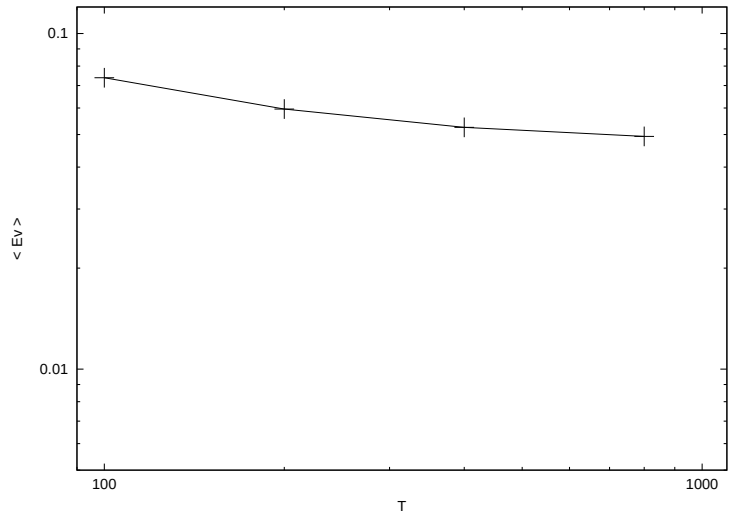

Figure 5.9: First order error behaviour as a function of T at $\alpha = 8.4661$, $R_e = 10$ and 2.2815 for a 3D oscillatory tube flow with the curved bounce back and linear interpolation.

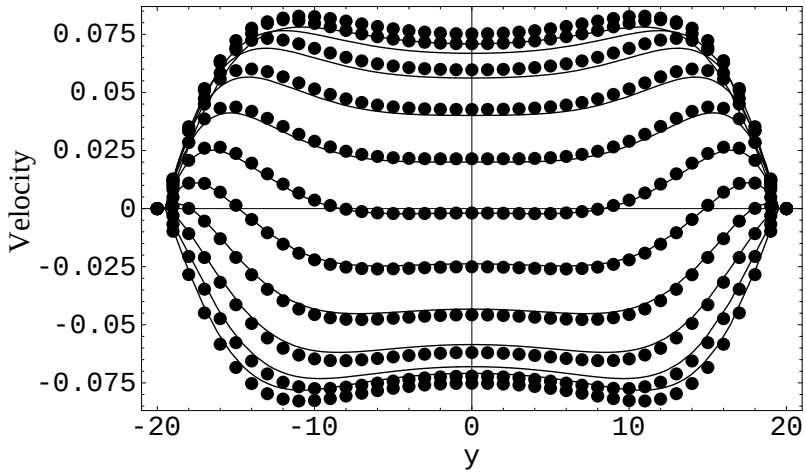

Figure 5.10: Velocity profiles with $\tau = 0.6, T = 1200, d = 39$, $\alpha = 7.7284$, $R_e = 1250$ and $St = 0.0152$ in a 3D oscillatory tube flow. The dots are the lattice BGK results with BBC boundary condition. The lines are the analytical solutions

lytical solutions derived from analytical velocity profiles. With both BBL and BBC, excellent agreements have been obtained for both the oscillatory channel (see Fig. 5.11) and tube flows (see Fig. 5.12). The shear stress vanishes in the canter and grows up towards the walls, where the velocity gradients are large. As the Womersley parameter increases, the flat region increases and the shear stress decreases in

the central region. Similar agreement with the theory has been obtained for the other stress components in a range of Womersley and Reynolds numbers. The shift in time has no effect here and is absent during the collision process. We have noticed that the shear stress is slightly better when the bounce-back on the links is used. The average error is about 0.18 for the BBL and 0.19 for the BBC. This may be attributed to the fact that the spatial gradient of the slip velocity vanishes which enhances the BBL over the BBC which interpolates in a region of high velocity gradients.

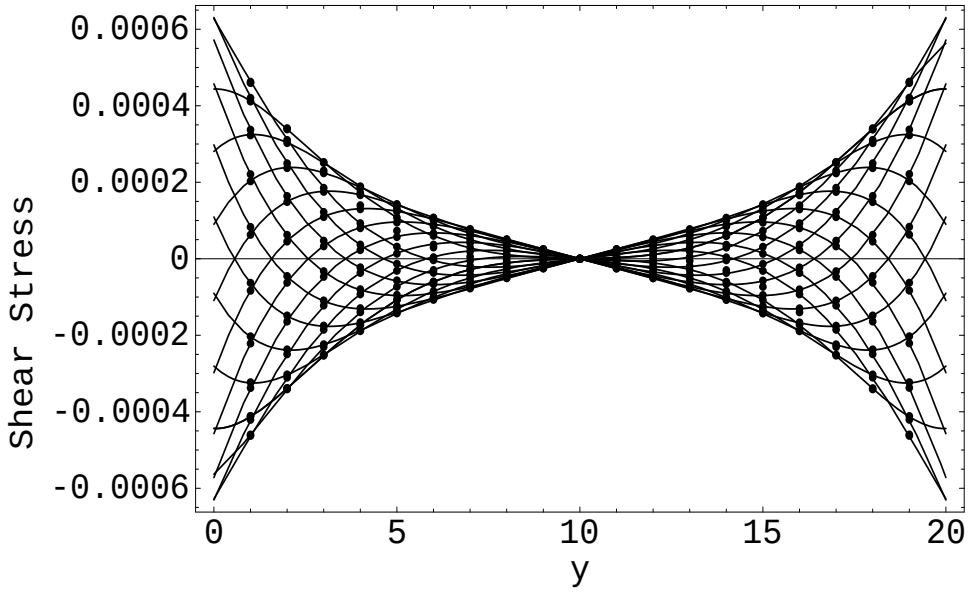

Figure 5.11: Shear stress (in Lattice Units) obtained from lattice BGK simulations (dots) for $\alpha = 4.34$, $R_e = 10$ and $St = 0.6$ in a 2D oscillatory channel flow, showing excellent agreement with the analytical solutions (lines). The effect of time shift is not observable.

5.6 Discussion and Conclusions

In this study, it has been shown that the lattice Boltzmann BGK model can be used to simulate time dependent flows in 2D within acceptable accuracy if suitable simulation parameters and accurate boundary conditions are used. We have conducted a number of 2D simulations for time-dependent flow in a channel with different boundary conditions. A shift in time has been observed and analysed. The lattice Boltzmann BGK model is more accurate when a half time step correction is added to the time coordinates. We have investigated the time shift association with the used boundary conditions, and have found that it is always present for the cases we have studied. However, the origin of this shift is not fully understood and is a subject for future research. The effects of the Womersley, the Reynolds and the Strouhal numbers have

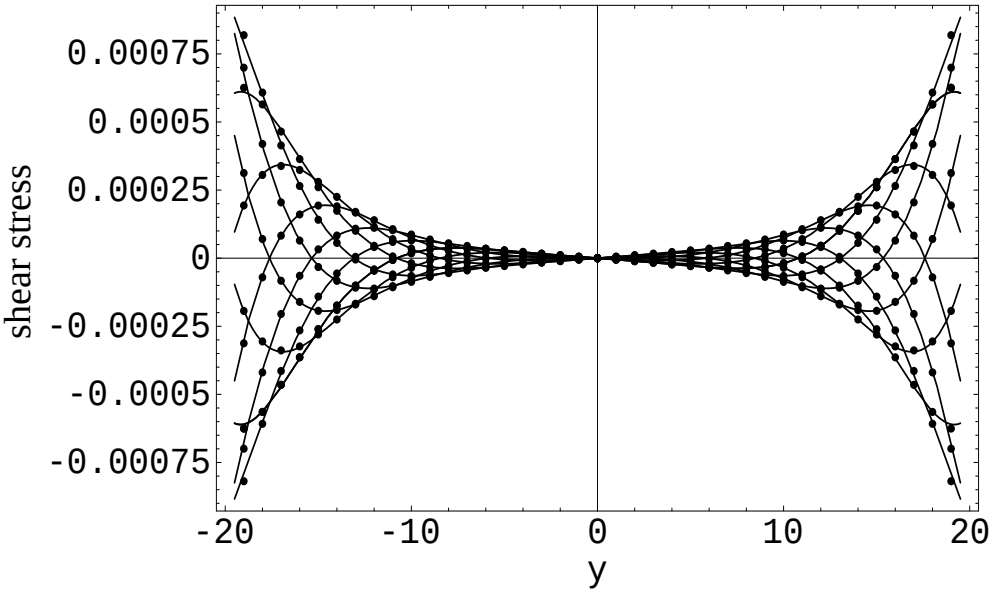

Figure 5.12: Shear stress (in Lattice Units) obtained from lattice BGK simulations (dots) for $\alpha = 7.7284$, $R_e = 1250$ and $St = 0.0152$ in a 3D oscillatory tube flow, showing excellent agreement with the analytical solutions (lines). The measurements are taken at each t = 0.1 nT where n = 0,1, ...,20.

also been studied in a number of simulations which showed that the shift in time is reduced at high Reynolds numbers. The obtained accuracy in time for time-dependent flows is of first order.

A quasi-incompressible D3Q19 model for the 3D simulations of oscillatory tube flow has recovered the analytical Womersley solution with average error of 15% when the bounce-back on the links boundary condition is used. The large error associated with the simple bounce-back rule may be attributed to the slip velocity, stair casing geometry and compressibility of the used lattice BGK model. The D3Q19 has been cited in the literature to result in large errors (He and Luo, 1997) when it is used to simulate time dependent flows, since the effect of the order $O(M^2)$ has to be taken into consideration. Incompressible models are encouraged and are under development in our group.

The bounce-back on a curved boundary recently proposed by Bouzidi *et al.* with linear interpolation has reduced the error to less than seven percent and didn't enhance the accuracy in the stress tensor calculations due to high velocity gradients close to the walls.

However, it has been reported that the lattice Boltzmann BGK model is thermodynamically inconsistent and that the forcing term leads to an incorrect energy balance equation if the acceleration is not constant in space (Luo, 2000). Therefore, it is argued that, it is better to use a general lattice Boltzmann model rather than the lattice BGK to overcome problems arising from artifacts in the lattice BGK model, since it

is not suitable for dense gases. Using the modified Lattice Boltzmann method that is derived from the Enskog equation confirms a proof of the Boltzmann H theorem and the forcing term recovers correct energy balance equations (Luo, 2000). On the other hand, the lattice BGK is simple and could yield satisfactory results if being used cautiously.

Chapter 6

Accuracy Versus Performance

The aim of this chapter is to tune the lattice Boltzmann parameters in order to achieve optimum accuracy and performance for time dependent flows. We present detailed analysis of the accuracy and performance of the lattice Boltzmann method in simulating pulsatile Newtonian flow in a straight rigid 3D tube and compare the obtained velocity profiles and shear stress to the analytical Womersley solutions. A curved boundary condition is used for the walls and the accuracy and performance are compared to that obtained by using the bounce-back on the links.

6.1 Introduction

Suitability and accuracy of the lattice Boltzmann method in simulating time dependent fluid flows has been demonstrated in the previous chapter. It was shown that use of curved boundary conditions noticeably enhances the accuracy as compared to using the simple bounce-back on the links.

Here, we further investigate the accuracy by considering the effect of Mach number on the accuracy and performance of the method. The aim of this study is to end up with optimum simulation parameters for a desired accuracy with minimum simulation time. Simulation parameters for fixed Reynolds and Womersley parameters are studied. We will present the relationship between the free parameters of the lattice Boltzmann and the constraints arising from running simulations under fixed Reynolds number and Womersley parameter at different Mach and Knudsen numbers. Then, we will discuss the convergence behaviour under different simulation choices; and set up the optimum conditions for best performance.

Time dependent LBM simulations involve higher density fluctuation, since the density and the unsteady pressure are tied up together through the ideal gas equation of state. Although there are a number of incompressible lattice Boltzmann models in existence, they are not yet popular as they degrade the simplicity and flexibility of the standard method. Therefore, we stick here to the standard quasi-incompressible D3Q19 model, previously described.

6.2 Simulations

In all simulations presented here, the flow rate in the tube is computed from a measured aortic pressure at the entrance; and its unsteady Fourier terms, up to the 8th harmonic, are used to set a suitable time dependent pressure gradient for obtaining an average Reynolds number $R_e = \frac{UD}{\nu} = 590$ and a Womersley parameter $\alpha = R\sqrt{\frac{\omega}{\nu}} = 16$, where $R = d/2$ is the radius of the tube, $\omega = 2\pi/T$ is the angular frequency and $T = 1/f$ is the period, with f being the number of heart beats per second. Pressure boundary conditions are used for the inlet and the outlet boundaries and, for the walls, either the bounce-back on the links (BBL) or the Bouzidi (Bouzidi *et al.*, 2001) boundary condition (BBC) is used. We have performed three different categories of simulations of systolic flow in a 3D rigid tube benchmark. The first set of simulations compares BBL with BBC. The second set deals with error behaviour and the third set investigates the convergence behaviour. They are all subsequently discussed.

6.2.1 Influence of the Wall Boundary Conditions

Since the lattice Boltzmann method is defined only for fluid nodes, distributions streaming into the fluid structure from non-fluid nodes need to always be evaluated. The way in which these distributions are defined imposes a boundary condition. A wall boundary condition is needed to evaluate distributions coming from solid boundaries, while inlet/outlet conditions are needed to drive the flow. For the walls, achieving the macroscopic non-slip boundary condition with correct momentum flux is always desirable. Boundary conditions in lattice Boltzmann algorithm may be evaluated in terms of these two constraints together with their convergence behaviour and viscosity independence. The first and still most popular wall boundary condition is the bounce-back on the links used previously by the lattice gas community (Lavalle *et al.*, 1991; Cornubert *et al.*, 1991). With the bounce-back rule, relevant distributions (coming from wall nodes) are simply reflected back to the direction they came from. The major drawbacks of the bounce-back rule are its slip velocity and first order behaviour. A number of enhanced bounce-back rules successfully increase the accuracy to second order and the slip velocity to zero (Skordos, 1993; Ziegler, 1993; Noble, 1995) but they increase the computational cost. Alternate, more complex and "computationally" more expensive body fitted second order boundary conditions have recently been introduced (Filippova and Hänel, 1998a; Yu *et al.*, 2002; Bouzidi *et al.*, 2001; Fang *et al.*, 2001). Apart from a few exceptions, these boundary conditions are viscosity dependent and slightly violate conservation laws. In the previous chapter, we have used oscillatory pressure gradient to compare the error associated with the body fitted Bouzidi boundary conditions (BBC) and the bounce-back on the links (BBL), in which we have reported that the accuracy associated with BBC is at least three times higher than that with BBL. In this work, we investigate the error behaviour for a complete systolic cycle which contains at least 16 harmonic terms. We find this necessary since the error doesn't scale linear in these harmonics because they have different ampli-

tudes with increasing Womersley parameters. Moreover, we compare here the error behaviour for the two boundary conditions at a fixed Mach number in order to know how much gain we get from using a more accurate, but rather sophisticated boundary condition, such as BBC, over the less accurate but rather simple BBL.
The diameter of the tube is represented by 74 lattice nodes and the tube length is $L = 148$ lattice nodes. First, BBL is used to simulate systolic flow in the tube. The simulation parameters are set to yield the required Womersley and Reynolds numbers which are kept fixed to the values mentioned above. For this simulation, $T = 2000, G = 1.1 \times 10^{-5}$, and $\tau = 0.55$. Samples of obtained velocity profiles at different times of the systolic cycle are shown in Fig. 6.1(a) compared to the real part of the analytical Womersley solutions

$$u(y,t) = \sum_{m=1}^{8} \left[-\frac{A_m}{\rho m\omega} e^{-im\omega t} \left(1 - \frac{J_0\left[\sqrt{mb}y\right]}{J_0\left[\sqrt{mb}R\right]} \right) \right], \tag{6.1}$$

where J_0 is the zeroth order Bessel function of the first type and $b = -i\omega/\nu = -im(\alpha/R)^2$ for the mth Fourier harmonic. The average Mach number is 0.05 for this simulation. As clearly shown in this figure, the agreement with the analytical solution is quite good. The relative error in velocity at each time-step is defined by

$$Ev = \frac{\sum_{i=0}^{n} |\vec{u}_{th}(\vec{x}_i) - \vec{u}_{lb}(\vec{x}_i)|}{\sum_{i=1}^{n} |\vec{u}_{th}(\vec{x}_i)|} \tag{6.2}$$

where $\vec{u}_{th}(\vec{x}_i)$ is the analytical solution for the axial velocity and $\vec{u}_{lb}(\vec{x}_i)$ is the velocity obtained from the lattice Boltzmann simulations. The overall relative error is averaged over the period and will be referred to as the average error. The bounce-back on the links yields an average error of 0.11 at a Mach number of 0.05 for this specific simulation. This indicates that, even with the bounce-back rule, acceptable accuracy can be obtained for engineering applications.
Using the same simulation parameters, we have conducted another set of simulations after replacing BBL with BBC. The agreement with analytical solutions enhances significantly, as shown in Fig. 6.1 (b) and the average error reduces to approximately 0.03.
In a separate study (Artoli *et al.*, 2002d), we have shown that it is possible to go for higher Mach numbers with curved boundary conditions while still having better accuracy than that associated with the BBL at a considerably low Mach number. We have shown that, even with a 10 times higher Mach number, the error associated with the curved boundary conditions is still better than that associated with BBL. It was also reported that using a curved boundary condition enhances the stability of the system and can reduce the simulation time since it allows higher Mach numbers than the simple bounce-back rule. It is therefore not recommended to use BBL for such case unless simulation parameters are changed towards low Mach numbers. However, reducing the Mach number slows down the convergence to equilibrium (Maier, 1996), unfortunately, as will be investigated in the next chapter.

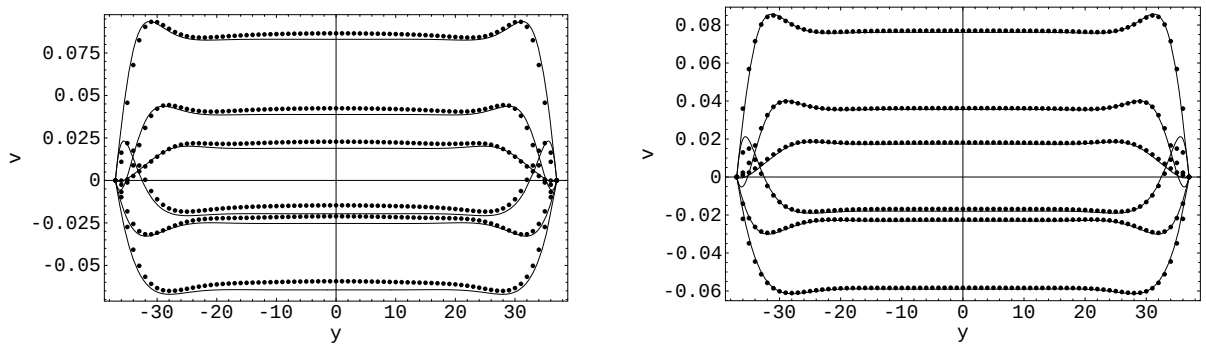

(a) (b)

Figure 6.1: Obtained samples of velocity profiles (dots) in lattice units during the systolic cycle in a 3D tube, compared to the analytical Womersley solution (lines) with: (a) BBL and (b)BBC2 wall boundary conditions.

6.2.2 Grid Refinement

In order to study the accuracy and convergence behaviour for the same physical problem under fixed Reynolds number (R_e) and Womersley parameter α, we need to tune our simulation parameters in a special way. The standard lattice Boltzmann method has several free parameters, but for pulsatile flow in rigid tubes, it is more convenient to tune the lattice viscosity ν, the Mach number M, the diameter D of the tube and the period T of the pulse. Changes in any of these parameters will result in changes in the space and time resolutions of the grid, and accordingly, the Mach and the Knudsen numbers. For lattice Boltzmann simulations the error behaviour is influenced by the Mach number, $M = \frac{U}{c_s}$, and the Knudsen number $\varepsilon \sim (2\tau - 1)/D$. The effect of these numbers arises as a compressibility error, given by (Holdych *et al.*, 2002)

$$\phi = \delta_x^2 \, R_e^2 \, \nu^2 \, c^2 \partial_t \rho \tag{6.3}$$

which increases with increasing Reynolds and Mach numbers, since $R_e = MDc_s/\nu$. As a function of Womersley number, the compressibility error can be written as

$$\phi = \frac{2\delta_x^2 c_s c^2}{\pi} \, \frac{\alpha^2 MD}{St} \, \partial_t \rho \tag{6.4}$$

where $St = Df/U$ is the Strouhal number. In this simulation, the dimensionless hydrodynamic numbers (R_e, α and St) and the Mach and the Knudsen numbers are all fixed. This implies that the grid must be refined, and/or the density gradients shall be small in order to reduce the compressibility error. Time-dependent flow with BGK involves high density gradients, as stated before. Therefore, we are only left with grid refinement. There are three different ways to do this;

1. **fixed M method**: in which the the diameter D, the period T and the viscosity ν are changed while keeping fixed the Mach number.

2. **fixed τ method**: by changing the diameter D, the period T and the Mach number M while keeping fixed the lattice viscosity ν, and

3. **fixed D method** : by keeping Fixed the diameter D while changing the viscosity, period and the Mach number.

The effects of these changes on the grid resolution are tabulated in Table 6.1, in which we assume an n times change in one of the parameters and compute the corresponding changes in the other parameters to return the fixed R_e and α. From this table, we can predict the computational efficiency of each approach. For instance, the fixed M approach involves n times decrement in δ_x (which increases the number of grids n^3 times) and n times reduction in δ_t which scales the simulation time by n^4. The fixed τ method scales the simulation time as n^5 and the fixed D method scales it as n. Although it is easy to tell that the last method is faster while the second one is more accurate, a combination of accuracy and performance is not trivial. The fixed M method does not involve reduction of the Mach number, which is a major contributor to error enhancement when considering time dependent flows and, therefore, it is not attractive in this study. Accordingly, we have performed two sets of simulations corresponding to the two left methods. These are discussed below.

Table 6.1: Relative changes in simulation parameters under fixed Reynolds and Womersley numbers with respect to an n times change in one of the parameters of a reference simulation.

Lattice Parameter	D'/D	ν'/ν	T'/T	U'/U	δ'_x/δ_x	δ'_t/δ_t	M'/M	ε'/ε
Fixed D	1	$1/n$	n	$1/n$	1	$1/n$	$1/n$	1/n
Fixed τ	n	1	n^2	$1/n$	$1/n$	$1/n^2$	$1/n$	$1/n$
Fixed M	n	n	n	1	$1/n$	$1/n$	1	1

Accuracy and Performance with the Fixed D Method

Based on Table 6.1, we have selected three sets of parameters to study the error behaviour produced by this technique. First, we have performed a reference simulation at $M = 0.5$ and $\varepsilon = 1/74$ with $\tau = 1$ and $T = 200$. Then, two other parameter sets are selected with the aid of Table 6.1. These parameters are listed in Table 6.2 which also lists the changes in M and ε and their multiplication for each simulation set. In Table 6.2, n = 1 represents a reference simulation, in which we set $\tau = 1$, the magnitude of the pressure gradient as $G = 0.0011$ and $T = 200$ to yield a resulted Mach number $M = 0.50$. The Mach number is reduced n times through increasing the period n times, reducing the pressure gradient $1/n^2$ times, and τ by a factor $\frac{1+n}{2n}$ in order to have the same Reynolds and Womersley numbers. In all simulations, the system is initialised from rest and the simulation ends after 40 complete periods. The BBL, BBC with first order interpolation (BBC1) and BBC with second interpolation (BBC2) were used separately for each parameter set to end up with 9 simulations. The simulations were

performed on 8 nodes of a Beowulf cluster using slice decomposition. The mean time per iteration is about 0.45 seconds using BBL and 0.47 seconds using BBC.

Table 6.2: Simulation parameters with respect to the reference simulation for which $\tau = 1, M = 0.50$ and $\varepsilon = 1/74$, . The average error associated with each set is shown for BBL, BBC1 and BBC2 boundary conditions.

T	200	2000	20000
n	1	10	100
τ	1	0.55	0.505
$\frac{G'}{G}$	1	1/100	1/10000
$\frac{M'}{M}$	1	1/10	1/100
$\frac{\varepsilon'}{\varepsilon}$	1	1/10	1/100
$\frac{\varepsilon' M'}{\varepsilon M}$	1	1/100	1/10000
Eav, BBL	instable	0.120	0.027
Eav, BBC1	0.0627	0.0352	0.0253
Eav, BBC2	0.0615	0.0102	instable

Samples of BBC1 obtained velocity profiles during the systolic cycle are shown in Fig. 6.2 for $M = 0.5$, compared to the analytical Womersley solutions. Although M is relatively high, the agreement with the analytical solution is still better than those obtained by a 10 times smaller Mach number with BBL shown in Fig. 6.1 (a). The last three rows in Table 6.3 list the average error associated with the three wall boundary conditions.
The combined influence of the boundary conditions and the Mach $\times$ Knudsen numbers is shown in Fig. 6.3 in which the three boundary conditions are tested at a fixed Mach number ($M = 0.05$). From this figure it is apparently clear that it would be necessary to use a curved boundary condition at the same Mach number. In Fig. 6.4 we show the computational time as a function of the Mach number, which assures a first order behaviour, as predicted above.
From this set of simulations, we conclude that it would be faster, more stable and more accurate to use a curved boundary condition than the simple bounce-back. In addition, we have noticed that the first order BBC, which interpolates data up to the first fluid node is more stable than the second order interpolation scheme, BBC2, which interpolates data using two neighbouring fluid nodes. This may be attributed to effects from interpolation in a region of large velocity gradients in the case of BBC2. It is worth noting that the error behaviour as a function of the sampling period T has been studied in the previous chapter (see also Artoli *et al.*, 2003e), showing error enhancement as the number of sampling points representing the period increases and behaves as first order in time instead of second order due to the compressibility effect of the D3Q19 model.

In summary, to obtain better accuracy, it would be more accurate to still use the

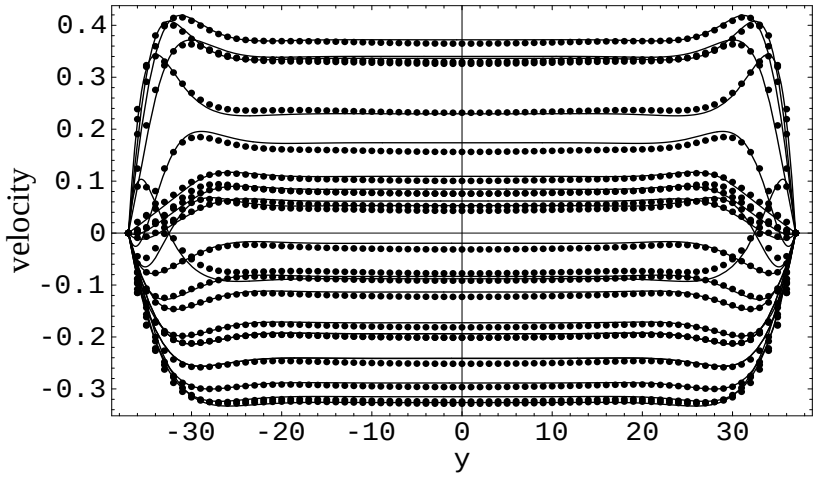

Figure 6.2: Velocity profiles at $M = 0.50$ using the BBC1 boundary condition with overall average error of about 0.07, still less than the BBL results at a 10 times lower Mach number. The system is instable with the BBL at this Mach number.

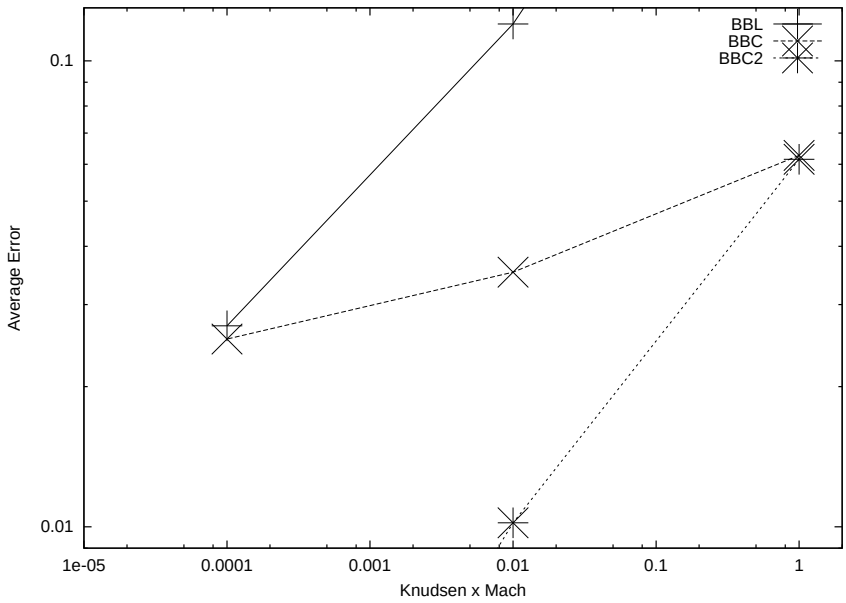

Figure 6.3: Average error behaviour as a function of Mach and Knudsen numbers, for the systolic tube flow using the BBL, BBC and BBC2 boundary conditions.

bounce-back on the links at lower Mach numbers than to use more sophisticated boundary conditions. For faster convergence, curved boundary conditions are pre-

Table 6.3: Simulation parameters used to enhance the spatial resolution. The mean relative error, Eav, is listed for each case.

D	21	65	105
n	1	3	5
T	40	360	1000
$\frac{G'}{G}$	1	1/27	1/125
$\frac{M'}{M}$	1	1/3	1/5
δ_t	1	1/9	1/25
Eav, BBL	0.2412	0.1189	0.0262
Eav, BBC	0.2301	0.0557	0.0262
Eav, BBC2	instable	0.0560	0.0266

Table 6.4: Temporal Local Relative Error, Ev (T) for BBL and BBC boundary conditions with $D = 65$ lattice nodes.

Time	0	10 T	20T	30 T	40 T	50 T
Ev(T), BBL	0.9950	0.2520	0.0698	0.0279	0.0200	0.0200
Ev(T), BBC	0.9950	0.2769	0.0615	0.0280	0.0200	0.0197
Ev(T), BBC2	0.9950	0.2747	0.2520	0.0866	0.0350	0.0560

Table 6.5: Mean, variance and mean deviation of the Relative error for BBL, BBC boundary conditions with $D = 65$ lattice nodes.

Boundary condition	Mean error (Eav)	Variance	Mean deviation
BBL	0.1189	0.0013	0.0219
BBC	0.0557	0.0027	0.0352
BBC2	0.0560	0.0027	0.0350

ferred than the bounce-back rule if the boundary is static.

Accuracy and Performance with the Fixed τ Method

In order to reduce simulation time, it is necessary to have a large time-step in a coarse grid at a high Mach number. To attain that, we use the fixed τ method to perform a set of simulations in which the period is set to a minimum possible value that leads to a stable solution on the coarsest grid. Then the corresponding values for the pressure gradient and the relaxation parameter are set to yield the desired Womersley and Reynolds numbers. The convergence behaviour is studied by grid refinement in both δ_x and δ_t, as explained in Table 6.1. The simulation parameters are listed in Table 6.3 together with obtained average errors associated with the three used boundary conditions. As this method results in reducing δ_x , δ_t and the pressure gradient,

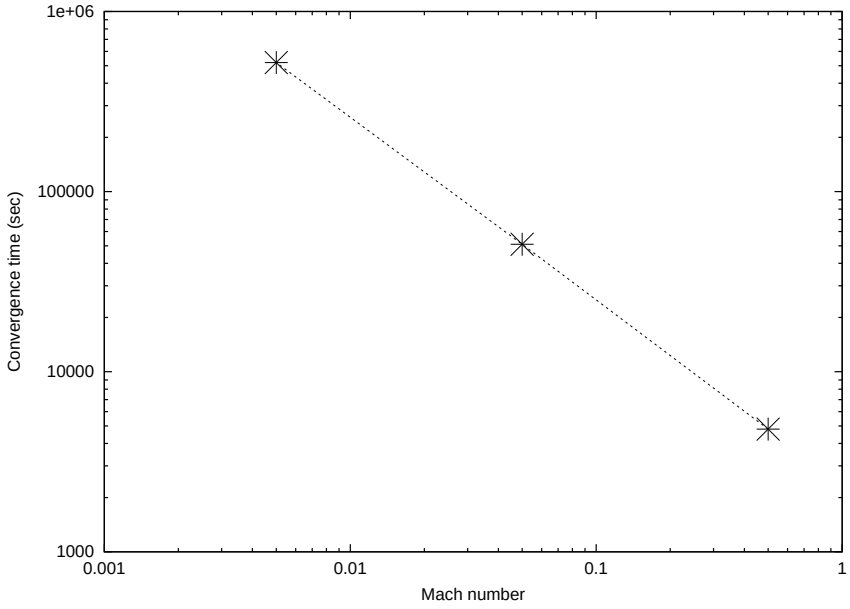

Figure 6.4: Convergence behaviour as a function of Mach number at fixed δ_x , obtained by using 8 processors and applying the BBC1 boundary condition.

both accuracy and performance are significantly enhanced, since all parameters influencing the error are under control. As is shown in Fig. 6.5, at least second order convergence behaviour is guaranteed with this method. Moreover, with this method, solutions with periods smaller than the fixed D method are stable and therefore the simulation time is less, but it scales as n^2.

The convergence behaviour as a function of time for this method is shown in Fig. 6.6, which shows the difference between the analytical and obtained velocity profiles at different simulation times. From this figure, we observe that the method converges to a reasonable accuracy after 40 complete periods, similar to the fixed D method, but with a major computational gain, since the length of the period is smaller (i.e. δ_t is larger). This figure also illustrates that the error localises near to the walls, where large gradients exist, and does not enhance noticeably near to the walls on the same grid. Table 6.4 lists the error dependence as a function of simulation times for BBL, BBC1 and BBC2 boundary conditions for a tube with $D = 65$ lattice nodes, with its mean, variance and mean deviations tabulated in Table 6.5. The error is reasonably comparable to that obtained by using the fixed D method. In conclusion, this method is computationally more feasible than the fixed D method and is recommended to use while keeping D and T to their minimum values that returns stable solutions.

6.2.3 Convergence Behaviour

Convergence of the lattice Boltzmann method to steady state is significantly affected by two local processes; initialisation and boundary conditions. In this section, we focus on the influence of these processes on the convergence behaviour.

Convergence and Walls Boundary Conditions

As mentioned above, boundary conditions need to be defined at walls, inlets and outlets. For the walls, two categories of boundary conditions can be recognised; bounce-backs and curved boundaries. The bounce-back rule is a very efficient boundary condition since it only involves a single memory swapping process for each relevant distribution on each node on the surface of the simulated object. For all curved boundaries, the exact position of the walls is determined at least once if the boundary is fixed and needs to be computed dynamically for moving boundaries. On its own this is more costly than using the bounce-back rule. In addition, using curved boundary conditions involves first or second order interpolation or extrapolation for velocity, distribution functions or density or a combination of some or all of them. As demonstrated above, use of a curved boundary condition enhances the accuracy but is computationally more intensive compared to the simple bounce-back at the same Mach number. To gain the accuracy of a curved boundary condition and a performance similar to the bounce-back, an accelerating technique recently introduced by the author (Artoli et al., 2003a) may be applied, as will be described in the next chapter.

Inlet and Outlet Conditions

For lattice Boltzmann simulations, a number of inlet and outlet conditions are available. The most commonly used are periodic boundary conditions, in which distributions leaving the simulation box at the outlet are re-injected at the inlets and vice-versa. Periodic boundary conditions involve only memory swapping operations which count as at least 10 times the cross section of the simulation box per time-step. Although they are fast, and accurate, they can only be used for periodic geometry. For non-periodic geometry, inlets and outlets need to be treated differently in the following manner:

- Velocity and pressure : assign one and compute the other (Zao and He, 1997), assign both (only for inlets) extrapolate or no flux normal to the walls (only for outlets).

- unknown distributions: compute explicitly, set to their equilibrium, copy from nearest neighbours, interpolate or extrapolate.

For the first item, if the velocity or the pressure are computed one from the other, at least 15 additions and two multiplications are needed per node on the boundary and

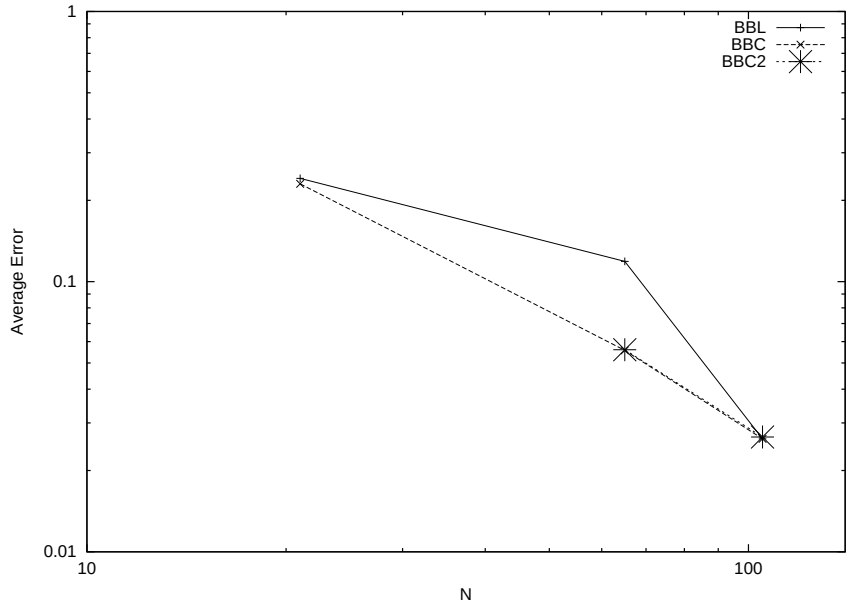

Figure 6.5: Convergence behaviour obtained by reducing the grid spacing n times, time-step n^2 times and increasing the period n^2 times, for the BBL, BBC and BBC2 boundary conditions as a function of grid points representing the diameter of the tube. The relaxation parameter is kept constant and the body force is reduced n^3 times to return the same Reynolds and Womersley parameters at $R_e = 1250$ and $\alpha = 16$.

therefore is at least 15 times more expensive than periodic boundary conditions. Extrapolation and no-flux schemes are far better in terms of accuracy and performance than computing velocity or pressure from one another, but they are only suitable for the outlets. A reasonable choice for time-dependent flow in irregular geometry is then to assign pressure and compute velocity at the inlet, no-flux at the outlets and set the unknown distributions to their equilibrium values. If the outlets are far enough from inflow, copying from upstream would be the most efficient outlet condition.

Initial Conditions

Time dependent flow involves large density fluctuations. Although it increases compressibility errors, this reduces the initialisation influence on convergence behaviour. However, the way in which the simulation box is initialised has little effect on the final flow fields. Since the Boltzmann equation assumes that the system is not far from equilibrium, a correct and reasonable initialisation technique is to set each distribution to its equilibrium with a small perturbation. We have adopted this initialisation process in all our simulations. It is noted that more sophisticated initialisation techniques such as second order interpolations from the boundaries may be useful but

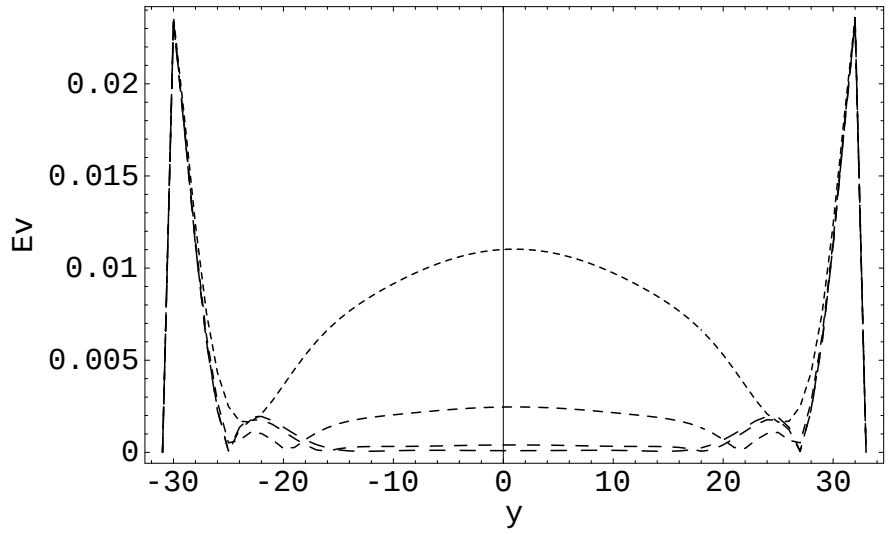

Figure 6.6: Local deviations from Analytical solutions, δE, computed for the velocity field at $t = 20T$ (top Curve), $30T, 40T$ and $50T$ (bottom curve). The diameter of the tube is represented by 65 nodes and the period is $T = 360$ sampling points. The average errors are tabulated in Table 6.3.

they complicate the standard lattice BGK scheme.

6.3 Summary

We have shown that the lattice Boltzmann BGK method is an accurate and efficient method as a solver for time-dependent flows. Different methods for performing time dependent flows at fixed simulation parameters are tested in terms of accuracy and performance. An aortic pressure is used as an inlet condition to drive the flow in a 3d rigid tube and the Womersley solution is recovered to an acceptable accuracy. Different grid refinement techniques to study error analysis and convergence behaviour are discussed. The influence of walls, inlet and outlet boundary conditions on accuracy and performance is studied in details as a function of Mach and Knudsen numbers. It is found that the bounce-back on the links could be more efficient if used at low Mach numbers when the Mach number annealing technique is used, as will be demonstrated in the next chapter.

Chapter 7

Optimisation Techniques

We present two adaptation techniques for the lattice Boltzmann method. First, the Mach number annealing is proposed for fast convergence of simulations of laminar time-dependent flows. The second technique is a test for the robustness of the method for interactive simulations. The first technique is an extension to the recent accelerated procedures for steady flow computations. Being based on Mach number annealing, the present technique substantially improves the accuracy and computational efficiency of the lattice Boltzmann method for such unsteady flows.

7.1 Necessity for Optimisation

In the previous chapters, we have demonstrated the suitability and investigated the accuracy of the standard lattice Boltzmann method in simulations of time-dependent fluid flows. We have also shown that use of curved boundary conditions significantly enhances the accuracy as compared to the bounce-back on the links. However, the bounce-back rule is still the most popular boundary condition, for its simple implementation and easy adaptation to complex geometry. Figure 7.1 shows temporal error behaviour in simulating a systolic cycle as a function of time, boundary conditions and Mach number. From this figure, it is shown that with the bounce-back, high order accuracy is only obtainable when the Mach number is very small (see the legend of the figure). This can be explained as follows. It is known that the bounce-back rule produces large errors of first order behaviour. In addition, simulations of time-dependent flows with the standard lattice Boltzmann model involve another major source of error: the compressibility errors. These two sources of error can be reduced significantly by reducing the Mach number. This, unfortunately, blows up the computational time needed for the simulation to converge. A current computational interest for all CFD solvers is to optimise simulation parameters for a desired accuracy with minimum computational cost. Within the lattice Boltzmann community, many efforts have been reported in this direction, mainly via implicit techniques (Tölke *et al.*, 1998; Verberg and Ladd, 1999) local grid refinement (Filippova and Hänel, 1998; Yu *et al.*, 2002) and scaling of the Reynolds number (Bernaschi *et al.*, 2002). Most of these techniques

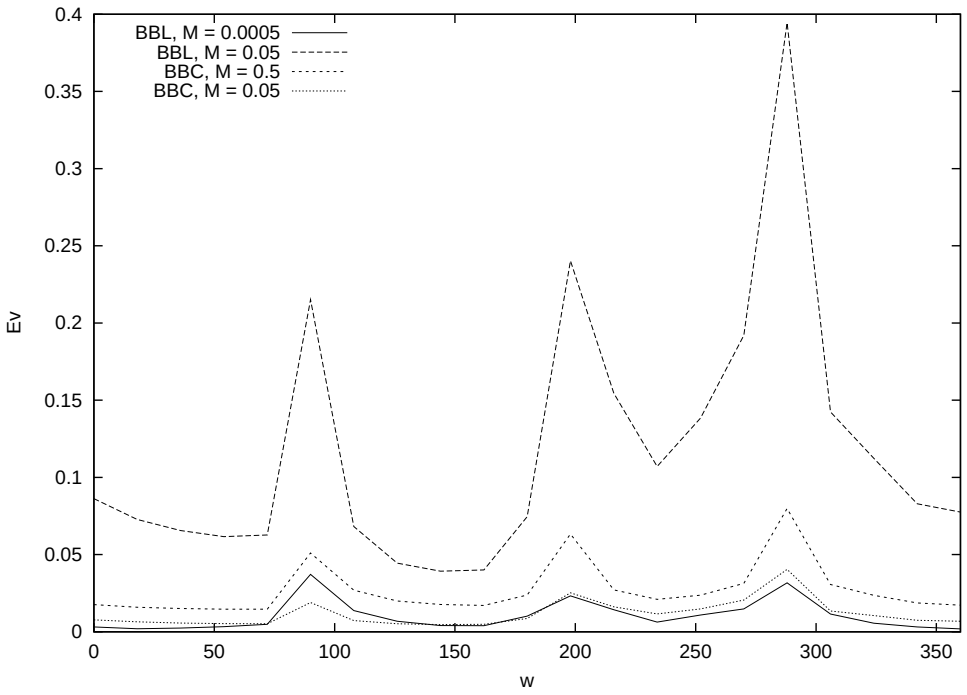

Figure 7.1: Error in velocity as a function of Mach number and boundary conditions for systolic flow in a rigid tube with $\alpha = 16$ and $R_e = 1150$.

are applied to steady flows and/or affect the uniformity of the Cartesian grid and hence complicate parallelism in the computations. For unsteady flows, time evolution cannot be avoided and the method is computationally expensive, especially when the physical time scale is very small (which is a characteristic feature of dynamic complex systems).

In this study, we extend these acceleration techniques to unsteady flows. The idea is based on stepwise reduction of the Mach number after the simulation converges with a higher Mach number. We call this process Mach number *annealing*.

The standard lattice Boltzmann model works pretty well as long as the Mach number M_a is low ($M_a^2 << 1$) and the density fluctuations are small. However, modelling unsteady flows involves higher density fluctuations, since the density and the unsteady pressure are tied up together through the ideal gas equation of state. Also, compressibility errors at high Mach numbers are expected. Although there exist a number of incompressible versions of lattice Boltzmann (e.g. He and Luo, 1997a; Guo *et al.*, 2000) they have not been clearly formulated and tested in three dimensions, and are not yet highly thought of. A number of generalised lattice Boltzmann equations are recently gaining more attention (e.g. D'Humiéres, 1992). They provide more stable and accurate solutions, but at relatively higher computational cost. Here, we have applied the widely used quasi-incompressible D3Q19 model previously explained.

7.2 Mach Number Annealing

The Mach number is defined as the ratio between the speed U of an object to the speed of sound

$$M_a = \frac{U}{c_s}. \tag{7.1}$$

Low-speed fluids ($M_a << 1$) can be considered as incompressible. As the Mach number approaches unity, compressibility effects need to be considered. The lattice BGK scheme involves a low-Mach number expansion of the Maxwell equilibrium distribution function and therefore, it introduces compressibility errors at relatively high Mach numbers.
In addition to the kinematic viscosity ν, the diameter D and the velocity U which define the Reynolds number as $R_e = \frac{UD}{\nu}$, a non-steady flow is characterised by a characteristic time interval, included in the Womersley parameter $\alpha = \frac{D}{2}\sqrt{\frac{\omega}{\nu}}$ or the Strouhal number, $St = \frac{Df}{U} = \frac{2\alpha^2}{\pi R_e}$ where $\omega = 2\pi f = \frac{2\pi}{T}$ is the angular frequency with f being a typical frequency and T the associated period of oscillation. An additional constraint comes from the fact that the accuracy of the lattice Boltzmann method reduces with increasing Mach number, especially for unsteady flows. The flow problem is completely defined by the geometry and these dimensionless numbers which take certain constant values. Now, in order to simulate at low-Mach number, we must decrease the velocity U and consequently decrease the viscosity ν to produce the same Reynolds number. However, since the Womersley and the Strouhal numbers are dependent on the viscosity and the velocity, the frequency must also be reduced. Explained in formulae, the velocity U is given by

$$U = \frac{R_e \nu}{D} = \frac{Df}{St} = M_a c_s \tag{7.2}$$

from which

$$M_a = \frac{R_e \nu}{c_s\, D}\ , \tag{7.3}$$

and

$$R_e = \frac{D^2 f}{\nu\ St}\ . \tag{7.4}$$

From these relations, we recognise that the Mach number M_a and the kinematic viscosity ν are directly proportional to the frequency of oscillation through

$$M_a = \frac{fD}{St\ c_s}\ , \tag{7.5}$$

$$\nu = \frac{fD^2}{St\ R_e}\ , \tag{7.6}$$

and

$$\nu = \frac{\pi D^2 f}{2\ \alpha^2}\ . \tag{7.7}$$

Eq. (7.5) implies that the frequency domain has to be reduced in order to have a low Mach number. This results in a considerable delay in the convergence behaviour. Eq. (7.6) shows that decreasing the frequency unfortunately results in pushing the simulation towards the instability region of the lattice BGK. Eq. (7.7) tells us that, for highly dynamic simulations (high α), we need to consider both low frequency and viscosity. These constraints end up with a computationally expensive slowly time evolving simulation. This poses a high demand on a prospective acceleration method. An annealing process to accelerate the lattice Boltzmann method was first reported by Bernaschi *et al.* (2002). It allows fast convergence by combining viscosity annealing with powerful linear iterative solvers for computing the inverse Liouville operator. Different from those for steady flows, time-dependent lattice Boltzmann simulation parameters are not easy to control within a running simulation since, among others, new physical and hydrodynamic constraints need to be satisfied. The flow is now characterised by the Womersley number, the Reynolds number, and the Strouhal number, as discussed above. These parameters need to be fixed during annealing since the dynamics of the flow is highly time-dependent. We apply the same idea for unsteady flows, but anneal the Mach number instead of the Reynolds number on a strictly fixed spatial grid. We assume that the Mach number is to be annealed n times and recall n as the annealing factor. In order to do that

$$n = \frac{M_a}{M_a'} = \frac{U}{U'} = \frac{f}{f'} = \frac{\nu}{\nu'} \ , \tag{7.8}$$

which implies that all the velocity (in terms of the driving force), the frequency of oscillation and the viscosity are to be reduced n times. This annealing strategy can be direct (1 level annealing) or multi-level. In the direct annealing strategy, after the simulation converges with a higher Mach number, the viscosity, the frequency and the driving force are reduced n times in a single step and the simulation converges to the final solution. The multi-level annealing strategy involves gradual reduction of these parameters towards n, depending on the stability and tolerance constraints. In other words, there are different ways to decide when to start the annealing. Examples of both direct and multi-level annealing methods are discussed in the next section.

7.3 Simulations

We consider time-dependent systolic flow in a rigid tube of diameter $D = 63$ lattice units as a benchmark for our simulations. The first 8 harmonics of a pressure pulse, measured at the entrance of the human abdominal aorta, are used to apply an inlet condition for the tube. We have selected this complex time series for the sake of generality. For the outlets, constant density is applied. The velocity and the unknown distributions are computed from the density. For the walls, the bounce-back on the links is used. For all simulations the Womersley number is kept constant at $\alpha = 16$ and the average Reynolds number is $R_e = 270$. The simulation starts at average $M_a = 0.5$ ($T = 360$ and $\nu = 0.068$) and waits until the system builds up its knowledge

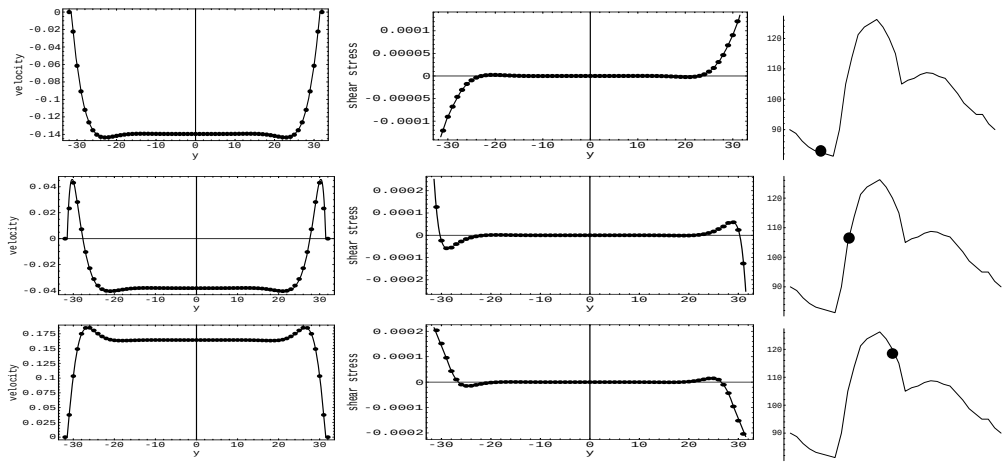

Figure 7.2: Obtained (dots) velocity profiles (left) and shear stress (middle) in lattice units during the systolic cycle (right), compared to the analytical Womersley solution (lines) for the 3D tube benchmark. The dots in the right column indicate times at which the profiles are shown. For this simulation $\alpha = 16$, $R_e = 270$, and $M_a = 0.1$.

about the pulsatility and non-linear behaviour and converges after about 40 complete periods. Obtained simulation results are compared with the real part of the analytical Womersley solution given by Eq. (6.1).
The average error at $M_a = 0.5$ is 15%, originating from both compressibility effects and wall boundary conditions. Next, we reduce the Mach number to obtain good agreement with the analytical solution. We have previously studied the effect of reducing the Mach number on the accuracy for this benchmark (Artoli *et al.*, 2002d). Fig. 7.2 shows sample simulation results for three different time frames after reducing the Mach number to $M_a = 0.1$. The new simulation parameters are computed from Eq. (7.8) after substituting $n = 5$ and including the initial simulation parameters. The average error is reduced to less than one per cent. However, since the period increases 5 times, the computational time increases with the same factor. The aim of Mach number annealing is to accelerate convergence to equilibrium by reducing the percentage tolerance in mass and momentum, computed by comparing similar points for each two successive periods. The mass tolerance is defined as

$$M\ tolerance\ \% = \frac{M(t) - M(t-T)}{M(t-T)} * 100 \tag{7.9}$$

and the momentum tolerance is defined accordingly.
In typical simulations, we accept convergence below 0.1% for the momentum. We have performed three simulation sets for the systolic tube flow benchmark - one without annealing with the lowest desired Mach number, having $T = 1800$ and $\nu = 0.01353$. The pressure gradient is scaled to obtain a Mach number of 0.1 . Fig. 7.3 (a, b) shows the relaxation of tolerance in mass and momentum from which we see that it takes

quite a long time to dampen the initial oscillations in tolerance (more than 72000 time-steps). The second set of simulations is conducted using 4 levels of annealing by reducing the Mach number after each 60 periods of the basic simulation. In detail, the Mach number is reduced to 0.4, 0.3, 0.2 and finally 0.1 directly after 60, 120, 180 and 240 complete periods of the basic simulation, respectively. The results are shown in Fig. 7.3 (c, d), from which we notice that the mass and more strongly the momentum converge much faster with the annealing process. The momentum tolerance is usually several orders of magnitudes higher than that for the mass, and hence, has more influence on the accuracy of the flow fields.
The third set shows a one-step annealing in which simulation parameters are directly tuned to the final Mach number ($M_a = 0.1$) after convergence of the basic simulation in which $T = 360$ and $M_a = 0.5$. The direct annealing strategy significantly accelerates the relaxation towards equilibrium (see Fig. 7.3 (e,f)), since it significantly reduces compressibility errors earlier than the multi-level annealing process. For the non-annealed case, it takes a long time for the momentum to relax with a tolerance similar to the directly annealed simulations. In terms of numbers, the direct annealing strategy is at least 3 times faster for a 5 times annealed Mach number. The gain in computational time is higher if the ratio between the two Mach numbers is larger, since the order in the tolerance seems to depend only on the tolerance of the initial simulations rather than the annealing factor. The short-living spikes in Fig. 7.3 may be attributed to two reasons. First, since the systolic cycle is composed of many harmonic terms, values of point mass and momentum do not converge simultaneously. Compressibility errors at high velocities are also large. This explains why the spikes disappear with direct annealing, since the Mach number is reduced significantly.

7.4 Changing Geometry

In this section, we present the capability of the lattice Boltzmann method as a robust technique for interactive blood flow simulations, by considering the case of a phototypical symmetric bifurcation with a changing geometry. During vascular surgical planning, we envision that different geometrical solutions need to be tested on the patient's anatomical image provided by a suitable imaging technique. Conventionally, with NS solvers, for each newly suggested geometrical solution S_N, the previous solution S_O is discarded, a new grid G_N has to be generated and the simulation has to be restarted to obtain the solution S_N. This may take considerable amount of simulation time. However, there are some CFD methods which are fully adaptive, such as the finite difference methods. In this section, we present primitive results on adaptivity of lattice Boltzmann method. Given a geometry $G(t_0)$ at time t_0, we first run the lattice Boltzmann solver towards obtaining the solution $S(t_0)$ while monitoring for a new geometry, not too different from the previous geometry. If at time t_i the user introduces a new geometry $G(t_i)$, the simulation instantaneously adapts to the new grid and resumes towards obtaining the solution $S(t_i)$ without a need to restart. The user may end up with a solution S_N for the geometry $G(t_N)$. If the lattice Boltzmann

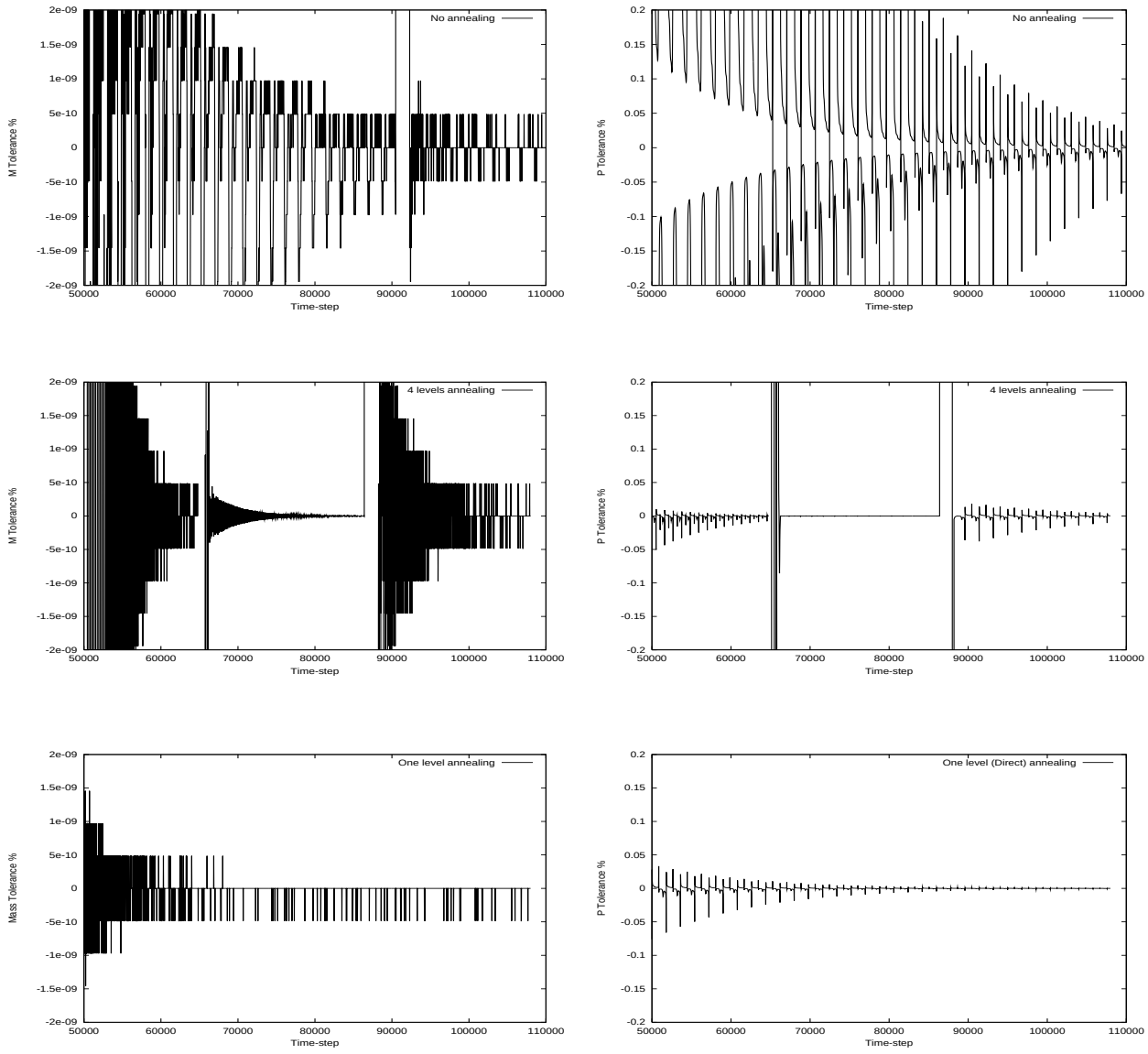

Figure 7.3: Comparison in mass- (left) and momentum (right) tolerance as a function of the number of time-steps , between non-annealed (upper row), 4 levels annealed (middle row) and directly annealed (bottom) simulations. The Mach number is reduced 5 times in the annealed simulations (from 0.5 to 0.1).

method is robust enough, the simulation time from t_0 to t_N could be less than the sum of convergence times T_i^0 for each individual simulation, i.e. $t_N - t_0 < \sum_{i=0}^{N} T_i^0$. Moreover, the accuracy in S_N must be the same as the solution $S_N(restart)$ which is obtained by restarting the simulation. This is shown consequently.

We have conducted a number of 2D simulations on the bifurcation benchmark in-

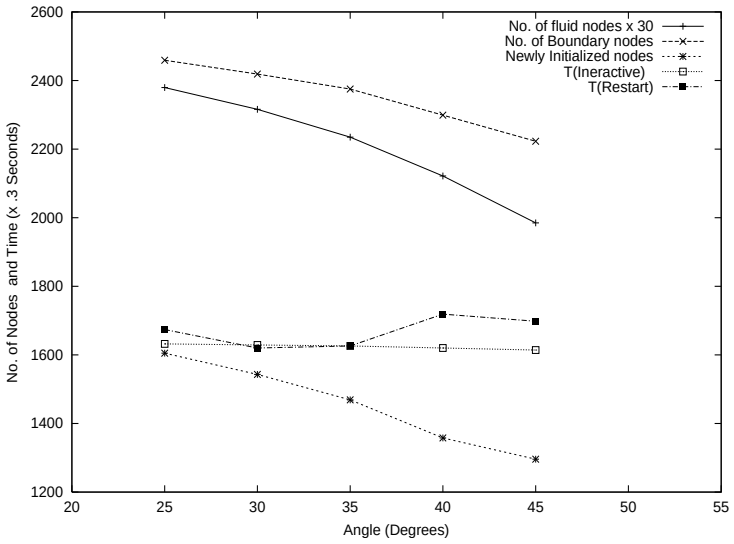

Figure 7.4: A lattice Boltzmann Comparison between interactive simulations and restarted simulations in terms of simulation time for a symmetric bifurcation benchmark.

troduced in the previous section, though allowing the bifurcation angle θ to change during the simulation after equal number of time steps. We have selected this benchmark for its similarity to the planning of a bypass for a diseased artery, where, the surgeon tries different paths to implant the host artery.

The simulation starts at $t_0(\theta)$ at $\theta = 20^o$ and the system evolves towards the solution $S(0)$ a number of time steps i. At time $t = i$, the angle is increased by $\delta\theta$ and the simulation resumes towards the solution $S(i)$ for the geometry $G(i)$ another i number of time step after which the geometry $G(2i)$ is introduced and so on, till we end up with $\theta = 80^o$ as our final G(N) geometry. The simulation then converges to the solution $S(G_N(ni))$. In lattice Boltzmann method, the system converges directly after the mass and momentum reach a given tolerance, chosen to be less than 10^{-5} for momentum and less than 10^{-9} for mass.

Technically speaking, the initialisation and the update of the new geometry are the critical factors which have direct influence on the total simulation time, while the choice of boundary conditions affects both stability and simulation time. In this experiment, we have tested two simple initialisation techniques. In both methods, only if the status of a node in the simulation box is changed from fluid to solid or from solid to fluid, will the node need initialisation. One way to initialise is to put these nodes to their equilibrium distributions which involves more computational time than the other simpler initialisation method such as assigning them to an average value. It is noted that the system forgets about the initialisation method in a short transitional time t_{trans}. Figure 7.4 shows the total number of nodes, the number of nodes to be updated and the total simulation time for interactive and restarted simulations. As shown in this figure, the total simulation time during an interactively changing geometry is in general smaller than the total simulation time for each individual sim-

ulation. This reflects a nice feature of the lattice Boltzmann method and makes it quite suitable for interactive simulation environments. However, the computational gain is less than 10% in this specific case. Application of acceleration techniques has proven to be feasible (Bernaschi *et al.*, 2002). It is noted that other Cartesian grid CFD techniques may share this feature with the lattice Boltzmann method, but the body fitted grid solvers such as the finite element methods will be faced with the time it takes to adapt the new mesh. We are now using the lattice Boltzmann as a core simulation system for an interactive virtual vascular treatment environment using high level architecture (HLA)and a virtual 4D CAVE environment for interaction and visualisation (Belleman *et al.*, 2000; Zhao *et al.*, 2002).

7.5 Conclusions

In this chapter we have presented a numerical technique to accelerate laminar time-dependent lattice Boltzmann simulations through annealing of the Mach number during simulations, either directly or in a multi-level strategy. In both cases, the simulation is performed on a fixed grid and the viscosity, the Mach number, and the frequency are annealed by the same annealing factor. Considerable gain in computational time compared to that for the non-annealed standard lattice Boltzmann simulations is observed. We have shown that direct annealing of the Mach number is faster than the multi-level one. Since it works on the same grid, the Mach number annealing technique does not affect the parallelism of the uniform lattice Boltzmann Cartesian grid. Our current research concentrates on the optimisation of different annealing strategies of the Mach number for best acceleration. The capability of the lattice Boltzmann method for interactive simulations has shortly been demonstrated through studying flow in a changing geometry. It has been demonstrated that the lattice Boltzmann solver can be an adaptive flow solver without considerable difficulties.

Chapter 8

The Real Thing

Based on the arguments raised on the previous chapters, in this chapter, simulation results of steady and unsteady flow in a realistic model of the human aortic bifurcation reconstructed from Magnetic Resonance Angiography are presented as a typical haemodynamic application. Velocity fields and shear stress are computed and results are compared to those available in the literature.

8.1 Introduction

Flow characteristics near branches and bifurcations are quite important in haemodynamics: Cardiovascular diseases are considered as a leading cause of death in the developed world and are now becoming more prevalent in developing countries (World Health Organisation, 2002). Most of these diseases localise in regions of complex geometry of the arterial tree. The flow fields and shear stress play important roles in understanding, diagnosis and treatment of such diseases. Although being studied by many authors (e.g. McDonald, 1960; Caro *et al.*, 1974; Ku *et al.*, 1985; Moore *et al.*, 1994a, 1994b and 1994c; Reneman *et al.*, 1993; Taylor *et al.*, 1996; Gijsen *et al.*, 1997; Vorp *et al.*, 1998; Wootton, 1999; Ku, 1999), the relation between flow fields and cardiovascular diseases is still not fully understood, and is currently receiving more and more attention (Botnar *et al.*, 2000, Berthier *et al.*, 2002; Cheng *et al.*, 2002).
There have been many reports relating low and oscillatory shear stress to atherosclerosis in large arteries. For a recent review, we refer to Shaaban and Duerinckx (2000). Frequently, the treatment of an arterial disease involves implanting a new host artery as an additional or a replacement to the diseased one, or design of a cardiovascular device. These are quite difficult to plan and have to be tailor made for each specific patient.
Recently, two major developments in the field of vascular surgery planning have made it possible to better and faster plan risk reduced implantation: firstly, magnetic resonance imaging angiography (MRA)[1] has been significantly enhanced to provide ex-

[1] use of Magnetic Resonance Imaging to produce detailed pictures of the blood vessels.

cellent images of the arterial tree and non-invasive dynamic data acquisition is made possible (Goyen *et al.*, 2001). Secondly, the development of cheap computing power and interactive simulation environments have made near real time simulations not far from reach (Taylor *et al.*, 1999; Bellemann and Sloot, 2000; Zao *et al.*, 2002). With these in hand, an efficient and robust flow solver can be used as an interactive modelling environment. There are various successful computational fluid dynamics (CFD) methods commonly used here, such as the finite element methods, the finite difference methods and the finite volume methods. All these techniques are well established, but they yield two major difficulties. These are the non-trivial and time consuming grid generation, and the necessity to solve the Poisson equation for the pressure field.

On the other hand, the conventional flow solvers such as the finite element methods and the finite difference methods are accurate and efficient. However, their applicability to problems involving complex and moving geometry is complicated, due to their strong dependence on time consuming mesh generation. The Navier-Stokes (NS) equations can now be solved with mesh-free algorithms (Batina, 1993) which are unfortunately not flexible enough due to errors attributed to numerical viscosity and to difficulty in improving the space and time accuracy. Dynamic mesh generating techniques have been reported recently (Taylor *et al.*, 1998).

New particle based methods such as dissipative particle dynamics, lattice gases and lattice Boltzmann methods have been developed and matured (Mcnamara and Zanetti, 1988; Higuera and Succi, 1989; Qian *et al.*, 1992; Aharonov and Rothman, 1993; Behrend, 1995). These mesocopic techniques may be quite useful for haemodynamic research, as, among other features, they are more flexible in dealing with multicomponent fluid flow problems. In this study, we use the lattice Boltzmann BGK method, shortly described in the next section.

Since the shear rate in the aorta is higher than $0.1s^{-1}$, we consider blood to be Newtonian. We also ignore the elastic behaviour of the aortic walls for its minor effects on the flow fields in the aorta.

As time dependent flow simulations are known to be computationally expensive, a need for an efficient flow solver is crucial. Traditional Navier-Stokes solvers frequently use artificial compressibility and pressure projection methods to accelerate convergence. In this study, we present the capability of the lattice Boltzmann BGK method as a robust technique for systolic Newtonian flow in a a complex model of the human abdominal aorta reconstructed from MRA images of a volunteer.

Different from the traditional CFD methods which obtain the velocity and pressure by solving the Navier-Stokes equations and compute the shear stress from the velocity profiles, the lattice Boltzmann BGK method is a special finite difference equation of the simplified Boltzmann BGK equation which describes transport phenomena at the mesoscopic level. From the previous chapters, it has been realised that solving the lattice Boltzmann equation has three main advantages over solving the Navier-Stokes equations: first, it works with fast and easy to generate Cartesian grids while it still yields accurate results of second order in space and time. Secondly, the pressure is simply a linear function in the speed of sound ($p = \rho c_s^2$) while the NS solvers need to

solve the Poisson equation. Finally and most important for the field of haemodynamics, is the fact that the stress tensor can be directly obtained from the non-equilibrium parts of the distribution functions, independent of the velocity fields, while a need to get the derivative of obtained velocity profiles is not avoidable when NS solvers are used. The non equilibrium parts of the distribution functions are computed during collision steps to relax the system towards equilibrium. Therefore, no considerable computational cost is needed to compute the stress. All these advantages make the lattice Boltzmann method a promising candidate for simulating time-dependent blood flow in arteries.
In the last two chapters, it has been demonstrated that the lattice Boltzmann method can easily be adapted to simulate time dependent flows. Since it is a linear function in the pressure, time dependent density gradients can be implemented to represent a systolic flow rate quite easily. A range of values of Womersley parameter can be simulated without affecting the stability of the model. All kinds of inlet and outlet boundary conditions, usually used in computational haemodynamics can equivalently be implemented. The robustness of the method appears in the straightforward parallelisation of the easy to generate Cartesian grid. On the other hand, since it is implemented on a Cartesian grid, very fine grids need to be generated to simulate flow in complex geometry. Filippova and H*ä*nel (1998) have overcome this problem by considering local grid refinement.

8.2 Flow in the Abdominal Aorta

Atherosclerosis mainly occurs in focused locations of large and medium arteries such as the carotid bifurcation, the coronary arteries, the abdominal aorta and the iliac and femoral arteries at regions of low and oscillating shear stress, independent of other risk factors (Shaaban and Duerinckx, 2000). In the human abdominal aorta, the lateral and posterior walls of the aorta distal to the inferior mesenteric artery (IMA) are highly susceptible for Atherosclerosis. These regions are known to have low and oscillating shear stress (Gibson *et al.*, 1993; Oshinski *et al.*, 1995; Taylor *et al.*, 1998). From the arguments raised previously and the conducted benchmark experiments presented earlier in this thesis, we are further encouraged to explore the capability of the lattice Boltzmann method in simulating a more realistic geometry of interest to Biomechanics. We choose to study flow in a model of the human abdominal aorta as an example. The model is reconstructed from a magnetic resonance angiography of a volunteer. The pressure gradient at the entrance of the aorta is averaged from flow rate obtained from literature (Moore *et al.*, 1994c; Taylor *et al.*, 1999). The computational model under study involves only the bifurcation region, directly after the IMA, and includes parts of the left and right iliac arteries (see Fig. 8.1). The complete model of the abdominal aorta, including the celiac, mesenteric and renal branches is currently under study.
Many studies on the flow in the abdominal aorta have been reported, all related the cause of the focal nature of the disease mainly to the complex nature of the shear

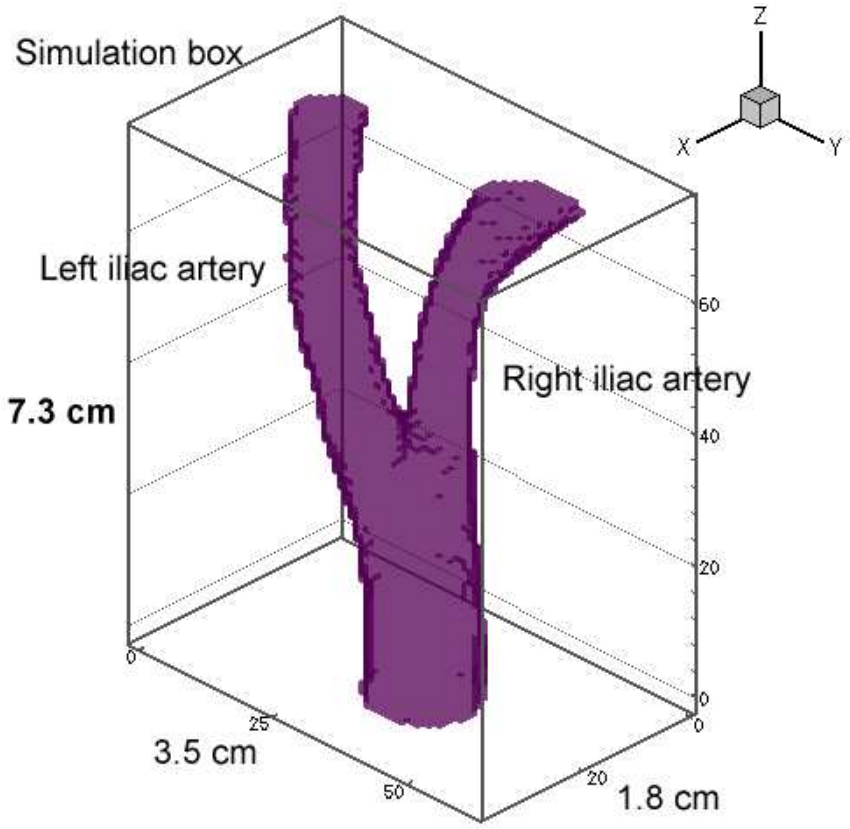

Figure 8.1: An MRA reconstructed model of the aortic bifurcation with left and right iliacs. The right iliac is more bent than the left one. The computational grid size is $37 \times 61 \times 73$ nodes.

stress profiles in these regions. Several investigations have been discussed in literature. Moore *et al.* (1994a) computed the shear stress in a model of the human abdominal aorta under resting and exercise conditions from MRA measured velocity data and extracted six shear stress indices influencing the locality of Atherosclerosis: mean (over the cardiac cycle), maximum and minimum, pulse (maximum - minimum), negative index, NEG (fractional time during which the shear stress stays negative) and oscillatory shear stress index (OSI). Reneman *et al.* (1993) used experimental and computational models to study flow in bifurcation regions. Gijsen *et al.* (1997) suggested a new experimental technique to determine the wall shear stress *in vivo*. Vorp *et al.* (1998) used a coupled fluid structure interaction model to combine the influence of mechanical stress and wall shear stress and concluded that the arterial diseases most probably localise in regions of high mechanical stress and low wall shear stress. However, the mechanical stress within the wall cannot easily be extracted unless further development in imaging techniques and image segmentation algorithms are achieved. In this study, we use Eq.(3.22) to compute the 9 components of the sym-

metric stress tensor, i.e $\sigma_{\alpha\beta}$ which represents the stress component in the β-direction acting on the element with outward normal in the α-direction. Since the components of any second order tensor can be reduced to an eigenvalue problem, it is possible to transform the second order stress tensor into an eigenvalue problem and extract the principal stresses λ_1, λ_2 and λ_3 with their eigen vectors. These can be visualised as a quadric surface (elliptical glyph), but in biomechanics, the traction forces, shear stress and the von Mises effective stress are commonly used. The traction forces are orientation dependent and need the surface normals. However, the von Mises effective stress, usually available in visualisation packages, is computed from the second invariant of the stress tensor (see the next section) and is more suitable for Cartesian grids than the surface traction, as the Cartesian grids introduce more approximation when computing surface normals. The von Mises stress is commonly used in biomechanics to determine the effective stress (e.g.. Raghavan and Vorp, 2000). In this study, we will focus on the time-behaviour of the effective von Mises stress.
For our simulations, a smoothed MRA image was provided by Charles Taylor, Stanford University, U.S.A, with original resolution of 512 x 512 x 64 voxels, each voxel occupies 1 byte. The spacing between each two successive recorded cut planes is 0.9375 mm. An image segmentation algorithm is applied to the original data set to extract the aorta and the segmented aorta is then cropped and filtered to end up with the simulation model shown in Fig. 8.1. It is worth noting that there is a limitation

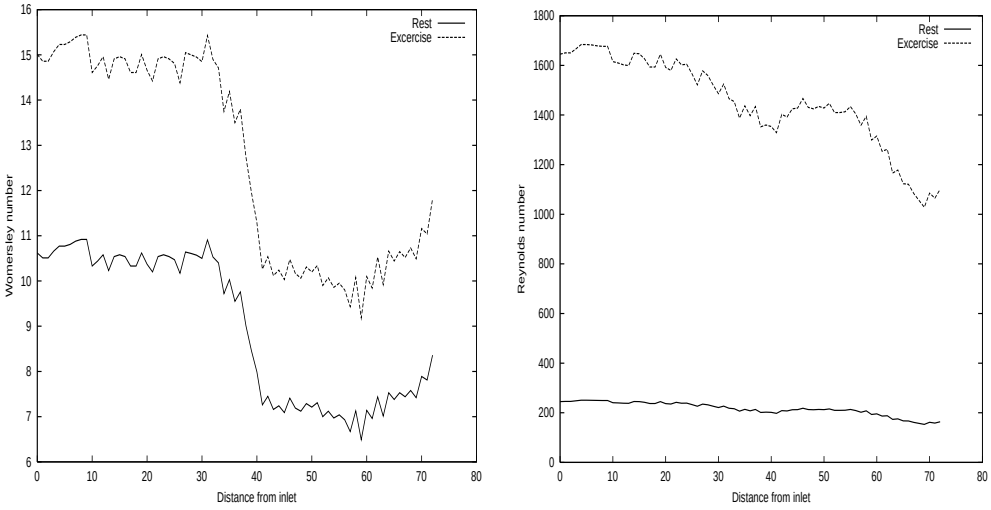

Figure 8.2: Change in Womersley parameter(left) and Reynolds number (right) along the segmented aorta during resting and exercise conditions.

to obtaining high resolution non-invasive and low noise images. To have a stable solution in the lattice Boltzmann method, the relaxation time τ must be greater than 0.5 in order to have a positive fluid viscosity. Having a Reynolds number R_e within a diameter nD, n being the spatial resolution of the image, for a fluid of blood viscosity, will result in a relaxation time of $0.5 + 0.3nD/R_e$. Therefore, the stability scales linearly with the spatial resolution. We have conducted a number of steady and

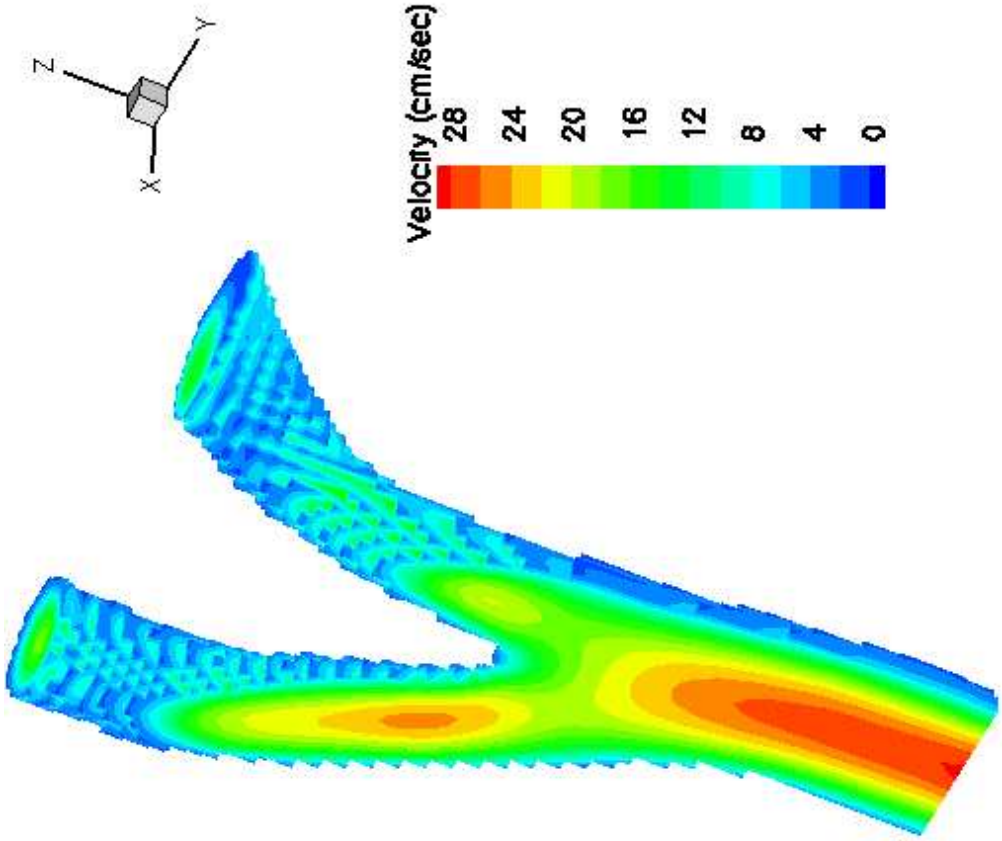

Figure 8.3: Steady flow in the aortic bifurcation. The maximum Reynolds number is 1500.

unsteady flow simulations for the aorta model. As the cross section of each slice is irregular, the Reynolds number is redefined as $Re = 4mU/\nu = \frac{4Q}{\nu P}$ and the Womersley number is defined as $\alpha = 2m\sqrt{\omega/\nu}$, where m is the mean hydraulic depth which is the ratio between the vascular bed A and the perimeter P. Figure 8.2 shows changes in the Reynolds and the Womersley numbers downstream of the aortic model under resting and exercise conditions, assuming a flow rate of 0.8 l/min with 65 beats/min under resting and 5.36 l/min with 130 beats/min for exercise conditions (Moore and Ku, 1994d).

The steady flow simulations are performed to asses the steady flow behaviour and to check the validity of the used inlet and outlet conditions. We have used the bounce-

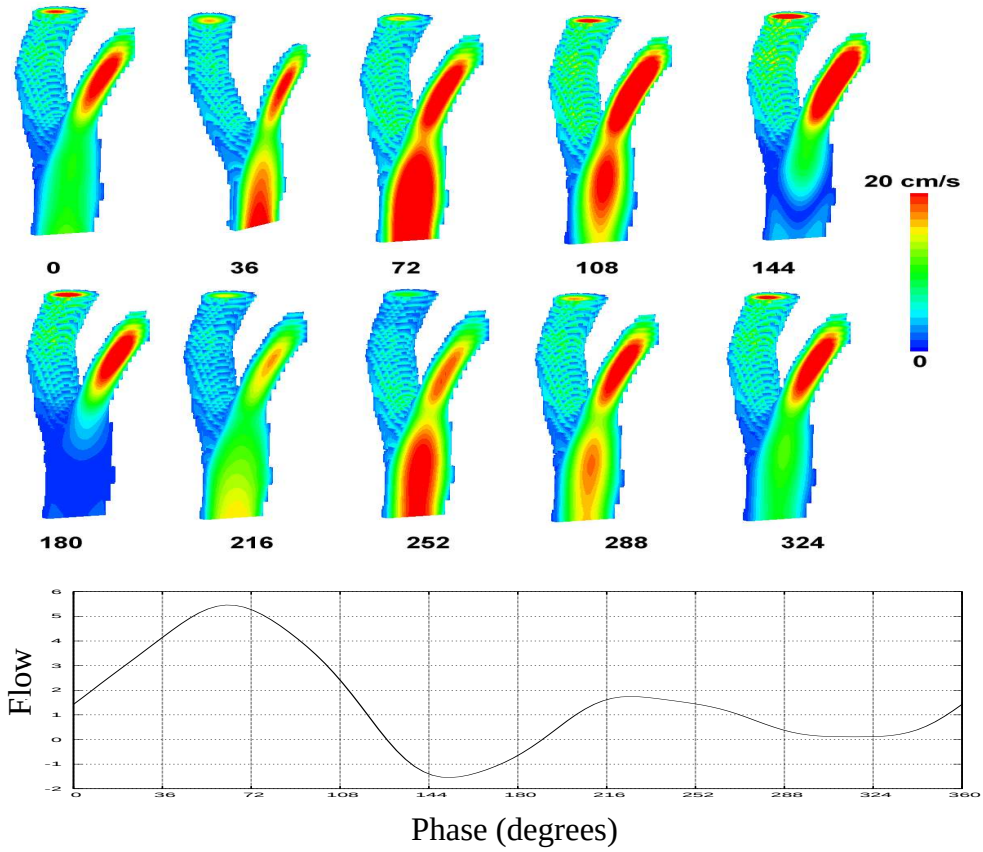

Figure 8.4: Velocity profiles in the aortic bifurcation computed at every 36^o of the cardiac cycle, at 120 heart beats/min and a flow rate of 90 cm^3/sec

back rule as a wall boundary condition. For the inlet, we use an assigned inlet pressure to compute the inlet velocity (Zou and He, 1997) and assign equilibrium values for unknown distributions. The outlet conditions are assigned accordingly with an outlet pressure. The maximum Reynolds number is 1500. A velocity snapshot of steady flow is shown in Fig. 8.3, from which we observe that the bended branch of the aorta (the right iliac in this case) has less entrance velocity than the less curved one (the left iliac). The velocity gradients before the bifurcation are smaller near to the right lateral wall than those on the left lateral wall and the shear stress is expected to be smaller. Also, the posterior wall receives less flow than the anterior wall and a similar conclusion may be drawn. However, the unsteady nature of the locality of low shear stress may be different as will be explained later.

For the unsteady flow simulations, an aortic pressure waveform is applied at the entrance of the aortic model. Velocities are then computed from the distribution functions coming from downstream, and the unknown distributions are set to their equilibriums. At the two outlets, constant pressure is applied. The total simulation time is 2 hours on a single processor and reduces to 40 minutes when using 4 nodes. We assume that the system converges after the change in conserved quantities (mass and

momentum) is less than 2×10^{-5}%. This results in an error that is less than 1% when simulating rigid circular tubes, as claimed in the previous section. At least 40 complete periods are needed to converge to the simulation criterion. Although it seems longer than the required periods when using a finite element solver, the total simulation time per period is far less. On a single processor, a period represented by 240 time-steps takes approximately 3 minutes. Flow fields and shear stress are recorded during the last cycle as separate frames for each time-step. The phase of the full cardiac cycle (360^o) is split into a number of frames (vertical lines in Fig. 8.4) and each frame is named after the corresponding phase angle. Vector magnitudes of velocity profiles at 10 frames are visualised in Fig. 8.4.

At the beginning of systole (frame 0), the flow is relatively simple through the bifurcation model, except for a small velocity of maximum magnitude 5.0 cm/sec near to the walls of the main branch. As the flow is increased (frames 36 and 72), the velocity increases rapidly in the main branch and slowly in the iliacs. The left iliac receives more flow than the right one (see the change in the red dot on top of the branch). Close to the Aortic bifurcation, negative velocities of small magnitudes are frequently observed (see Fig. 8.5). The flow then relaxes towards the end of systole (frame 108). After that, a complex nature of the flow takes place in the main branch (see frames 144 and 180), involving two conjugate vortexes and flow mixing. This is clearly illustrated by streamlines shown in Fig. 8.6. It is worth noting that, although the flow reverses in the main branch during this period, the flow at the exits is forward on average. This demonstrates the function of the aorta as a reservoir that provides blood to the organs when the flow reverses. The second half of the cycle represents the diastole (frames 216-324) during which the flow oscillates till it reaches the beginning of systole where frame 0 is repeated.

Velocity magnitudes near the posterior wall are approximately the same as those close to the anterior wall, as shown by the symmetry in colour. Throughout most of the cardiac cycle, the flow is slightly skewed towards the anterior wall (Fig. 8.4).

Close to the bifurcation, the flow becomes quite complex. At about 15 mm proximal to the bifurcation, the flow reverses near the walls during most of the cardiac cycle. It was reported that the walls proximal to the aorta are frequently subjected to occlusive atherosclerosis, although this region does not involve bifurcation or area expansion which are two major factors that complicate the flow pattern (Moore *et al.*, 1994c). The locality of atherosclerosis in this straight segment is attributed to the low and oscillatory near wall velocity profiles, which may result in mass transfer from blood to the walls (Moore *et al.*, 1994c; Taylor *et al.*, 1996).

After the bifurcation, the flow is laminar. The left iliac receive more flow during systole. In order to have a clearer picture about the flow, streamlines are plotted for the whole cardiac cycle. Except for periods of back flow, the streamlines are in general uniform and show forward direction of the flow (data not shown). Vortex rings set up during flow reversal at the end of systole (See Fig. 8.6), but they progressively damp out when the flow is re-established. These vortices form a trap for fluid elements and disturb the flow across the whole vessel. The reason for formation of vortices may be attributed to the rapid flow reversal and the damp-out may be forced by the inher-

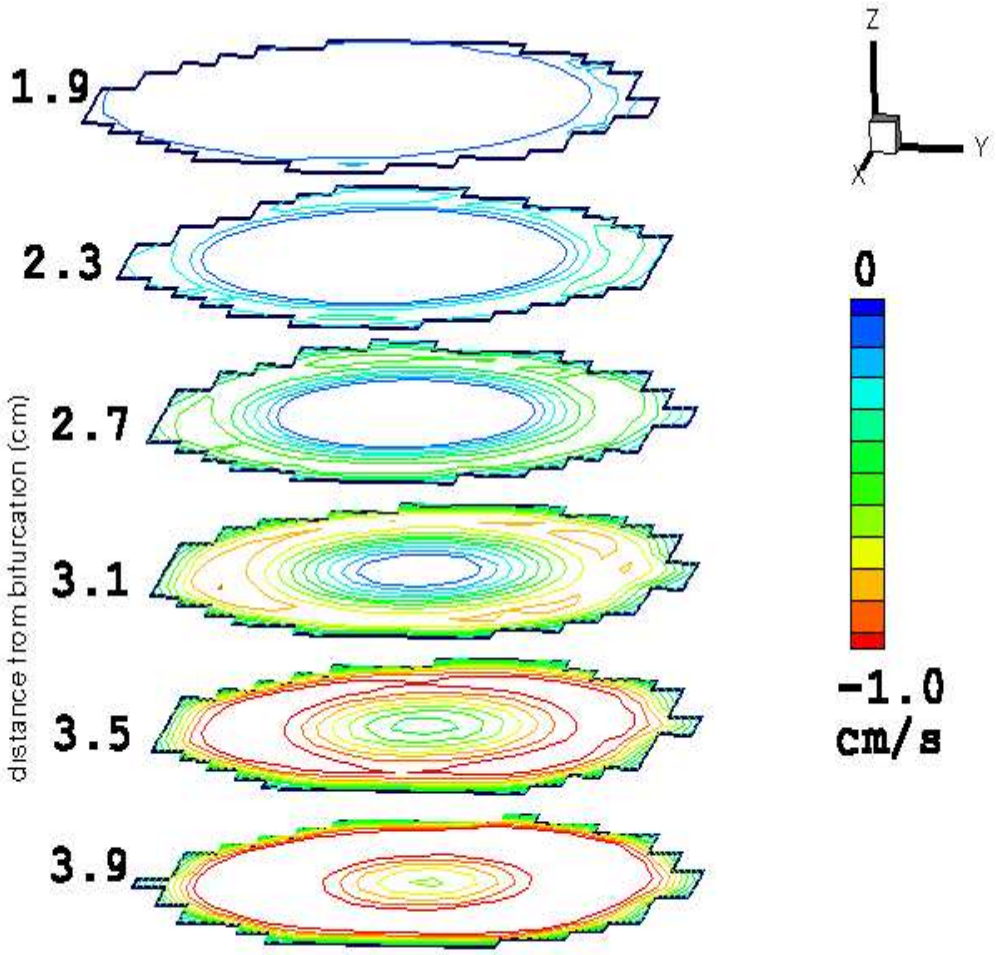

Figure 8.5: Negative velocity profiles during the systole are frequently observed close to the aortic bifurcation. The figure shows two snapshots of velocity 2.0 cm proximal to the bifurcation.

ent stability of the flow. Some of these observations have been previously reported by Moore *et al.* (1994c) in their extensive experimental MRA velocity measurements of a glass blown idealised model of the abdominal aorta and by Taylor *et al.* (1996) who observed large vortex development along the wall of the abdominal aorta, which shrinks considerably under moderate exercise condition. It is worth noting that although the models investigated by Moore *et al.* (1994c) and by Taylor *et al.* (1996) are idealised, similar qualitative results could be observed.

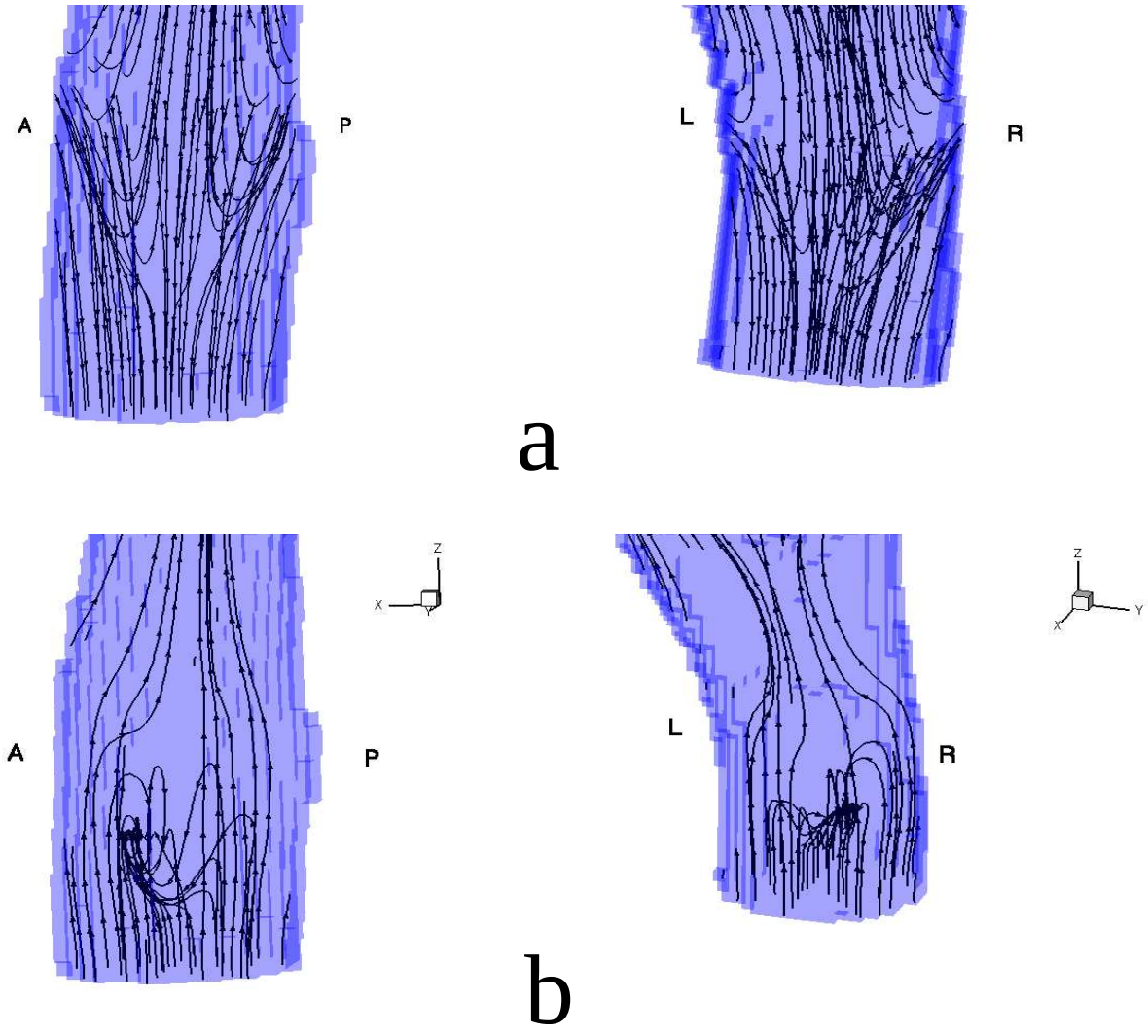

Figure 8.6: Velocity streamlines showing (a): Vortex formation during diastole (at $t = 0.4T$) and (b) flow mixing (at $t = 0.5T$).

8.3 Shear Stress

Shear stress for a Newtonian fluid is conventionally estimated from gradients of measured or simulated velocity components, and the fluid viscosity. This process involves some approximations which may lead to underestimation on the order of 10%–45% (Luo *et al.*, 1993) when the lumen is not circular. This large error is due to nonlinear velocity profile at the wall and ignorance of the radial derivatives. An enhancement was recently reported by Cheng *et al.* (2002) by introducing piecewise Lagrangian basis functions and segmenting the vessel lumen with a level set method.
With LBM, the nine Cartesian components of the local stress tensor are directly obtained using Eq. (3.22), as stated above without any further approximation than the Cartesian geometry. The stress at any given point is completely determined by this

stress tensor. A real benefit of the lattice Boltzmann solver is that these components are computed independently from velocity gradients. In this study, we compute and visualise the von Mises effective stress (Geiringer, 1953), defined as

$$\sigma_{eff} = \sqrt{\frac{A+6B}{2}} \tag{8.1}$$

where

$$A = (\sigma_{xx} - \sigma_{yy})^2 + (\sigma_{yy} - \sigma_{zz})^2 + (\sigma_{zz} - \sigma_{xx})^2 \tag{8.2}$$

and

$$B = \sigma_{xy}^2 + \sigma_{yz}^2 + \sigma_{zx}^2 \ . \tag{8.3}$$

This quantity is one of the three invariants of the stress tensor and therefore, is orientation independent. In addition, it includes the effect of small directional variations in the octahedral normal stress (the mean pressure) on the walls. The quantity B vanishes in the principal coordinate system.

The effective stress in $dynes/cm^2$ is shown in Fig. 8.7 , from which we observe that the effective stress at the posterior and lateral walls is always small (less than 40 $dynes/cm^2$) throughout the cardiac cycle. The stress is uniformly distributed along the lateral walls. The minimum stress values are observed during the flow reversal where the stress is very small through the whole vessel. The stress also oscillates in magnitude and the stress vector oscillates rapidly. The high stress values near the exits of the left iliac are attributed to the fact that this branch is subject to a small curvature at these locations. Effects of outlet conditions are minor and are hardly seen. The stress behaviour during the systole is described below. Let us first describe the stress behaviour in the main branch. At the beginning of systole (frame 0), the shear stress is small (less than 20 $dynes/cm^2$) and is least around the walls, with the posterior and right lateral walls having minimum values close to zero. The lateral walls of the left iliac have higher shear stress than the lateral walls for the right iliac, as predicted by the steady flow simulations.

The shear stress increases close to the walls as the systolic pressure is increased (frame 36) a strip-like island of zero shear stress splits the region just before the bifurcation into a left and right regions, with the left region having higher stress than the right one. The left anterior walls receive more stress (frame 72) of magnitude greater than 60 $dynes/cm^2$. Then the walls around the main are released from regions of minimum stress (frame 108), with the posterior walls released first while the anterior walls are not (frame 144). When the systole ends and the diastole begins (frame 180), the shear stress becomes again very small at regions far from the bifurcation, with small islands in the centre with minimum shear stress. The stress on the anterior lateral walls then increases, except for a small island in the middle of posterior wall, just before the bifurcation (frame 216). The shear stress comes again to its minimum on the centres and at the distal posterior walls (frame 252), with maximum shear stress ($40 dynes/cm^2$) on the walls. Then it gets smaller again, except near the left anterior walls (frame 288). Near the end of the cardiac cycle (frame 324), the

shear stress is low around the walls and on islands close to the bifurcation, spreading from left posterior to right anterior and covering the right anterior sides. The left anterior walls clearly has larger shear stress than the right side. At the end of the cycle, frame 0 is repeated.
In summary, the posterior wall receives stresses greater than 60 $dynes/cm^2$ during one third of the cycle, less than 5 $dynes/cm^2$ during another third and between $20-40$ $dynes/cm^2$ during the rest of the cycle. The shear stress after the bifurcation is higher in magnitude than the main branch, except for some islands and edges.
At the beginning of systole (frame 0), the regions directly after the bifurcation have minimum shear stress in an island on the right iliac spreading toward the right lateral and posterior walls, while the left iliac has higher magnitudes on the outer walls and minimum values on the inner walls. The bend near the exit makes the shear stress highest at these locations (> 150 $dynes/cm^2$). The stress is also maximum in the centre of the exit of left iliac artery and one-third from the exit of the right iliac. The inner walls of the right iliac receive minimum shear stress. The near-end (after the bend) outer walls receive minimum shear stress. In summary, at the beginning of systole, the inner walls have less stress than the outer ones and the right iliac artery has less shear stress than the left one.
As the systole develops, the stress first goes higher towards the bifurcation (frame 36), but remains minimum for some islands on the right iliac: close to the bifurcation and near the inner posterior walls (frame 72). Near the exits, the stress at the anterior walls of the left iliac becomes minimum at the bend (frame 108), and gets less for the inner walls. The islands in the right iliac are shifted towards the posterior inner walls (frames 144 and 180) till they are accompanied by high stress islands spreading toward the outer and anterior walls of both iliacs (frame 216). The stress reaches its maximum directly after the beginning of diastole (frame 252) and oscillates around lesser values (frames 288 and 324) till the systole begins again (frame 0).
From this description, we see that the effective von Mises stress is minimum close to the lateral and posterior walls of the abdominal aorta segment before the bifurcation, at the inner walls of the iliacs, and at islands in the right iliac artery; and is maximum at anterior walls, outer walls of the iliacs and at islands on both iliacs. Comparable results have been obtained in the literature (e.g. Raghavan and Vorp, 2000; Moore *et al.*, 1994b; Taylor *et al.*, 1996) leading to similar conclusions about the relationship between locality of cardiovascular diseases and the complex nature of stress. However, in this study, we did not measure the oscillatory shear index, although it is known to have an influence on the locality of cardiovascular diseases. This will be presented in a future article in which the full abdominal aorta will be studied.

8.4 Summary

We have demonstrated that the lattice Boltzmann method is a successful mesoscopic solver to time dependent blood flow in the arterial system. Simulated results of sys-

tolic flow in a 3D rigid tube at haemodynamic Reynolds and Womersley parameters have recovered the analytic Womersley solutions within acceptable accuracy. Steady and unsteady flow fields in a realistic aorta geometry, reconstructed from Magnetic Resonance Angiography have been successfully obtained and compared to the available literature, showing qualitative agreements. As the shear stress plays a crucial role in cardiovascular diseases and since it is directly and independently computed in the lattice Boltzmann solver, we strongly encourage researchers from haemodynamics to consider this method as an alternative blood flow solver. More benefits are seen from easy grid generation and straightforward parallelism, easy and feasible adaptation to changing geometry. Further investigation of the complete aorta model and experimental validations are under development in our group.

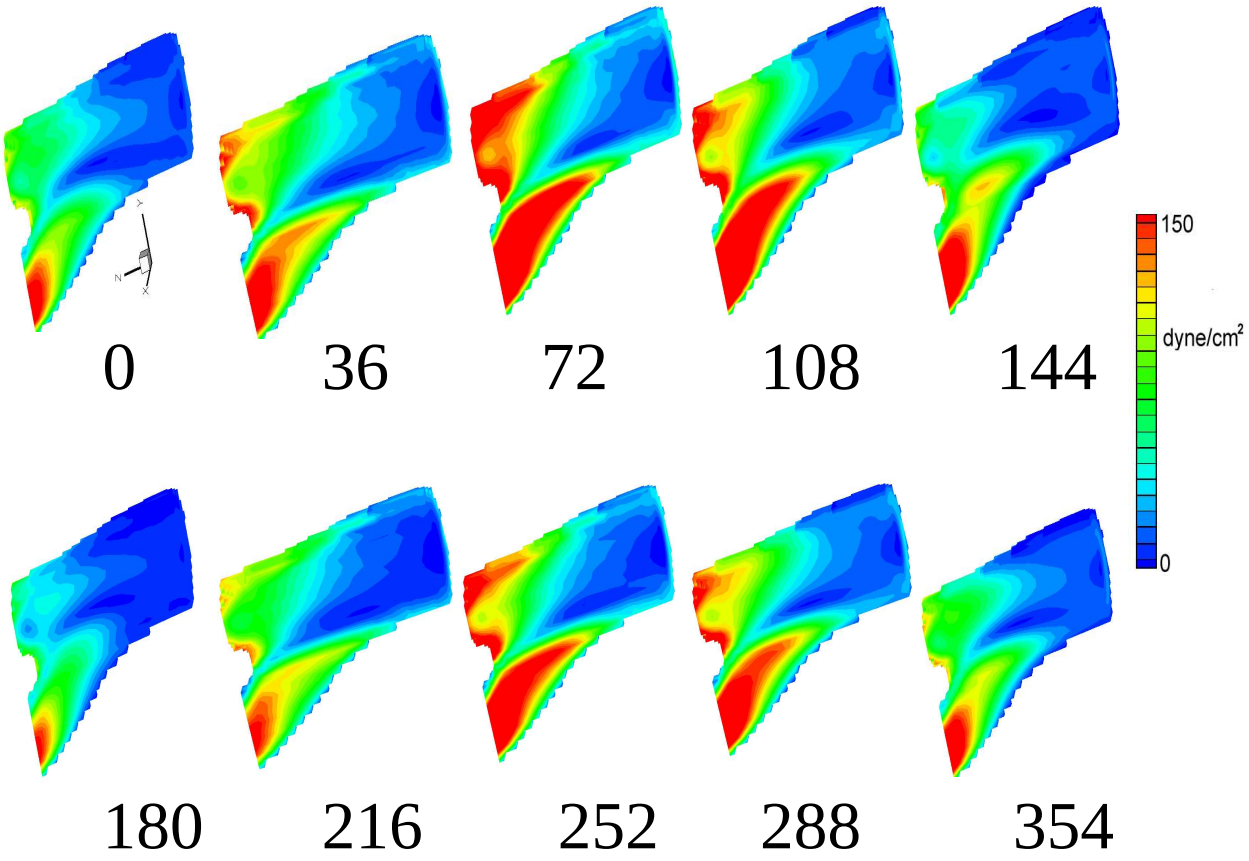

Figure 8.7: Effective stress on the walls of the aortic bifurcation computed at every 36^o of the cardiac cycle. The posterior wall has low values throughout the whole systolic cylce, while relatively high values of the stress near the curved exits are observed.

Chapter 9

Summary and Conclusions

In this final chapter, we summarise the main result and conclusions presented in this thesis, and future work to enhance the numerical model.

In the present study, the lattice Boltzmann method is presented as a robust and accurate haemodynamics numerical solver at mesoscale. The capabilities and shortcomings of the method are discussed. It is demonstrated that the lattice Boltzmann is of second order in space and time at low Mach numbers. The stress tensor is obtained from the non-equilibrium parts of the distribution functions without any need to approximate the shear-rate.

Various steady and unsteady numerical simulations are performed, all yielding excellent agreement with analytical solutions, other numerical methods, and/or available experimental data. Machine accuracy was obtained for some simple flow problems such as the channel and the Couette flows, even with the bounce-back rule, which is known to be of first order behaviour.

For 2D unsteady flows driven by a body force, a shift in time has been observed and analysed. The lattice Boltzmann BGK model is found to be more accurate when a half time step correction is added to the time coordinates. The effects of the Womersley, the Reynolds and the Strouhal numbers have also been studied in a number of simulations which showed that the shift in time is reduced at high Reynolds numbers. The obtained accuracy in time for time-dependent flows is of first order.

Using a quasi-incompressible D3Q19 model for the 3D simulations of oscillatory tube flow we have recovered the analytical Womersley solution with an average error of about 15 % with bounce-back on the link at relatively high Mach number which reduces to less than a percent at low Mach numbers, at a cost to computational time. A body fitted curved boundary condition, recently proposed by Bouzidi *et al.* (2001) is found to produce better results and is of second order accuracy.

As the purpose of building this numerical solver is to use it as an interactive flow solver in the promising Cross Grid environment now under development, performance of the method was enhanced by introducing the Mach number annealing as an acceleration technique for unsteady flows. With Mach number annealing, it is possible to perform simulations that are of the order of the annealing factor times faster than non-annealed simulations. Composite annealing procedures in which both

Reynolds and Mach numbers may be annealed would be adopted for further acceleration in the future.
The influence of walls, inlet and outlet boundary conditions on accuracy and performance is studied in detail as a function of Mach and Knudsen numbers. It is found that the bounce-back on the links could be more efficient if used at low Mach numbers when the Mach number annealing technique is used. With the Mach number annealing, we recommend the bounce-back on the links as a better alternative than other sophisticated boundary conditions which are difficult to use in the field of haemodynamics.
Another application of interest in simulation environments is changing the geometry on-the fly and investigating the robustness of the numerical method in producing accurate results without a need to restart the simulation. The lattice Boltzmann method is found to be fully adaptive, as demonstrated by simple test cases. More investigation is necessary to demonstrate the real benefit of this feature. This is recently under study in our group.
Simulation results of steady and unsteady flow in a model of the human aortic bifurcation reconstructed from Magnetic Resonance Angiography are presented as a typical haemodynamic application. The computational model under study involves only the bifurcation region, directly after the IMA, and includes parts of the left and right iliac arteries.We have conducted a number of steady and unsteady flow simulations for the aorta model. Results on velocity fields and stress are successfully obtained and are qualitatively compared to literature.
As the shear stress plays a crucial role in cardiovascular diseases and since it is directly and independently computed in the lattice Boltzmann solver, we strongly encourage researchers from haemodynamics to consider this method as an alternative blood flow solver. More benefits are seen from easy grid generation and straightforward parallelism, easy and feasible adaptation to changing geometry. Further investigation of the complete aorta model and experimental validations are under development in our group.
A main conclusion in the thesis is that, even with the most simple lattice Boltzmann methods, comparable results to the most sophisticated traditional solvers are possible. However, the thesis has left open many questions to be answered. Some of them are

- The method is not yet matured in solving models involving fluid-structure interactions. Some recent developments based on coupling the fluid lattice Boltzmann with solid models (Chopard[1] *et al.*, 2002, personal communication) to investigate thrombosis are promising.

- The lattice Boltzmann method with simplified BGK approximation has many troubles at high Mach and Reynolds numbers, but not at haemodynamic Womersley numbers. However, this issue is quite sensitive to the boundary conditions

[1]It is worth noting that Chopard suggested to the author in 2000 that this coupling would be useful if applied in Haemodynamics. At that time we were not sure if even the lattice BGK yields acceptable results. When that has been cleared out, there is no time left for this interesting direction.

and the lattice BGK boundary conditions are known to be viscosity dependent, except for a few of them. This has direct influence on the stability of the method. A solution is to consider using generalised lattice Boltzmann equations (GLBE). However, the computational cost raised by using GLBE needs to be investigated versus the accuracy and compared to the engineering accuracy.

- It is well known that the non-Newtonian models produce significantly different results than Newtonian ones. Although the global structure remains similar, the profile of the stress tensor is significantly different near the walls. It is relatively easy to perform non-Newtonian flows in lattice Boltzmann models, but GLBE may be a better option than the lattice BGK.

- As early turbulence may build up in the circulation, turbulent models need to be approached in an ideal haemodynamic solver. A number of turbulent models are available in previous literature, most of which use GLBE.

- With the development in imaging techniques and the increase in microscopic understanding of atherosclerosis, traditional CFD solvers may not be useful and mesoscopic models may join wider acceptance.

In conclusion, the lattice Boltzmann methods are accurate and robust computational fluid dynamics solvers in the mesoscale, with elegant computational characteristics. This makes them feasible alternates to traditional macroscopic solvers in a wide range of applications.

Bibliography

[1] Abe T (1997): Derivation of the Lattice Boltzmann Method by Means of the Discrete Ordinate Method for the Boltzmann Equation. *Journal of Computational Physics***131**: 241–246.

[2] Aharonov E, Rothman DH (1993): Non-Newtonian flow (through porous-media)- A Lattice-Boltzmann Method. *Geophysical Research Letters* **30**: 679–682.

[3] Aidun CK, Lu YN (1995): Lattice Boltzmann Simulation of Solid Particles Suspended in Fluid. *Journal of Statistical Physics* **81**: 49–61.

[4] Argyris JH (1952): Energy Theorems and Structural Analysis. *Aircraft Engineering* **26**: 347-56, 383-87.

[5] Artoli AM, Kandhai BD, Hoekstra AG, Sloot PMA (2000): Accuracy of shear stress calculations in the Lattice Boltzmann Method. In: Proceedings of the 9th International Conference on Discrete Simulation of Fluid Dynamics, New Mexico USA, http://cnls.lanl.gov/Conferences/DiscreteSimulation/agenda.htm.

[6] Artoli AM, Hoekstra AG, Sloot PMA (2002a): Time dependent flow in a rigid tube using the Lattice Boltzmann Method. In: Boon JP, Coveney PV, Succi S (Editors), International Conference on Discrete Simulation of Fluid Dynamics, in series Europhysics Conference Abstracts, **25**:3.

[7] Artoli AM, Kandhai BD, Hoefsloot HG, Hoekstra AG, Sloot PMA (2002b): Shear Stress in Lattice Boltzmann Simulations. In: F. Hossfeld and K. Binder (Editors), Europhysics Conference on Computational Physics. Aachen, Germany, 5-8 September 2001. Book of Abstracts, John von Neumann Institute for Computing, in series Publication Series of the John von Neumann Institute for Computing, **8**: A127. 2001.

[8] Artoli AM, Hoekstra AG, Sloot PMA (2002c): Accuracy of 2D pulsatile flow in the lattice Boltzmann BGK method, in Sloot PMA; Tan CJK; Dongarra JJ; Hoekstra AG (Editors), Computational Science - ICCS 2002, Lecture Notes in Computer Science, **2329**: 361-370. Springer Verlag, April 2002. ISBN 3-54043591-3.

[9] Artoli AM, Hoekstra AG, Sloot PMA (2003a): Accelerated Lattice BGK method for unsteady flow simulations through Mach number annealing, Accepted, *International Journal of Modern Physics C*.

[10] Artoli AM, Hoekstra AG, Sloot PMA (2002d): 3D Pulsatile flow with the lattice Boltzmann BGK method. *International Journal of Modern Physics C* **13**: 1119–1134.

[11] Artoli AM, Hoekstra AG, Sloot PMA (2003b): Simulation of a systolic cycle in a realistic artery with the Lattice Boltzmann BGK method, textitInternational journal of Modern Physics B **17**: 95-98.

[12] Artoli AM, Hoekstra AG, Sloot PMA (2003c): Mesoscopic simulations of systolic flow in the Human abdominal aorta, Submitted, *Journal of Biomechanics*.

[13] Artoli AM, Hoekstra AG, Sloot PMA (2003d): Lattice Boltzmann, a robust and accurate solver for interactive computational haemodynamics. In: Sloot PMA; Abramson D; Bogdanov AV; Dongarra JJ; Zomaya AY; Gorbachev YE (Editors), Computational Science - ICCS 2003, *Lecture Notes in Computer Science* **2657**: 1034–1043. Springer Verlag, Berlin, June 2003. ISBN 3-540-40194-6.

[14] Artoli AM, Hoekstra AG, Sloot PMA (2003e): Simulations of a systolic cycle with lattice Boltzmann method: Accuracy versus performance, submitted, *Computers and Fluids*.

[15] Artoli AM, Hoekstra AG, Sloot PMA (2002d): Proceedings of the 11th international conference of Discrete simulation of fluid dynamics and soft condensed matter, Shanghai, China, August 5–9 (2002).

[16] Aziz AK (Ed.) (1972): The Mathematical Foundations of the Finite Element Method with Applications to Partial Differential Equations. *Academic Press, New York*.

[17] Baker RC (1991): Responce of Bulk flowmeters to Multiphase flows. In: Proceedings of the Institution of Mechanical Engineers Part C. *Journal of Mechanical Engineering Science* **205**, pp 217–229.

[18] Balakrishnan R, Agarwal RK (1997): Numerical simulation of Bhatnagar-Gross-Krook-Burnett equations for hypersonic flows. *Journal of Thermophysics and Heat Transfer* **11**: 391–399.

[19] Batina T (1993): A gridless Euler/Navier-Stokes solution algorithm for complex aircraft applications. In: 31st Aerospace Sciences Meeting and Exhibition. American Institute of Aeronautics and Astronautics. Reno, NV.

[20] Behrend O, (1995): Solid-Fluid boundaries in Particle suspension simulations via the Lattice Boltzmann method. *Physical Review E* **52**: 1164–1175.

[21] Belleman RG, Sloot PMA (2000): The Design of Dynamic Exploration Environments for Computational Steering Simulations. In: Proceedings of the SGI Users Conference. Academic Computer Centre CYFRONET AGH Krakow, Poland.

[22] Belleman RG, Sloot, PMA (2001): Simulated vascular reconstruction in a virtual operating theatre. In: H.U. Lemke; M.W. Vannier; K. Inamura; A. G. Farman and K.Doi, (Editors). *Computer Assisted Radiology and Surgery*. Excerpta Medica International Congress Series 1230. Elsevier Science B.V., Berlin.

[23] Benzi R, Succi S (1990): 2-Dimensional Turbulence with the Lattice Boltzmann-Equation. *Journal of Physics A* **23**: L1–L5.

[24] Benzi R, Succi S, Vergassola M (1992): The lattice Boltzmann Equation: Theory and applications. Physics Reports **222**: 145–197.

[25] Berger SA (1993): Flow in Large Blood Vessels. *Contemporary Mathematics* **141**: 479–517.

[26] Berger SA, Jou LD (2000): Flows in stenotic vessels. *Annual Review of Fluid Mechanics* **32**: 347–382.

[27] Bernaschi M, Succi S, Chen HD, Zhang RY (2002): *International Journal of Modern Physics C* **13**: 675–687.

[28] Berthier B, Bouzerar R, Legallais C (2002): Blood flow patterns in an anatomically realistic coronary vessel: influence of three different reconstruction methods. *Journal of Biomechanics* **35**: 1347–1356.

[29] Bhatnagar PL, Gross EP, Krook M (1954): A model for collision processes in gases. I. Small amplitude processes in charged and neutral one-component system. *Physical Review* **94**: 511–525.

[30] Bird RB, Stewart WE, Lightfoot EN (1960): *Transport Phenomena*. John Wiley & Sons. New York.

[31] Boltzmann L (1872): Weitere Studien *ü*brt fsd W*o*rmegleichgewicht unter Gasmolekulen, Sitzungsber. Akad. Wiss. Wein **66**: 275-370. Cited in Lebowitz and Montroll, Editors (1983).

[32] Botnar R, Rappitsch G, Scheidegger MB, Liepsch D, Perktold K, Boesiger P (2000): Haemodynamics in the carotid artery bifurcation: a comparison between numerical simulations and in vitro MRI measurements. *Journal of Biomechanics* **33**: 137–144.

[33] Bouzidi M, Firdaouss M, Lallemand P (2001): Momentum transfer of a Boltzmann-lattice fluid with boundaries. *Physics of Fluids* **13**: 3452–3459. *Computers and Structures***79**: 2031–2037.

[34] Caflisch RE (1983): Fluid Dynamics and the Boltzmann Equation. In: Lebowitz JL, Montroll EW (Editors) *Nonequilibrium Phenomena I. The Boltzmann Equation*. North-Holland Publishing Company: 195–226.

[35] Caro CG, Fitzgerald JM, Schroter RC (1969): Arterial wall shear and distribution of early atheroma in man. *Nature* **223**: 1159–1161.

[36] Caro CG, Pedley TJ, Schroter RC, Seed WA (1978): *The mechanics of the circulation*, Oxford University Press.

[37] Carrel A (1912): In: Nobel Lecuture in Physiology or Medicine, 1901–1970. Elsevier Publishing Company, Amsterdam.

[38] Cauchy AL (1823): Researches sur l'équilibre et le mouvement intérieur des corps solides ou fluides, élastiques ou nonélastiques. Bull. Soc. philomath. Paris: 9–13.

[39] Cercignani C (1983): Solution of the Boltzmann Equation. In Montroll and Lebwitz (Editors): 123–192.

[40] Cercignani C (1975): *Theory and Application of the Boltzmann equation*. Elsevier, Amsterdam.

[41] Cercingnani C (1971): Methods of solution of the linearized Boltzmann equation for rarefied gas dynamics. *Journal of Quantitative Spectroscopy and Radiative Transfer* **11**: 973–985.

[42] Chapman S, Cowling TG (1970): *The Mathematical Theory of Non-Uniform Gases*. Cambridge University Press.

[43] Cheng CP, Parker D, Taylor CA (2002): Quantification of wall shear stress in large blood vessels using largrangian interpolation functions with cine phase-contrast magnetic resonance imaging. *Annals of Biomedical Engineering* **30**, 1020–1032.

[44] Chen H, Chen S, Matthaeus WH (1992): Recovery of the Navier-Stokes equations using a lattice-gas Boltzmann method. *Physical Review A*, **45**: R5339.

[45] Chen S, Doolen G (1998): Lattice Boltzmann method for fluid flows. *Annual Review of Fluid Mechanics* **30**: 329–364.

[46] Chen H, Kandasamy S, Orszag S, Shock R, Succi S, Yakhot V (2003): Extended Boltzmann Kinetic equation for Turbulent Flows. *Science* **301**:633–636.

[47] Chopard B, Droz M (1998): *Cellular Automata modeling of Physical Systems*, Cambridge University Press.

[48] Chopard B, Marconi S (2002): Lattice Boltzmann solid particles in a lattice Boltzmann fluid. *Journal of Statistical Physics***107**: 23–37.

[49] Clough RW (1960): The Finite Element Method in Plane Stress Analysis. In: Proceedings of the second ASCE Conference on electronic Computation. Cited in Nash (1990) page 164.

[50] Cole JS, Watterson JK, O'Reilly MJG (2002): Numerical investigation of the haemodynamics at a patched arterial bypass anastomosis. *Medical Engineering & Physics* **24**: 393–401.

[51] Coppola ED (1957): The discovery of the pulmonary circulation: A new approach. *Bulletin of the History of Medicine* **31**: 44–77.

[52] Cornubert R, D'Humiéres D, Levermore D (1991): A Knudsen layer theory for lattice gases. *Physica D* **47**: 241–259.

[53] Crochet MJ, Walters K (1983): Numerical methods in non-newtonian fluid mechanics. *Annual Review of Fluid Mechanics* **15**: 241–260.

[54] D'Humiéres D, Ginzburg I, Krafczyk M, Lallemand P, Luo LS (2002): Multiple-relaxation-time lattice Boltzmann models in three dimentions. *Philosophical Transactions of The Royal Society London A* **360**: 437–451.

[55] D'Humiéres D (1992): Generalized lattice Boltzmann equations. Rarefied gas dynamics: theory and simulations (ed. Shizgal BD and Weaver DP). *Prog. Aeronaut.* Astrnaut **159**: 450–458.

[56] D'Humières D, Ginzburg I, Krafczyk M, Lallemand P, and Luo LS (2002): Multiple-relaxation-time lattice Boltzmann models in three dimensions. *Philosophical Transactions of The Royal Society of London A* **360**: 437–450.

[57] DeBakey ME, Lawrite GM, Glaeser DH (1985): Patterns of atherosclerosis and their surgical significance. *Annals of Surgery* **201**: 115–131.

[58] Dubroca B, Klar A (2002): Prise en compte d'un fort désèquilibre cinétique par un modèle aux demi-moments: Half moment model to take into account strong kinetic non-equilibrium. *Comptes Rendus Mathematique* **335**: 699–704.

[59] Euler L (1755): Principes g*é*n*é*raux du mouvement des fluides. *Histoire de l'Acacdernie de Berlin* **11** (1755):274–315.

[60] Fang HP, Wang ZW, Lin ZF, Liu MR (2002): Lattice Boltzmann method for simulating the viscous flow in large distensible blood vessels. *Physical Review E* **65**: art. no. 051925

[61] Fedkiw R, Liu XD, Osher S (2002): A general technique for eliminating spurious oscillations in conservative schemes for multiphase and multispecies Euler equations. *International Journal of Nonlinear Sciences and Numerical Simulation* **3**: 99–105.

[62] Filippova O, Hänel D (1998a): Boundary-fitting and local grid refinement for lattice-BGK models. *International Journal of Modern Physics C* **9**: 1271–1279.

[63] Filippova O, H*ä*nel D (1998b): Grid refinement for lattice-BGK models *Journal of Computational Physics* **147**: 219-228.

[64] Flekkϕy EG, Herrmann HJ (1993): Lattice Boltzmann Models for Complex Fluids. *Physica A* **199**: 1–11.

[65] FLUENT 4.5, 1998. Fluent Inc., http://www.fluent.com

[66] Foster I, Kesselmann C (Eds.) (1999): *The Grid: BluePrint for a new computing Infrastructure*. Morgan Kaufmann.

[67] Frank O (1903): Kritik der elastischen Manometer. Zeitschrift fur Biologie, **44**: 445–613.

[68] Frederick D, Chang TS (1972): *Continuum Mechanics*. Scientific Publishers Inc. Boston.

[69] Friedmann MH, O'Brien V, Ehrlich LW (1975): Calculations of pulsate flow through a branch: implications for the haemodynamics of atherogenesis, *Circulation Research* **36**: 277 (1975).

[70] Frisch U, Hasslacher B, Pomeau Y(1986): Lattice gas automata for the Navier-Stokes equations. *Physical Review Letters* **56**: 1505–1508.

[71] Fung YC (1993): *Biomechanics: Mechanical Properties of Living Tissues. Second edition*. Springer Verlag, New York.

[72] Fung YC (1997): *Biomechanics: Circulation*, 2nd Edition. Springer, New York.

[73] Geiringer H (1953): Recent results in the theory of plasticity. In: von Mises, R., von Karmen (Editors), Advances in Applied Mechanics III. Academic Press, New York: 200–201.

[74] Gibson CM, Diaz L, Kandarpa K, Sacks FM, Pasternak RC, Sandor T, Feldman C, Stone PH (1993): Relation of vessel wall shear-stress to Atherosclerosis progression in human coronary-arteries. *Arterioscherosis and Thrombosis* **13**: 310–315.

[75] Gijsen FJH, Allanic E, van de Vosse FN, Janssen JD (1999): The influence of the non-Newtonian properties of blood on the flow in large arteries: unsteady flow in a 90 degrees curved tube. *Journal of Biomechanics* **32**: 705–713.

[76] Gijsen FJH, Goijaerts AM, van de Vosse FN, Janssen JD (1997): A new method to determine wall shear stress distribution. *Journal of Rheology* **41**: 995–1006.

[77] Ginsbourg I, Adler PM (1995): Surface-tension Models with Different Viscosities. *Transport in Porous Media* **20**: 37–76.

[78] Giraud L, d'Humieres D, Lallemand P (1997): A lattice-Boltzmann model for visco-elasticity. *International Journal of Modern Physics C* **8**: 805–815.

[79] Girault V, Raviart PA (1979): *Finite element approximation of the Navier - Stokes equations*. Springer-Verlag.

[80] Gnasso A, Carallo C, Irace C, De Franceschi MS, Mattioli PL, Motti C, Cortese, C (2001): Association between wall shear stress and flow-mediated vasodilation in healthy men. *Atherosclerosis* **156**: 171–176.

[81] Goyen M, Ladd ME, Debatin JF, Barkhausen J, Truemmler KH, Bosk S, Ruehm SG (2001): Dynamic 3D MR angiography of the pulmonary arteries in under four seconds. *Journal of Magnetic Resonance Imaging* **13**: 372–377.

[82] Grunau D, Chen S, Eggert K (1993): A lattice Boltzmann model for multiphase fluid flows. *Physics of Fluids* **5**: 2557–2562.

[83] Guo ZL, Shi BC, Wang NC (2000): Lattice BGK model for Incompressible Navier-Stokes Equations. *Journal of Computational Physics.* **165**: 288–306.

[84] Guo Z, Zhao TS (2002): Lattice Boltzmann model for incompressible flows through porous media. *Physical Review E***66**: 036304.

[85] Haddad TE, Khairallah AA (1936): A forgotten chapter in the circulation of the blood. *Annals of Surgery* **104**: 1–8.

[86] Harvey W (1628): *De Motu Cordis*, Frankfurt: William Fitzer.

[87] He X (1997): Error analysis for the interpolation-supplemented lattice-Boltzmann equation scheme. *International Journal of Modern Physic C* **8**: 737–745.

[88] He X, Luo LS (1997a): Lattice Boltzmann model for the incompressible Navier-Stokes equation. *Journal of Statistical Physics* **88**: 927–944.

[89] He X, Luo LS (1997b): Theory of the Lattice Boltzmann method: From the Boltzmann equation to the lattice Boltzmann equation, *Physical Review E* **56**: 6811–6817.

[90] He X, Luo LS (1997c): A priori derivation of the lattice Boltzmann equation. *Physical Review E* **55**: R6333–R6336.

[91] He X, Luo LS (1997d): Lattice Boltzmann Model for the Incompressible Navier-Stokes Equation, *Journal of Statistical Physics* **88** 927–944.

[92] He X, Doolen GD (1997): Lattice Boltzmann method on curvilinear coordinates system: vortex shedding behind a circular cylinder, *Physical Review* **51**: 434–440.

[93] He X, Zou QS, Luo LS, Dembo M (1997): Analytical solutions of simple flow and analysis of non-slip boundary conditions for the lattice Boltzmann BGK model, *Journal of Statistical Physics* **87**: 115–136.

[94] Higuera F, Jimenez J (1989): Boltzmann approach to lattice gas simulations. *Europhysics Letters* **9**: 663–668.

[95] Higuera FJ, Succi S, Benzi R (1989): Lattice gas dynamics with enhanced collisions,*Europhysics Letters* **9**: 345–349.

[96] Higuera F, Succi S (1989): Simulating the flow around a circular-Cylinder with a Lattice Boltzmann-Equation. *Europhysics Letters* **8**: 517–521.

[97] Hoekstra AG, van't Hoff J, Artoli AM, Sloot PMA (2003): Lattice BGK simulations of unsteady flow in a 2D elastic tube. In: Sloot PMA; Abramson D; Bogdanov AV; Dongarra JJ; Zomaya AY; Gorbachev YE (Editors), Computational Science - ICCS 2003, *Lecture Notes in Computer Science* **2657**: 997–1006. Springer Verlag, Berlin, June 2003. ISBN 3-540-40194-6.

[98] Holdych DJ, Noble DR, Georgiadis JG, Buckius RO (2002): Submtted to *Journal of Computational Physics* and presented in the Proceedings of Discrete Simulations of Fluid Dynamics and Condensed Mattar Physics, Shanghai China, August 5–9 (2002).

[99] Hou S, Zou Q, Chen S, Doolen G, Cogley AC (1995): Simulation of cavity flow by the lattice-Boltzmann method. *Journal of Computational Physics* **118**: 329–347.

[100] Igra D, Takayama K (2002): A high resolution upwind scheme for multicomponent flows. *International Journal for Numerical Methods in Fluids* **38**: 985–1007.

[101] Inamuro T, Yoshino M, Ogino F (1997): Accuracy of the lattice Boltzmann method for small Knudsen number with finite Reynolds number. *Physics of Fluids* **9**: 3535–3542.

[102] Junk M, Klar A (2000): Discretizations for the Incompressible Navier–Stokes Equations Based on the Lattice Boltzmann Method. *SIAM Journal on Scientific Computing* **22**: 1–19.

[103] Junk M, Klar A, Luo LS (2002): Theory of the Lattice Boltzmann Method: Mathematical Analysis of the Lattice Boltzmann Equation., Preprint.

[104] Kaandorp JA, Lowe CP, Frenkel D, Sloot PMA (1996): The effect of nutrient diffusion and flow on coral morphology. *Physical Review Letters* **77**: 2328–2331.

[105] Kandhai D, Vidal DJ, Hoekstra AG, Hoefsloot H, Iedema P, Sloot PMA (1999): Lattice-Boltzmann and Finite element simulations of fluid flow in a SMRX static mixer reactor. *International Journal of Numerical Methods in Fluids* **31**: 1019–1033.

[106] Kandhai D, Koponen A, Hoekstra AG, Kataja M, Timonen J, Sloot PMA (1998): Lattice-Boltzmann hydrodynamics on parallel systems. *Computer Physics Communications* **111**: 14–26.

[107] Kasser U, Heimburg P, Walitza E (1989): Viscoelasticity of Whole-Blood and its Dependence on Laboratory Parameters. *Clinical Hemorheology* **9**:307–312.

[108] Koponen A, Kandhai D, Kataja M, Timonen J (1998): Simulations of single fluid flow in porous media. *International Journal of Modern Physics C* **9**: 1505–1521.

[109] Koponen A, Kandhai D, Hellen E, Alava M, Hoekstra AG, Kataja M, Niskanen K, Sloot PMA, Timonen J (1998): Permeability of three-dimensional random fibre webs. *Physical Review Letters* **80**: 716–719.

[110] Krafczyk M, Cerrolaza M, Schulz M, Rank E (1998): Analysis of 3D transient blood flow passing through an artificial aortic valve by Lattice-Boltzmann methods. *Journal of Biomechanics* **31**: 453–462.

[111] Krafczyk M, Tolke J, Rank E (2001): Two-dimensional simulation of fluid-structure interaction using lattice-Boltzmann methods. *Computers & Structures* **79**: 2031–2037.

[112] Ku DN (1983): Hemodynamics and atherogenesis at the human carotid bifurcation. Ph.D. Thesis, Georgia Institure of Technology.

[113] Ku, DN, Giddens DP, Zarins CK, Glagov S (1985): Pulsatile flow and atherosclerosis in the human carotid bifurcation: positive correlation between plaque location and low and oscillating shear stress. *Arteriosclerosis* **5**: 293–302.

[114] Ku DN (1997): Blood Flow in Arteries. *Annual Review of Fluid Mechanics* **29**: 399–434.

[115] Ku JP, Draney MT, Arko FR, Lee WA, Chan FP, Pelc NJ, Zarins CK, Taylor CA (2002): In vivo Validation of numerical prediction of blood flow in arterial bypass grafts *Annals of Biomedical Engineering* **30**: 743–752.

[116] Ladd AJC (1994): Numerical simulations of particulate suspensions via a discretized Boltzmann equation. Part I. Theoretical foundation. *Journal of Fluid Mechanics* **271**: 285–309.

[117] Landau LD, Lifshitz EM (1975): *Fluid Mechanics*. Pergamon Press, Elmsford, New York.

[118] Lavalle P, Boon JP, Noullez A (1991): Boundaries in Lattice Gas–Flows. *Physica D* **47**: 233–240.

[119] Lebowitz JL, Montroll EW (Editors) (1983): *Nonequilibrium Phenomena I: The Boltzmann Equation*. North Holland.

[120] Lindenmayer A (1968): Mathematical models for cellular interactions in development, Part I and II **18**: 280–315.

[121] Lowe GDO, Barbenel JC (1988): Plasma and blood viscosity, *Clinical Blood Rheology* **1** ed. by Lowe GDO, CRC Press, Boca Ration Florida, 11–44.

[122] Luo LS (1997): Analytic solutions of linearized lattice Boltzmann equation for simple flows. *Journal of Statistical Physics* **88**: 913–926.

[123] Luo LS (2000): Theory of the lattice Boltzmann method: Lattice Boltzmann models for non-ideal gases. *Physical Review E* **62**:4982-4996.

[124] Luo LS, Chen HD, Chen SY, Doolen GD, Lee YC (1991): Generalized Hydrodynamic Transport in Lattice-Gas Automata. *Physical Review A* **43**: 7097–7100.

[125] Luo Z, Yang WJ, Stein PD (1993): Errors in the estimate of arterial wall shear rated that result from curve fitting of velocity profiles. *Journal of Biomechanical Engineering* **26**: 383–390.

[126] Maier RS, Bernard RS, Grunau DW (1996): Boundary conditions for the lattice Boltzmann method. *Physics of Fluids* **8**: 1788–1801.

[127] Maier SE, Meier D, Boesiger P, Moser U, Vieli A (1989): Human abddominal aorta: Comparative Measurements of blood flow with MR Imaging and Multigated Doppler US. *Radiology* **171**: 487–492.

[128] Majumdar A (1996): Development of a Multiple Perturbation Monte Carlo method for Eigenvalue Problems and Implementation on Parallel Processors. Ph.D. thesis, The University of Michigan.

[129] Mantle MD, Bijeljic B, Sederman AJ, Gladden LF (2001): MRI velocimetry and Lattice-Boltzmann simulations of viscous flow of a Newtonian liquid through a dual porosity fibre array. *Magnetic Resonance Imaging* **19**: 527–529.

[130] Mattheus WH (2001): Bartol Research Institute, University of Delware, personal communication, International Conference on Discrete Simulation of Fluid dynamics, Cargese, July(2001).

[131] Maxwell, JC (1867): On the dynamical theory of gases. *Philosophical Transactions of the Royal Society of London* **157**: 49–88.

[132] McDonald DA (1955): The relation of pulsatile pressure to flow in arteries. *Journal of Physiology* **127**: 533–552.

[133] McDonald DA (1960): Blood flow in arteries. Monog. Physiol. Society London: Edward Arnold (Publishers) Ltd.; Baltimore: Williams & Wilkins.

[134] McDonald DA (1974): *Blood flow in arteries*. Edward Arnold (Publishers).

[135] McNamara GR, Garcia AL, Alder BJ (1995): Stabilization of Thermal Lattice Boltzmann Models. *Journal of Statistical Physics* **81**: 395–408.

[136] McNamara GR, Zanetti G (1988): Use of the Boltzmann-Equation to simulate Lattice-gas Automata. *Physical Review Letters* **61**: 2332–2335.

[137] Mei R, Shyy W, Yu D, Luo LS (2000): Lattice Boltzmann method for 3-D flows with curved boundary. *Journal of Computational Physics* **161**:680–699.

[138] Mei RW, Luo LS, Shyy W (1999): An accurate curved boundary treatment in the lattice Boltzmann method. *Journal of Computational Physics* **155**: 307–330.

[139] Mercie P, Thiebaut R, Lavignolle V, Pellegrin JL, Yvorra-Vives MC, Morlat P, Ragnaud JM, Dupon M, Malvy D, Bellet H, Lawson-Ayayi S, Roudaut R, Dabis F (2002): Evaluation of cardiovascular risk factors in HIV-1 infected patients using carotid intima-media thickness measurement. *Annals of Medicine* **34**: 55–63.

[140] Mettler CC (1947): *History of Medicine*. Philadelphia, PA, USA. The Blakiston Co. : 40–59 and 113–128.

[141] Mohamed T and Andrés S (2001): Non-Newtonian Poiseuille flow of a gas in a pipe. *Physica A* **289**: 336–358.

[142] Moore JE, Maier SE, Ku DN, Boesiger P (1994a): Haemodynamics in the abdominal aorta: a comparison of in vitro and in vivo measurements. *Journal of Appl Physiology* **76**: 1520–1527.

[143] Moore JE, Xu C, Glagov S, Zarins CK, Ku DN (1994b): Fluid wall shear stress measurements in a model of the human abdominal aorta: oscillatory behavior and relationship to atherosclerosis. *Atherosclerosis* **110**: 225–240.

[144] Moore JE, Ku DN (1994c): Pulsatile Velocity Measurements in a Model of the Human Abdominal Aorta Under Resting Conditions. *Journal of Biomendical Engineering* **116**: 337–346.

[145] Moore JE, Ku DN (1994d): Pulsatile Velocity Measurements in a Model of the Human Abdominal Aorta Under Resting Simulated Excercise and postprandial Conditions. *Journal of Biomendical Engineering* **116**: 107–116.

[146] Moore JA, Steinman, DA, Ethier CR(1998) Computational blood flow modelling: Errors associated with reconstructing finite element models from magnetic resonance images. *Journal of Biomechanics* **31**: 179–184.

[147] Nannelli F, Succi S (1992): The Lattice Boltzmann-Equation on Irregular Lattices. *Journal of Statistical Physics* **68**: 401–407.

[148] Nash SG (Ed.) (1990): *A History of scientific computing*. ACM Press History Series.

[149] Navier L: Memory sur les lois de mouvements des fluides. *Mémoires de l'Académie Royale des Sciences de l'Institut de France* **6** (1822): 389–440.

[150] Nazemi M, Kleinstreuer C (1989): Analysis of Particle Trajectories in Aortic Artery Bifurcations with Stenosis. *Journal of Biomedical Engineering* **111**: 311–315.

[151] Newton (1687): *Philosophiae Naturalis Principia Mathematica*. London.

[152] Noble DR, Georgiadis JG, Buckius RO (1995): Direct Assessment of Lattice Boltzmann Hydrodynamics and Boundary-conditions for Recirculating-flows. *Journal of Statistical Physics*. **81**: 17–33.

[153] Oden JT (1970): A finite Element Analogue of the Navier-Stokes Equations. *Journal of Engineering Mechanics* **96**: 529–534.

[154] Oden JT, Somogyi D (1968): Finite Element Applications in Fluid Dynamics. *Journal of Engineering Mechanics* **95**: 821–826.

[155] Ojha M (1994): Wall shear stress temporal gradient and anastomotic intimal-hyperplasia. *Circulation Research* **74**: 1227–1231.

[156] Oldroyd JG (1950): On the formulation of rheological equations of state. In: Proceedings of the Royal Society of London, A **200**: 523–541.

[157] Oldroyd JJ (1958): Non-Newtonian effects in steady motion of some idealised elastico-viscous liquids. In: Proceedings of the Royal Society of London, A **245**: 278–297.

[158] Oshinski JN, Ku DN, Mukundan S, Loth F, Pettigrew, RI (1995): Determination of wall shear stress in the aorta with the use of MR phase velocity mapping. *Journal of Magnetic Resonance Imaging* **5**: 640–647.

[159] Pareschi L, Russo G (2001): Time relaxed Monte Carlo methods for the Boltzmann equation. *Siam Journal on Scientific Computing* **23**: 1252–1272.

[160] Picioreanu C, van Loosdrecht MCM, Heijnen JJ (2000): Effect of diffusive and convective substrate transport on biofilm structure formation: A two-dimensional modeling study. *Biotechnology and Bioengineering* **69**: 504–515.

[161] Pontrelli G (1997): Mathematical Modeling for Viscoelastic Fluids. *Nonlinear Analysis, Theory, Methods & Applications*. **30**: 349–357.

[162] Pontrelli G (2001): Nonlinear problems in arterial flows. *Nonlinear Analysis* **47**: 4905–4915.

[163] Pontrelli G (1998): Pulsatile blood flow in a pipe. *Computers & Fluids***27**: 367–380.

[164] Pontrelli G (1997): Mathematical modelling for viscoelastic fluids. *Nonlinear Analysis* **30**: 349–357.

[165] Pozrikidis C (1997):*Introduction to Theoretical and Computational Fluid Dynamics*, Oxford University Press.

[166] Przemieniecki (1985): *Theory of Matrix Structural Analysis*. Dover Publications, New York.

[167] Przemieniecki JS, Bader RM, BOZICH WF, JOHNSON JR, MYKYTOW WJ(Eds.) (1966): In Proceedings, Conference on Matrix Methods in Structural Mechanics, AFFDL-TR-66-80, (Oct. 26-28,1965), Wright-Patterson AFB, Ohio.

[168] Qian YH, D'Humieres D, Lallemand P (1992): Lattice BGK models for Navier-Stokes Equations. *Europhysics Letters* **17**: 479–484.

[169] Qian YH, Deng YF (1997): A lattice BGK model for viscoelastic media, *Physical Review Letters* **79**: 2742–2745.

[170] Qiu Y, Tarbell JM (2000): Numerical simulation of pulsatile flow in a compliant curved tube model of a coronary artery. *Journal of Biomedical Engineering* **122**: 77–85.

[171] Raghavan ML, Vorp DA (2000): Toward a biomechanical tool to evaluate rupture potential of abdominal aortic aneurysm: identification of a finite strain constitutive model and evaluation of its applicability. *Journal of Biomechanics* **33**: 475–482.

[172] Ramaswamy S (2001): Issues in the statistical mechanics of steady sedimentation. *Advances in Physics* **50**: 297–341.

[173] Raviart PA (1984): Mixed finite element methods. In: The mathematics basis of finite element methods., Ed. Griffiths D. F., Clarendon Press, Oxford.

[174] Reneman RS, Hoeks APG, van de Vosse FN, Ku DN (1993): Three-dimensional blood flow in bifurcations: computational and experimental analyses and clinical applications. *Cerebrovascular Diseases* **X**: 185–192.

[175] Richtmyer RD, Metropolis N (1949): Modern Computing. *Physics Today* **2**: 8–15.

[176] Rivet JP, Boon JP (2001): *Lattice gas hydrodynamics*. Cambridge University Press.

[177] Roache PJ(1972): *Computational fluid dynamics*. Hermosa Publ.

[178] Rothmann DH, Zaleski S (1997): *Lattice-Gas Cellular Automata, Simple Models of Complex Hydrodynamics* Cambridge University Press.

[179] Schellbach K (1851): Probleme der Variationsrechnung. *Journal für die Reine und Angewandte Mathematik*. **41**: 293–363.

[180] Shaaban AM, Duerinckx AJ (2000): Wall Shear Stress and Early Atherosclerosis: A Review. *American Journal of Roentgenology* **174**: 1657–1665.

[181] Shan XW, He XY (1998): Discretization of the velocity space in the solution of the Boltzmann equation. *Physical Review Letters* **80**: 65–68.

[182] Sharpa MK, Thurstonb GB, Moore JE (1996): The effect of blood viscoelasticity on pulsatile flow in stationary and axially moving tubes. *Biorheology* **33**: 185–208.

[183] Skordos PA (1993): Initial and Boundary conditions for the lattice Boltzmann Method*Physical Review E*, **48**: 4823–4842.

[184] Spadling DB (1981): A general-purpose computer program for multidimensional one- and two-phase flow. *Math. Comp. Simulation* **23**: 267–276.

[185] Sone Y, Bardos C, Golse F, Sugimoto H (2000): Asymptotic theory of the Boltzmann system, for a steady flow of a slightly rarefied gas with a finite Mach number: General theory. *European Journal of Mechanics B-Fluids* **19**: 325–360.

[186] Stokes GG (1845): On the theories of the internal friction of fluids in motion, and of the equilibrium and motion of elastic solids. *Transactions of Cambridge Philosophical Society* **8** (1845): 287 ff, Cited in von Mises, 1958.

[187] Stone HL (1968): Iterative solution of Implicit Approximations on Multidimensional Partial Differential Equations. *SIAM Journal of Numerical Analysis* **5**: 530–58.

[188] Succi S, (2001): *The Lattice Boltzmann Equation for Fluid Dynamics and Beyond*. Oxford University Press.

[189] Succi S, Benzi R, Massaioli F (1993): A Review of the Lattice Boltzmann Method. *International Journal of Modern Physics C* **4**: 409 –415.

[190] Succi S, Foti E, Higuera F (1989): *Europhysics Letters* **10**, 433

[191] Taylor CA, Hughes TJR, Zarins CK (1996): Computational Investigations in Vascular Disease. *Computers in Physics* **10**: 224–232.

[192] Taylor CA, Hughes, TJR, Zarins CK (1998): Finite element modeling of blood flow in arteries. *Computer Methods in Applied Mechanics and Engineering* **158**: 155–196.

[193] Taylor CA, Darney MT, Ku JP, Parker D, Steele BN, Wang K, Zarins CK (1999): Predictive medicine: Computational techniques in therapeutic decision making. *Computer Aided Surgery* **4**: 231–247.

[194] Tölke J, Krafczyk M, Schulz M, Rank E, Berrios R (1998): Implicit discretization and nonuniform mesh refinement approaches for FD discretizations of LBGK models. *International Journal of Modern Physics C* **9**: 1143–1157.

[195] Thubrikar MJ, Robicsek F (1995): Pressure-induced arterial-wall stress and atherosclerosis. *Annals of Thoracic Surgery* **59**: 1594–1603.

[196] Thurston GB (1972): The viscoelasticity of human blood. *Biophysical Journal* **12**: 1205–1217.

[197] Turing AM (1952): The chemical basis of Morphogenesis. *Philosophical Transactions of the Royal Society of London* **B237**:37–72.

[198] Turner ML, Clough RW, Marin HC, Topp LJ (1956): Stiffness and Deflection analysis of Complex Structures. *Journal of the Aeronautical Sciences* **23** (1956): 805–823.

[199] van de Vosse FN (1987): Numerical analysis of carotid artery flow. PhD. Thesis, Eindhoven University of Technology, Eindhoven, The Netherlands.

[200] Verberg R, Ladd A (1999): Simulation of low-Reynolds-number flow via a time-independent lattice-Boltzmann method. *Physical Review E* **60**: 3366–3373.

[201] Von Mises R (1958): *Mathematical Theory of Compressible fluid flow*. Academic Press.

[202] von Neumann J (1961): Collected works, Elmsford, NY: Pergamon Press.

[203] Vorp DA, Raghavan ML, Webster MW (1998): Mechanical wall stress in abdominal aortic aneurysm: Influence of diameter and asymmetry. *Journal of Vascular Surgery* **27**: 632–639.

[204] Vorp DA, Steinman DA, Ross CE (2001): Computational Modeling of Arterial Biomechanics. *Computing in Science and Engineering* **3**: 51–64.

[205] Weaver JB, van Houten EEW, Paulsen KD (2001): Magnetic resonance elastography using 3D gradient echo measurements of steady-state motion. *Medical Physics* **28**: 1620–1628.

[206] Weber EH, Weber W (1825): *Wellenlehre auf Experimente gegrundet oder uberdie Wellen tropfbarer Flussigkeiten mit Anwendung auf die Schall-und Lichtwellen.* Leipzig: Gehard Fleischer, Cited in McDonald (1976).

[207] Womersley JR (1955a): Oscillatory flow in arteries: effect of radial variation in viscosity on rate of flow. *Journal of Physiology* **127**: 38–39P.

[208] Womersley JR (1955b): Method for calculation of velocity, rate of flow and viscous drag in arteries when the pressure gradient is known. *Journal of Physiology* **127**: 553–563.

[209] Womersley JR (1955c): Oscillatory motion of a viscous liquid in a thin-walled elastic tube-I: The linear approximation for long waves. *Philosophical Magazine* **46** 199–221.

[210] Wootton D, Ku DN (1999): Fluid Mechanics of Vascular Systems, Diseases, and Thrombosis. *Annual Review of Biomedical Engineering* **1**: 299–329.

[211] World Health Organization (2002): The World Health Report 2002 Reducing risks, promoting healthy life. World Health Organization. http://www.who.int/whr/en/

[212] Yeleswarapu KK(1996): Evaluation of continuum model for characterizing the constitutive behavior of blood. Ph.D. thesis. University of Pittsburg.

[213] Yeleswarapu KK, Kameneva MV, Rajagopal, KR, Antaki JF (1998): The flow of blood in tubes - theory and experiment. *Mechanics Research Communications* **25**: 257–262.

[214] Young T (1809): On the functions of the heart and arteries. The Croonian lecture. *Philosophical Transactions of The Royal Society* **99**: 1–31.

[215] Yu DZ, Mei RW, Shyy W (2002): A multi-block lattice Boltzmann method for viscous fluid flows. *International Journal for Numerical Methods in Fluids* **39**: 99–120.

[216] Zamir M (1977): The role of shear forces in arterial branching. *Journal of General Physiology* **67**:213–222.

[217] Zhao Z, Belleman, RG, van Albada, GD, Sloot, PMA (2002): AG-IVE: an Agent based solution to constructing Interactive Simulation Systems. In Computational Science - ICCS 2002.In: Lecture Notes in Computer Science **2329**: 693–703.

[218] Ziegler DP (1993): Boundary Conditions for Lattice Boltzmann Simulations. *Journal of Statistical Physics* **71**: 1171-1177.

[219] Zou Q, He X (1997): On pressure and velocity boundary conditions for the lattice Boltzmann BGK model. *Physics of Fluids* **9**: 1591–1598.

[220] Zou QS, Hou SL, Doolen GD (1995): Analytical Solutions of the Lattice Boltzmann BGK Model. *Journal of Statistical Physics* **81**: 319–334.

[221] Zou Q, Hou S, Chen S, Doolen GD (1995): An improved incompressible lattice Boltzmann model for time independent flows. *Journal of Statistical Physics* **81**: 35–48.

Samenvatting

In dit laatste hoofdstuk vatten wij de belangrijkste resulaten en de conclusies samen die in dit proefschrift worden besproken, samen met toekomstig onderzoek om het numerieke model te verbeteren.
In dit proefschrift wordt de rooster–Boltzmann methode beschreven als een robuuste en nauwkeurige hemodynamische numerieke oplossingsmethode op mesoscopische schaal. Zowel de mogelijkheden als de tekortkomingen van deze methode worden besproken. Er wordt aangetoond dat de rooster–Boltzmann methode van tweede orde is in ruimte en tijd bij lage Mach–getallen. De spanningstensor wordt daarbij verkregen uit de niet-evenwichts delen van de distributiefuncties, zonder de afschuif snelheid te benaderen.
Diverse numerieke simulaties zijn uitgevoerd, die allen een uitstekende overeenkomst opleveren met analytische oplossingen, andere numerieke methodes, en/of beschikbare experimentele gegevens uit de literatuur. Machine-precisie nauwkeurigheid werd verkregen voor enkele eenvoudige stromingsproblemen, zoals Poiseuille en Couette stroming, zelfs met de ”bounce-back”regel, van welke bekend is dat deze van eerste orde is.
Een quasi-onsamendrukbaar D3Q19 model voor de 3D simulaties van een oscillerende buisstroom reproduceert de analytische oplossing van Womersley opnieuw opgelever met een gemiddelde fout van ongeveer 15 procent met ”bounce-back” op de verbinding met een vrij hoog Mach–getal en minder dan een procent bij lage Mach–getallen. Een gebogen randvoorwaarde, zoals onlangs door Bouzaidi *et al.* (2001) is voorgesteld, aangepast aan het object, levert betere resultaten op en is tot op tweede orde nauwkeurig.
Aangezien het doel van het ontwikkelen van deze numerieke methode het gebruik is als interactieve oplossingsmethode in het CrossGrid project dat momenteel in ontwikkeling is, werden de prestaties van de methode verbeterd door simulaties op een hoog Mach getal te starten en vervolgens tijdens de simulatie te verlagen naar de gewenste waarde (Mach-Annealing).
Hiermee is het mogelijk om simulaties uit te voeren die in de orde van de annealing factor sneller zijn. Samengestelde procedures waarin zowel de Reynolds– als Mach–getallen dynamisch worden ingesteld, kunnen voor verdere versnelling in de toekomst in aanmerking komen.
De invloed van de wand–, in– en uitvoer–randvoorwaarden op de nauwkeurigheid en prestaties is in detail bestudeerd als functie van de Mach– en Knudsen–getallen. Er is zo aangetoond dat de ”bounce-back” op de verbindingen efficiënter zou kunnen zijn

indien toegepast bij de lage Mach–getallen wanneer de annealing techniek wordt gebruikt. Met de Mach–annealing techniek adviseren wij opnieuw de ”bounce-back” op de verbindingen als beter alternatief in vergelijking met andere verfijnde randvoorwaarden die moeilijk te gebruiken zijn op het gebied van de hemodynamica.

Een andere toepassing van belang in simulatieomgevingen is het interaktief veranderen van de geometrie en het bestuderen van de robuustheid van de numerieke methode bij het produceren van nauwkeurige resultaten zonder de simulatie opnieuw op te hoeven starten. De rooster–Boltzmann methode blijkt volledig aanpasbaar te zijn, zoals in eenvoudige tests is aangetoond. Meer onderzoek is noodzakelijk om het echte voordeel van deze eigenschap aan te tonen. Dit maakt onderdeel uit van huidig onderzoek.

De resultaten van de simulatie van een stabiele en instabiele stroming in een model van de menselijke aortavertakking die met behulp van een angiografie op basis van Magnetische Resonantie gereconstrueerd wordt, zijn beschreven als een typische hemodynamische toepassing. Voor onze simulaties werd een MRA beeld geleverd door Charles Taylor van de Universiteit van Stanford, U.S.A, met een oorspronkelijke resolutie van 512 x 512 x 64 voxels, elke voxel ter grootte van 1 byte. De afstand tussen elke twee elkaar opeenvolgende geregistreerde snijvlakken is 0.9375 mm. Een beeldsegmentatie algoritme is toegepast op de originele gegevensreeks om de aorta te extraheren waarna de gesegmenteerde aorta eruit gelicht wordt en gefiltreerd om uiteindelijk het simulatiemodel uit Fig. 8.1 over te houden. De drukgradiënt bij de ingang van de aorta wordt verkregen uit een gemiddelde van de stroomsnelheid uit de literatuur (Moore *et al.*, 1994c; Taylor *et al.*, 1999). Het bestudeerde computationeel model betreft slechts het vertakkingsgebied, direct na IMA, en omvat delen van de linker en rechter iliac–slagaders. Het gehele model is onderwerp van studie. Wij hebben een aantal stabliele en instabiele stroomsimulaties voor het aortamodel uitgevoerd. Resultaten voor snelheidsvelden en de spanning zijn met succes verkregen en zijn kwalitatief vergeleken met de literatuur.

Aangezien de schuifspanning een essentiële rol bij cardiovasculaire ziekten speelt en aangezien deze direct wordt berekend, bevelen wij onderzoekers op het gebied van hemodynamica deze methode sterk aan als een alternatieve methode voor bloedstroming. Meer voordelen worden duidelijk door eenvoudige rooster generatie en recht–toe–recht–aan parallellisme en een eenvoudige en uitvoerbare aanpassing aan een veranderende geometrie. Verder onderzoek van het complete aorta model en experimentele validatie is in ontwikkeling in onze groep.

Een hoofdconclusie uit dit proefschrift is dat zelfs met de eenvoudigste rooster–Boltzmann methoden resultaten mogelijk zijn vergelijkbaar met de meest verfijnde traditionele oplossings methoden. Nochtans heeft dit proefschrift vele vragen onbeantwoord moeten laten. Enige opgelaten vragen zijn:

- De methode is nog niet rijp voor het oplossen van modellen die vloeistof–structuur interactie betreffen. Sommige recente ontwikkelingen gebaseerd op het koppelen van de vloeistof aan vaste stof rooster–Boltzmann modellen (Cho-

pard[1] *et al.*, 2002, persoonlijke mededeling) om trombose te onderzoeken zijn veelbelovend.

- De rooster–Boltzmann methode met BGK–benadering heeft vele problemen bij hoge Mach– en Reynolds–getallen, maar niet bij hemodynamische Womersley–getallen. Nochtans is deze kwestie vrij gevoelig voor de randvoorwaarden. Van de rooster–BGK grensvoorwaarden is bekend dat ze viscositeitsafhankelijk zijn, op enkele uitzonderingen na. Dit heeft directe invloed op de stabiliteit van de methode. Een oplossing is om gegeneraliseerde rooster–Boltzmann vergelijkingen te beschouwen (GLBE). Echter, de rekentijd die voor GLBE benodigd is moet worden afgewogen tegen de nauwkeurigheid en met de engineering–precisie worden vergeleken.

- Het is bekend dat de niet–Newtoniaanse modellen beduidend verschillen van Newtoniaanse. Hoewel de globale structuur gelijk blijft, is het profiel van de spanningstensor beduidend anders in de buurt van de wanden. Het is vrij gemakkelijk om niet–Newtoniaanse stromen in de modellen van rooster–Boltzmann uit te voeren, maar GLBE kan dan een betere optie zijn dan het rooster–BGK.

- Aangezien vroege turbulentie zich in de circulatie kan opbouwen, zijn turbulentie modellen noodzakelijkerwijs benaderd door een ideale hemodynamische oplossings methode. Een aantal turbulentie modellen zijn beschikbaar uit de literatuur, waarvan GLBE de meeste gebruikte is.

- Met de ontwikkeling in beeldtechnieken en het toegenomen microscopisch begrip van atherosclerose, kunnen traditionele CFD solvers niet nuttig blijken te zijn en kunnen mesoscopische modellen een plaats vinden.

Samenvattend zijn de rooster–Boltzmann methoden nauwkeurige en robuuste CFD oplossings methoden met elegante berekeningskarakteristieken die hen tot alternatieve technieken maken, meestal zonder enige beperkingen.

[1]Het dient opgemerkt te worden dat Chopard aan de auteur in 2000 voorstelde dat deze koppeling, toegepast op de Hemodynamica, nuttig zou zijn. Op dat ogenblik waren wij er echter zelfs niet zeker van of de rooster–BGK methode aanvaardbare resultaten oplevert. Toen dat duidelijk was, was er geen tijd meer voor deze interessante suggestie.

Dankwoord

Alhamdu lil-Allahi Rab-il Aalamin.
I would like to thank my promoter Peter Sloot for giving me the opportunity to pursue my doctorate as a member of his group and his many efforts to guarantee continuous funding for me. Thanks Peter for giving me the many opportunities I enjoyed to teach and guide your students. The discussion with you brings me to the edge of science and shows me how computational science “emerges”! I’m very appreciative of all the support you have given me.
Alfons Hoekstra is a patient critical and keen co-promoter, still a friend. I enjoyed the discussion we used to have on daily basis. I enjoyed travelling with Alfons to participate in various conferences. Without his throughgoing persuasion, this work wouldn’t have seen the light. Thanks are extended to Jet and Pepijn.
Special thanks to Drona Kandhai for introducing me to the field of lattice Boltzmann and his worm-up code. We had a very close and useful interaction that made safe my initial “swimming ” in the sea of lattice Boltzmann particle distributions.
My full respect and gratitude to Abdel Galil Karrar, my Sudanese supervisor, without whom, it would not have been easy for me to study abroad. I have learned a lot from you Karrar and I wish that we would continue our research in the future.
I continue to be Grateful to my friends Bastien Chopard and Sauro Succi for their very fruitful assistance during many occasions. Their insightful guidance have enhanced my work effectively. Many thanks to librarians of Uva, NIKHEF and CWI. Special thanks to you Liesbeth.
I didn’t loose the chance to interact with the smart family of Lattice Boltzmann during the successful workshop in Erlangen. From that time, I couldn’t hide my bias to the method. Cargèse event was the most successful conference I participated in. I enjoyed the breaks talking to Dominique d’Humières Dominique, Bastien Chopard, Li-Shi Luo, Irina, Sauro, Gary Doolen, David Noble, Manfred and Zeiser about my problems. Thanks all for your valueless comments. Jean Boon “Merci Boque” for your special attention. I would also like to thank Ruibao Tao for visa arrangements to China and the organisers of the Discrete conferee in Shanghai. Special thanks to Fan Chen “nan wang” and Jiajia. I’ve enjoyed the pre-conference tours with Li-Shi Luo , Manfred Krafczyk, Thomas Zeiser, Alexandre Dupuis, Bastien Chopard and others.
Special thanks to Charles Taylor for the segmented images of the aorta and valuable advice. And for crossing the Atlantic for me.
Thanks to Huub Hoefsloot, Frans van de Vosse, Jack Eggels, David Ku and James Moore for their valuable scientific assistance.

Many thanks and best regards to the reading committee of my thesis. Thank you for your time and the very useful comments. I am grateful to Bert and Inna Zwart , Ron and Sofia, Rob Kordos and family, Harry and Vim, Maurits, Jessi and Tjitske, Rob and Lidy for their encouragement and emotional support. I owe you a lot Arend van Leeuwen. You have been so helpful to me. Peter, it is time to acknowledge your assistance. I will miss all of you!
Thanks to all members of the "Dutch Lattice Boltzmann Group" in Wageningen, Delft and Twente.
The possibility to obtain a PhD position in the Netherlands would have never happen without the efforts of Peter de Chatel and the generous financial support from Marten Durieux. Mart, your support to science students from Sudan is highly appreciated. In 1990 he already showed me a different way to deal with physics. Thanks are extended to Maurits Wijzenbeek for always being helpful.
Peter de Chatel is a scientist you enjoy listening to. I enjoyed the many times Peter and Schilla invited me and sheltered my soul.
A "Big thank you" to Eric Hennes for many ways of support. Without you Eric, life would have been more difficult in Amsterdam. Thanks for your valueless contributions. Thanks are extended Nina and Annejot Hoffman.
Throughout my life, I continue to receive full support from my parents Mohammed Ali and Fat-hia, my brothers Omar, Khalid and Eltayeb, and my sisters Nada and Nahla. I continue to be grateful to my uncle Bashir and family, Abdullahi Karoum and family, Sheikh Gabir and all the other members of my family..
Kamal, you are a real brother and a close friend. Thanks for all your support. Hassan Hamad, you proved to be a friend in need. "Khalis Al-Shukr" to all my colleagues and students at the School of Physics in Sudan.
I would like to thank Prof. Badr Eldin Khalil, Dean faculty of Science and Technology, Al Neelain University, Khartoum, Sudan for his valueless and friendly assistance. Thanks are extended to Prof. Abdel Aziz, the Principal, for limitless help and encouragement, Prof. Awad, the Vice-Chancellor and all the members of Al Neelain university for their support and encouragements. The many friends I came to know in Amsterdam made life easier for me. My close friend Ahmed, I will miss you so much. Sara ook! Tarig and Wafaa, I can find no words to express my gratitude. Ehrlichtstraat was a real home from home! Many thanks Isam Obeid for the true friendship and wish you and Dalal a happy life. Thanks Hala and all the best.
Special thanks to Isam and Muna for the good times we had together and their full support when we lost Omar. Laila and Noon, God zij met u! I am grateful to my colleagues Siddig, Gammar, Hassan "Abu Abi-Bakr" and Lamiaa, Mugahid, Yazeed, Sami, Uthman, Omar and Hala.
Am Abd Allah, thanks for your help and the fruitful discussion during the "Arabic-tea breaks". Thanks are extended to your family. Hette, what a great man you are!
Thanks Nahla Abdel Hadi, Yassir Abdo and Mahdi Yousuf for the nice weekend I enjoyed with you, "Shishia" Mohammed Eisa, Yuan, Galal, Ismael, Alnur and families for the Sudanese times in Shanghai, and "Vielen Dank" to the Berliners Salih, Mohamed Ali, Ibrahim, Abo and Christa and families.

During my holidays in Sudan, I enjoyed the very interesting mathematical discussion with Assawi, Sanousi and Bekri. Appreciations!
Despite all international crises, the international room is an ideal example that represents the ability of science to unite people. With Judhi (Indonesia), Zhiming (China), Roman (Russia), Alfredo, (Mexico) and Mike (United States) I enjoyed working while understanding other cultures. Shukran, shisia, spasibo, grasias and many thanks, with a lot more!
The variety of disciplines in our group defines what computational science is all about. I always find someone who knows something about what comes in mind. I particularly owe thanks to Dick van Albada for his scientific and personal advices and Jaap for the good friendship and fruitful discussion. I am grateful to Walter Hoffmann and Simon Portegeis.
I have received appreciated support from all my colleagues. Robert Belleman, you have been of real help in many aspects. Roel, Zeger and Kamil, thanks for the unlimited Beowulf and DAS2 support. I 've already missed the chocolate Kamil and Elena used to bring from abroad. Hartelijk dank Zeger voor het Nederlandse samenvatting. Thanks to Qui, Jos and Simon Engler with whom worked during their Msc. projects. Many thanks to Marianne Pieterse, Jacqueline, Erik, Virginie, Saskia and Richard for their friendly assistance. Special thanks to Willem, Elvire and Marianne of the Personnel Department.
Bob, you are a limitless source of information. I have had a chance to explore that during the trip to the the ASCI conference in Belgium in 2000. I also had a historic interview with de Nobel, a student of Einstein and Lorenz in Leiden in 2001. I feel very sad that I can not have another chance to meet you to tell me more about science in the 1930s.
The lunch breaks with Roel, Alfredo, Roman, Alessia, Piero, Michael and Peiro have a spatial taste. Grazie! Nights of Amsterdam with all of you together with Heidi, Yan Xu, Spetlana, Julia *et al.* were just fantastic!
Spasibo Dennis, Roman, Demtri and Ilia for all your help and for the good time. I would also like to thank Adam, Ammar and Abdul Salam for the good brotherhood. A word of "Shukran" to all the staff memebers of the Faculty of Science and Technology in Al Neelain University, to the director of the Institue of Natural Sciences, and all my previous teachers and colleagues in El Matamma, Shendi, Assiut, Khartoum, Wad-Medani, Obeid, Atbara, El-Fashir, Trieste, and Amsterdam.
Thanks are extended to the system group for keeping my account alive despite the many crashes I made and to Michael Williams for editing my manuscript.
So special times I spent with Ali El-Sadig and family, the Counsler of Sudanese Embassy in Den Haag, Ebtisam and sons, Husna and Tayseer, Aisha and "sunflower friends", Azza, Huda, Hiba and Solara.. Many Many thanks.
Thank you All!

Publications

- Artoli AM, Hoekstra AG, Sloot PMA (2002): Accuracy of 2D pulsatile flow in the lattice Boltzmann BGK method, in Sloot PMA; Tan CJK; Dongarra JJ; Hoekstra AG (Editors), Computational Science - ICCS 2002, *Lecture Notes in Computer Science* **2329**: 361-370. Springer Verlag, Berlin, April 2002. ISBN 3-540-43591-3.

- Artoli AM, Hoekstra AG, Sloot PMA (2002): 3D Pulsatile flow with the lattice Boltzmann BGK method, *International Journal of Modern Physics C* **13**: 1119-1134.

- Artoli AM, Hoekstra AG, Sloot PMA (2003): Accelerated Lattice BGK method for unsteady flow simulations through Mach number annealing, Accepted, *International Journal of Modern Physics C*.

- Artoli AM, Hoekstra AG, Sloot PMA (2003): Simulation of a systolic cycle in a realistic artery with the Lattice Boltzmann BGK method, *International Journal of Modern Physics B* **17**: 95–98.

- Hoekstra AG, van't Hoff J, Artoli AM, Sloot PMA (2003): Lattice BGK simulations of unsteady flow in a 2D elastic tube, in Sloot PMA; Abramson D; Bogdanov AV; Dongarra JJ; Zomaya AY; Gorbachev YE (Editors), Computational Science - ICCS 2003, *Lecture Notes in Computer Science* **2657**: 997–1006. Springer Verlag, Berlin, June 2003. ISBN 3-540-40194-6.

- Artoli AM, Kandhai D, Hoefsloot HCJ, Hoekstra AG, Sloot PMA (2003): Lattice Boltzmann, a Robust and Accurate Solver for Interactive Computational Hemodynamics, in Sloot PMA; Abramson D; Bogdanov AV; Dongarra JJ; Zomaya AY; Gorbachev YE (Editors), Computational Science - ICCS 2003, *Lecture Notes in Computer Science* **2657**: 1034–1043. Springer Verlag, Berlin, June 2003. ISBN 3-540-40194-6.

- Artoli AM, Hoekstra AG, Sloot PMA (2003): Mesoscopic simulations of systolic flow in the Human abdominal aorta, Submitted, *Journal of Biomechanics*.

- Artoli AM, Kandhai D, Hoefsloot HCJ, Hoekstra AG, Sloot PMA (2003): Robustness of the Lattice Boltzmann Method, submitted, *Future Generation Computer Systems*.

- Artoli AM, Hoekstra AG, Sloot PMA (2003): Simulations of a systolic cycle with lattice Boltzmann method: Accuracy versus performance, submitted, *Computers and Fluids*.

- Artoli AM, Hoekstra AG, Sloot PMA (2002): Time dependent flow in a rigid tube using the Lattice Boltzmann Method, in: Boon JP, Coveney PV, Succi S (Editors), International Conference on Discrete Simulation of Fluid Dynamics, in series *Europhysics Conference Abstracts* **25**:3.

- Artoli AM, Kandhai BD, Hoekstra AG, Sloot PMA (2000): Accuracy of shear stress calculations in the Lattice Boltzmann Method, in Proceedings of the 9th International Conference on Discrete Simulation of Fluid Dynamics, New Mexico USA, http://cnls.lanl.gov/Conferences/DiscreteSimulation/agenda.

- Artoli AM, Kandhai BD, Hoefsloot HG, Hoekstra AG, Sloot PMA (2001): Shear Stress in Lattice Boltzmann Simulations, in F. Hossfeld and K. Binder (Editors), Europhysics Conference on Computational Physics, Aachen, Germany, 5-8 September 2001, in series *Publication Series of the John von Neumann Institute for Computing* **8**: A127.